



Thesis Title

Characterization and Design of a Porous Core Photonic Crystal Fiber for THz Wave Guiding and Sensing

By

Md. Abdullah Al-Mahmud

A thesis submitted to Islamic University of Technology in partial fulfillment
of the requirements for the degree of

M.Sc. in Electrical and Electronic Engineering

Department of Electrical and Electronic Engineering

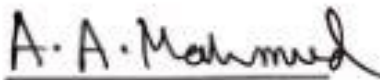
Islamic University of Technology (IUT)

Organization of Islamic Cooperation (OIC)

Board Bazar, Gazipur-1704, Bangladesh

DECLARATION OF CANDIDATE

I hereby declare that the work reported in the M.Sc. thesis entitled “ **CHARACTERIZATION AND DESIGN OF A POROUS CORE PHOTONIC CRYSTAL FIBER FOR THz WAVE GUIDING AND SENSING**” submitted at **Islamic University of Technology (IUT)**, OIC, Board Bazar, Gazipur, Bangladesh, is an authentic record of my work carried out under the supervision of **Prof. Dr. Mohammad Rakibul Islam**. I have not submitted this work elsewhere for any other degree or diploma. I am fully responsible for the contents of my M.Sc. thesis.



Md. Abdullah Al Mahmud

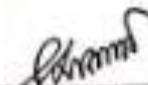
Student Number: 161021003


Academic Year: 2016-2017

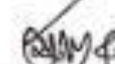
CERTIFICATE OF APPROVAL

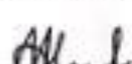
The thesis titled "CHARACTERIZATION AND DESIGN OF A POROUS CORE PHOTONIC CRYSTAL FIBER FOR THz WAVE GUIDING AND SENSING" submitted by Md. Abdullah Al Mahmud bearing Student No. 161021003 of Academic Year 2016-2017 has been found as satisfactory and accepted as partial fulfillment of the requirement for the degree of Master of Science in Electrical and Electronic Engineering on 24th February 2021.

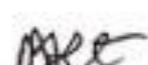
BOARD OF EXAMINERS

1. 

Dr. Mohammad Rakibul Islam
Professor
Department of Electrical & Electronic Engineering
IUT, Gazipur-1704, Bangladesh. Chairman
(Supervisor)
2. 

Dr. Md. Ruhul Amin
Professor and Head
Department of Electrical & Electronic Engineering
IUT, Gazipur-1704, Bangladesh. (Ex-Officio)
Member
3. 

Dr. Md. Ashraful Hoque
Professor
Department of Electrical & Electronic Engineering
IUT, Gazipur-1704, Bangladesh. Member
4. 

Dr. Ashik Ahmed
Professor
Department of Electrical & Electronic Engineering
IUT, Gazipur-1704, Bangladesh. Member
5. 

Dr. Masuma Akter
Professor
Department of Electrical & Electronic Engineering
DUET, Gazipur-1704, Bangladesh. Member
(External)

TO MY TEACHERS, COLLEAGUES & STUDENTS

TABLE OF CONTENTS

	Page No
DECLARATION OF CANDIDATE	i
CERTIFICATE OF APPROVAL	ii
LIST OF ACRONYMS AND ABBREVIATIONS	ix
LIST OF SYMBOLS	x
LIST OF FIGURES	xii
LIST OF TABLES	xv
ACKNOWLEDGEMENT	xvi
ABSTRACT	xvii
Chapter 1	1
Introduction	
1.1 Background and Current Status of Problem	1
1.2 Motivation	3
1.3 Objective	3
1.4 Outcomes	4
1.5 Organization of dissertation	4
1.6 Conclusion	4
Chapter 2	5
Development of THz Waveguide	
2.1 Waveguide	5
2.2 Terahertz Waveguide	5
2.3 THz Wave Propagation	5
2.4 Media of Guided Transmission	6
2.5 Background of THz Waveguide	6

2.5.1 Auston Switch	6
2.5.2 Microstrip	6
2.5.3 Circular Metallic Waveguide	7
2.5.4 Hollow Core Fiber	8
2.5.5 Plastic Sub Wavelength Fibers	8
2.5.6 Hollow Core Brag Fibers:	8
2.5.7 Photonic Crystal Fiber	9
2.5.8 Honeycomb Bandgap Fibers	10
2.6 Conclusion	11

Chapter 3 **12**
Photonic Crystal Fiber and Application of THz Wave

3.1 Classification	12
3.2 Construction of PCF	12
3.2.1. One-Dimensional Photonic Crystal Fiber	12
3.2.2. Two- Dimensional Photonic Crystal Fiber	13
3.2.3. Three- Dimensional Photonic Crystal Fiber	13
3.3 Development of Photonic Crystal Fiber	13
3.4 Advantages of Photonic Crystal Fiber	14
3.5 Definition, Generation and Detection of THz band	14
3.5.1 Generation of Terahertz Radiation	17
3.5.2 Detection Methods	18
3.6 Application of THz Wave	19
3.6.1 Breast Cancer	19
3.6.2 Skin Tumours	20

3.6.3 Dental	21
3.6.4 Detection of Impurities in the Pharmaceutical Industry	21
3.6.5 Security	22
3.6.6 Communication	22
3.6.7 Sensor	23
3.7 Conclusion	24
Chapter 4	
Losses and Factors of THz waveguide and Sensor Designing	
4.1 Effective Material Loss	25
4.2 Mode Power Propagation	26
4.3 Confinement Loss	26
4.4 Waveguide Dispersion	26
4.5 Effective Area	27
4.6 V- Parameter	27
4.7 Sensitivity	28
4.8 Origination of Finite Element Method (FEM)	29
4.8.1 PDE and the principle of physics	29
4.8.2 Different Elements	30
4.8.3 Finite Element Analysis (FEA) Software	31
4.8.4 Working Principle of software	32
4.8.5 Mathematical Model and Numerical Model	32
4.9 Well-Posed Mathematical Problems	32
4.10 Process of FEM	34

4.10.1 Geometry	34
4.10.2 Materials	34
4.10.3 Domain Settings, Boundary Conditions, Loads, and Constraints	34
4.10.4 Mesh	34
4.10.5 Solution	35
4.10.6 Results	36
4.11 Electromagnetic Waves in Media without Free Charges	36
4.12 Efficient solution of Maxwell's equations for optical fibers	38
4.13 Conclusion	39

Chapter 5

Design I: Proposed Sectorial Circular THz Waveguide for transmission	40
5.1 Design	41
5.2 Numerical Analysis	42
5.3 Fabrication Feasibility	52
5.4 Conclusion	52

Chapter 6

Design II: Proposed Sectorial Circular THz Sensor	54
6.1 Design Methodology	55
6.2 Simulation Results	56
6.3 Proposed sensor's experimental setup	73
6.4 Feasibility Assessment of Fabrication	74
6.5 Contribution of this research	75
6.6 Conclusion	75

	Chapter 7	
	Conclusion and Future Work	76
7.1	Conclusion	76
7.2	Future Work	76
	References	78

LIST OF ACRONYMS AND ABBREVIATIONS

Abbreviation	Definition
dB	Decibel
EML	Effective Material Loss
FEM	Finite Element Methode
NA	Numerical Aperture
PML	Perfectly Matched Layer
PCF	Photonic Crystal Fiber
CL	Confinement Loss
THz	Terahertz
TDS	Time Domain Spectroscopy
RIU	Refractive Index Unit
Ps	Pico Second
FEM	Finite Element Method
FEA	Finite Element Analysis

LIST OF SYMBOLS

Abbreviation	Definition
α_{eff}	Effective material loss
ϵ_0	Relative permeability
n_{mat}	Refractive index
α_{mat}	Bulk absorption loss
S_z	Z-component of the Poynting vector
E	Electric field component
H	Magnetic field component
L_c	Confinement loss
f	Operating frequency
c	Speed of light
$\text{Im}(n_{\text{eff}})$	Imaginary part of the complex effective refractive index
A_{eff}	Effective area
x	Area of the region of interest
n_{eff}	Effective refractive index
n_1	Effective refractive index core region
n_2	Effective refractive index cladding region
$I(f)$	Intensities of light with the presence of the analyte needed to be detected
I_0	Intensities of light without the presence of the analyte needed to be detected
r	Relative sensitivity
α_m	Absorption coefficient
l_c	Channel length
n_r	Refractive index of the sample
k	Light interaction
n_x	Effective refractive index of the x polarization mode

n_y	Effective refractive index of the y polarization mode
η	Core Power Fraction

LIST OF FIGURES

Figure Number	Caption	Page Number
2.1	(a) Geometry of a circular waveguide and (b,c) horizontal and vertical orientation of the electric field (Fundamental mode TE_{11}).	7
2.2	Transverse cross section of HC-BFs with (a) a conventional cladding and (b) with a defect layer. Black and gray, respectively mark the high- and low-index layers. The defect layer is marked by yellow.	9
2.3	Photonic-crystal fiber (PCF).	10
2.4	(Color online) Honeycomb fiber with (a) a seven-hole porous core and (b) a seven-cell hollow core. Dark regions represent air.	11
3.1	Terahertz range generation using a photoconductive switch.	16
3.2	Mastectomy from a 52 year old patient with invasive lobular carcinoma.	19
3.3	Lobular carcinoma (a) image from photomicrograph. (b) Terahertz image of E_{min} parameter. (c) Terahertz image of E_{min}/E_{max} parameter.	20
4.1	Node placement and geometry for 2D and 3D linear elements	31
5.1	Illustration of the cross-sectional details of core-cladding region with enlarged core.	42
5.2	Steps required to complete a finite element analysis	43
5.3	Fundamental electric field of mode for different values of porosity (a) 80% (b) 85% (c) 90%.	44
5.4	Effect of frequency on EML at different core diameter.	45
5.5	Effect of porosity on EML at different core diameter (D_{Core}).	45
5.6	Effect of frequency on core power fraction at different core diameter(D_{Core}).	47
5.7	Effect of frequency on confinement loss at different core diameters (D_{core}).	48

5.8	Effect of frequency on dispersion at different core diameter (D_{core}).	59
5.9	Effect of frequency on Effective area at optimal core diameter.	50
5.10	Characteristics of Effective Mode Index for proposed photonic crystal fiber.	50
5.11	V-Parameter as a function of frequency at different core diameters.	51
6.1	Illustration of the cross-sectional details of core-cladding region with enlarged core	56
6.2	Electric field distribution of proposed PCF at different refractive indices ($\mu = 1.33, 1.34, 1.35, 1.36, 1.37$)	57
6.3	Effect of frequency on the sensitivity at strut $5\mu\text{m}$	58
6.4	Effect of frequency on the sensitivity at strut $10\mu\text{m}$	59
6.5	Effect of frequency on the sensitivity at strut $15\mu\text{m}$	59
6.6	Sensitivity as a function of core diameter(D_{Core}) at strut $5\mu\text{m}$	61
6.7	Sensitivity with respect to frequency at strut $5\mu\text{m}$ for a bigger range of value of μ	61
6.8	Effect of frequency on the confinement loss at strut $5\mu\text{m}$	62
6.9	Effect of frequency on the confinement loss at strut $10\mu\text{m}$	62
6.10	Effect of frequency on the confinement loss at strut $15\mu\text{m}$	63
6.11	Effect of frequency on EML at strut $5\mu\text{m}$	64
6.12	Effect of frequency on EML at strut $10\mu\text{m}$	65
6.13	Effect of frequency on EML at strut $15\mu\text{m}$	65
6.14	EML as a function of core diameter(D_{Core}) at strut $5\mu\text{m}$	66
6.15	EML with respect to frequency at strut $5\mu\text{m}$ for a bigger range of value of μ	66
6.16	Effect of frequency on effective area at strut $5\mu\text{m}$	67
6.17	Effect of frequency on effective area at strut $10\mu\text{m}$	67
6.18	Effect of frequency on effective area at strut $15\mu\text{m}$	68

6.19	Effect of core diameter D_{Core} (μm) on effective area at strut $5\mu\text{m}$	69
6.20	Effect of frequency on effective area at strut $5\mu\text{m}$ for a bigger range of value of μ	69
6.21	Effect of frequency on Numerical aperture at strut $5\mu\text{m}$	70
6.22	Spot size as a function of frequency at strut $5\mu\text{m}$	71
6.23	Beam divergence as a function of frequency at strut $5\mu\text{m}$	72
6.24	Exploratory arrangement schematic of the proffered sensor for experimental sensing applications	74

List of Tables

Table Number	Title	Page Number
3.1	Overview of PCF Developments	13
5.1	Comparison between the design of existing PCF based THz waveguide and proposed design of PCF based THz waveguide	52
6.1	Performance comparison of the demonstrated design with previously designed sensors	73

ACKNOWLEDGEMENTS

First of all, I would like to express my deep and sincere gratitude to my supervisor Dr. Mohammad Rakibul Islam, Professor, Department of Electrical and Electronic Engineering (EEE), Islamic University of Technology (IUT), OIC, Dhaka, Bangladesh, for his kind guidance, support and encouragement. His regular helps and supervision on this thesis really made me to complete this work within very short time. His valuable advice and constructive criticism guided me to learn and enjoy the art of research. His ability to quickly understand the depth of the problem and suggesting a clear solution has always inspired me. In every sense, this thesis could never have come into existence without his help. Learning from him has been a very fruitful and enjoyable experience. I shall always remain grateful to him.

I would like to express my heartiest thanks to all of my board members, Prof. Dr. Md. Ruhul Amin, Prof. Dr. Md. Ashraful Hoque, Prof. Dr. Ashik Ahmed and External member Prof. Dr. Masuma Akter for their supporting and encouraging activities. I have acquired a lot of life time skills and positive things from them which will guide me through my life.

I would like to express my deepest cordial recognitions to my parents for their continuous support despite being far away from me.

Last but not the least I am thankful to Allah, who gave me enough patience, strength and courage to complete this work. I am highly grateful to the Almighty.

ABSTRACT

In this work, the main attention is to develop Photonic Crystal Fiber (PCF) geometry that is applicable for THz wave propagation as well as in analytes sensing applications. Recently lots of researchers have developed their PCFs with low losses and high sensitivity. Optical properties of PCF based devices depend on the geometrical properties. So it can be said that there is a huge scope to develop the properties by changing the geometrical parameters. Based on the above mentioned situation, a PCF with sectorized roundabout core is proposed. The cladding region follows the same sectorized circular design also. Topas is used as a background material for both cladding and core region of designed fiber because Topas contains low material absorption loss with a consistent refractive index inside at a wide range of frequency. Guiding properties of developed PCF are investigated through Comsol Multiphysics v5.3 a with finite element method. Due to the strategic geometrical optimization, it renders improved performances in most of the crucial cases. It exhibits ultra-low effective material loss of 0.022 cm^{-1} at 0.9 THz, besides, near-zero flatten dispersion is observed in the wide THz spectrum. Moreover, to ensure the suitability of proposed PCF, other significant guiding properties such as confinement loss, effective area, and v-parameter, etc. are observed in the same THz frequency range.

Lots of recent researches proved that PCF has the huge potentiality in analytes sensing cases. For example biomedical, gas sensing, analyte sensing, blood component sensing, alcohol and toxic sensing applications with high sensitivity and it is proved that PCF is a strong candidate in the field of sensing. Considering the above mentioned fact, our developed PCF structure has also been investigated for THz sensing cases with different analytes of various refractive indices. Cladding holes of the proposed geometry are filled with only air and core holes are filled with different liquid analytes having different refractive indices. At optimal design condition a high sensitivity of 91.8% , 92.0% , 92.2%, 92.3% and 92.4% and low confinement loss of $2.88 \times 10^{-9} \text{ cm}^{-1}$, $2.69 \times 10^{-9} \text{ cm}^{-1}$, $2.502 \times 10^{-9} \text{ cm}^{-1}$, $2.308 \times 10^{-9} \text{ cm}^{-1}$, $2.11 \times 10^{-9} \text{ cm}^{-1}$ have been achieved for refractive indices of 1.33, 1.34, 1.35, 1.36, and 1.37 respectively. Besides, a moderate effective area and low EML have also been achieved.

Fabrication feasibility of the demonstrated design is a key concern for any researcher. The proposed PCF based waveguide and sensor is constructed by circular sectorized core and cladding. By using extrusion technique, various types of structure have been fabricated by Max Plank Institute and the procedures of fabrication of the proposed design have been discussed in details. Finally, the outcomes and contribution of proposed design is highlighted in this research. The proposed design is applicable in both waveguide application for data transmission and in sensing application for detecting a wide variety of chemicals in industrial and chemical sector

Chapter 1

Introduction

The fiber optic networking is the ideal decision for information transmission in rate of order of gigabits or more. The transmission of information such as voice, video, telemetry over long distances and local area networks or computer networks fiber optic networking is widely used. Through converting electronic signals into light, a fiber optic communication framework utilizes light wave technology to transfer information over a cable.

Some outstanding trademark highlights of this sort of communication framework like enormous data transfer capacity, light weight, littler diameter, low weakening, transmission security, signal transmission over long distance, and so on make this form of communication a significant functional element in maximum telecommunication foundation. This section PCF based fiber optic communication framework features its background and current status, inspiration, results and other points of interest.

1.1 Background and Current Status of Problem:

The frequency range of 0.1-10 THz covered the transmission of THz wave. It is widely used in imaging [1], sensing[2], communication[3][4], drug testing[5], and medical analysis[6][7] applications. In recent years, researchers show significant attention in the field of THz production[8], detection[9][10] and THz wave guide designing. Recent THz system is dependable on the propagation of free space. All materials which are available for waveguide designing are light absorbent in the range of THz (0.1-10 THz) frequency band.

At initial stage circular shaped metallic waveguide was used but after few days that design was rejected because of lossy character. After that metal layer coated of hollow dielectric tube were designed[11], but that was also rejected because of its heavy weight. As a result, research interest was shifted to polymer materials due to low absorption loss. Because of this problem various types of polymers such as Teflon[12], Topas[13], Poly methyl methacrylate (PMMA)[14] had been used as first choice for THz waveguide. For avoiding absorption loss researchers concentrated their interest on guiding structure design. At the range of THz frequency, dry air is considered for negligible material absorption loss. On the basis of this concept, optical core of waveguide was designed by using sub wavelength air holes[15]. It created the problem of power dissipation. Later, foam of polystyrene was used but it created a major problem of large dimension. After that hollow core Bragg fibers was considered but it created the problem of narrow band properties. In photonic crystal fiber, light is internally reflected and its property of reflection depends on the discrepancy of refractive index betwixt the cladding & core. In general cladding is constructed by a group of air holes. Now a day's photonic crystal fiber (PCF)[16] is widely used because of their salient features, which is helpful for controlling their behavior.

Though some PCFs were made by solid core polymer [12][17] but that were not focused by the researchers because of their huge amount of losses. To solve this problem ratio of air filling was significantly incremented to ensure the light propagation through the air lattice of cladding. It also created a problem of large size of core and cladding in waveguide. To solve this problem, solid core PCF was rejected and porous core PCF came out as solution. By using the porous core, amount of solid material in the core was deducted & as an outcome material absorption loss or Effective Material Loss (EML) was reduced. Nielsen et al.[18] proposed a honey comb band gap THz wave guide, which was investigated both experimentally and numerically. Uthman et al. [19] proposed a PCF of hexagonal core with an EML of 0.012cm^{-1} where background material was considered as Teflon. Due to lower effective material loss of topas, Kajjage et al. [20] proposed a PCF of octagonal core-cladding with an EML of 0.07cm^{-1} but that paper didn't provide any elaborate discussion on dispersion properties and power fraction.

Now a days porous core photonic crystal fiber has drawn an attention due to its capability to create desired transmission properties. As a result, porous core photonic crystal fiber has created an attraction to researchers due to freely chosen design parameters. Hasan et al. introduced a circular PCF showed an EML of 0.056cm^{-1} [21]. Islam et al. [22] proposed a hexagonal PCF & showed an EML of 0.06cm^{-1} along with a dispersion variation of $1.06\pm 0.12\text{Ps/THz/cm}$. Again Islam et al.[23] introduced a hexagonal PCF along with reduced EML of 0.053cm^{-1} but variation of dispersion of $1.20\pm 0.25\text{Ps/THz/cm}$. Hasanuzzaman et al. [24] introduced a novel PCF incorporating hexagonal core and kagome lattice with an EML of 0.034cm^{-1} with a small confinement loss. They also achieved a zero flattened dispersion although the fabrication of kagome structure is more challenging compared to circular structure. For better improvement, in 2016 Saiful et al. [23] introduced a circular shape crystal structure along with an EML of 0.053cm^{-1} with a dispersion variation of 0.25Ps/THz/cm . Another square lattice porous core photonic crystal fiber was also processed in [25] along with an EML of 0.076cm^{-1} & confinement loss of 10^{-3}cm^{-1} .

On the other hand, different researches on PCF based sensor has been directed for a comprehensive variation of implementations, and they have successfully managed to gain minimized losses & high sensitivities. A typical PCF composition for observing formalin in food items were introduced by Arif et al. in [26] which demonstrated sensitivities among 22% and 29% for a comprehensive range of wavelengths. A surface plasmon resonance (SPR) based refractive index sensor was planned by Hasan et al. [27] along with gold as the plasmonic component & titanium oxide for altering the resonant wavelength. For a comprehensive range of wavelengths, this model demonstrated high linearity and a large wavelength sensitivity of $10,800\text{nm/RIU}$. With an indium titanium oxide (ITO) coating on the surface, another SPR based PCF sensor with a D-shaped structure was introduced in [28] which attained highest spectral sensitivity was $50,000\text{nm/RIU}$ with a high resolution of $4\times 10^{-4}\text{RIU}$. In 2019, Ahmed et al. developed 2 diverse PCF sensors for identifying blood ingredients, one with an elliptical dual-core [29] & the other with a concise hexagonal cladding and a crystalline core architecture [30].

The latter work directed to attain an insignificant confinement loss on the order of 10^{-12} dB/m along with a sensitivity as high as 80.93%. For analyzing the salinity and temperature of aqueous substances, an unprecedented tri-core sensor was introduced by Amiri et al. in [31]. The attained sensitivities were 5674 nm/RIU and 4 nm/oc for salinity & temperature accordingly. In recent days, a duo of propitious SPR-based PCF biosensors was introduced for identifying hemoglobin in blood[32]. These sensors combined a dual-core including a D-shaped formation along with various background components. Exceptionally amplitude sensitivities and high wavelength were attained for each transformation of the proposed sensor. The above mentioned works suggested a great scope for PCF based THz waveguide and sensor development.

1.2 Motivation

Several researchers proposed a variety of circular core-cladding design for PCF which is applicable for THz waveguide and sensor. Such as circular core-cladding, hexagonal core-circular cladding, Circular cladding - hexagonal core, Kagome structure cladding-hexagonal core, suspended elliptical core-hexagonal cladding and hollow-core- asymmetrical cladding etc. Every researcher was concerned about lower EML, higher effective area, lower dispersion, high mode power propagation for THz waveguide. Besides they also focused on high sensitivity, high effective area and low EML for THz based sensor designing. Achieving motivation from their research a sectored circular core-cladding based PCF has been proposed in this thesis which is applicable for both THz waveguide and liquid refractometric sensor also. From the demonstrated design an appreciable value of lower EML, Confinement loss (CL), high sensitivity, moderate effective area Numerical aperture(NA) have been achieved. There is the future scope for the development of the proposed design. For example, bending loss and total loss can be calculated by varying the geometry of the proposed design. Besides this perception of this design can be implemented for a new field of research such as surface plasma resonance (SPR).

1.3 Objective

The main focus in this thesis is to develop a very simple PC-PCF structure which is easily implementable for both waveguide and sensor also. Another focus should be given to reduce the losses with a high core power fraction. The proposed PC-PCF design may offer negligible EML, high Sensitivity and low confinement loss in THz waveguide and sensing applications.

The Objectives is summarized as below:

- i. To propose a simple PCF for THz regime and that should be applicable for both THz waveguide and sensor. Besides it will offer low confinement loss, negligible EML, high core power fraction and high sensitivity.
- ii. To analyze the design parameter variations, such as core size, porosity, frequency, pitch size.

- iii. To find an optimum value of design parameters so that they will provide the deserved outputs.
- iv. To assess the performance of the proposed design by using COMSOL multi physics (version 5.3a) software and display the results graphically.

1.4 Outcomes

- i. Simple PCF structure with negligible EML and low confinement loss for THz guidance, which is superior to the recently proposed framework[20][21][24][23][25][33][14][34][35].
- ii. High sensitivity for variety of various refractive indices of different liquid analytes.
- iii. Show the effect of variation for different design parameters such as core size, core diameter, strut size, frequency, porosity etc.

1.5 Organization of Dissertation

The thesis consists of seven chapters. A short explanation is introduced here:

Chapter 1 is an introductory chapter. It contains a short overview or background about related research, motivation, objective and possible outcome of this thesis.

Chapter 2 contains a discussion about waveguide and their evolution.

Chapter 3 contains brief information about photonic crystal fiber and their numerous applications in various sectors.

Chapter 4 describes various key factor for designing THz wave guide and sensor. For example, effective area, core power fraction, effective material loss (EML), confinement loss (CL), sensitivity etc.

A new design of PCF based THz waveguide is proposed in **chapter 5**, which is used for data transmission and which shows a comparatively lower value of EML[25][36].

Designed THz waveguide has been successfully implemented for sensing application in **Chapter 6**, which describes the sensing features of proposed design and which shows a comparable higher sensitivity, moderate effective area, lower EML and confinement loss also[37][38].

Chapter 7 contains conclusion and direction of future work.

1.6 Conclusion

In this research a sectorized circular core & cladding structured based on photonic crystal fiber (PCF) has been proposed which provides a minimum EML of 0.022 cm^{-1} . Moreover the improved performance parameters such as confinement loss, flattened dispersion, core power fraction, effective area and V- parameter has been discussed also. Again the same design have been implemented in sensing application. In sensing application a high sensitivity of 92.2% has been achieved. Besides other factors have been discussed also.

Chapter 2

Development of THz Waveguide

The unit of frequency measurement is Terahertz (THz) which is equivalent to 1 trillion Hz (10^{12} Hz). It ordinarily alludes to the frequency of an electromagnetic wave that is a portion of the electromagnetic spectrum not visible to the bare eye and situates in the middle of the microwave & the infrared range. T-rays are a case of a particular portion of the spectrum inside the ITU-labeled band and range from 0.3 to 3 THz that discovers utility in astronomy.

2.1 Waveguide

A waveguide is an electromagnetic feed line utilized in broadcasting, microwave communications, and radar establishments. A waveguide comprises of a cylindrical or rectangular metal pipe or tube. The electromagnetic field spreads lengthwise. Horn antennas & dish antennas utilized waveguides regularly.

An electromagnetic field can spread along a waveguide in different manners. Two normal modes are familiar as transverse-electric (TE) & transverse-magnetic (TM). The electric lines of flux in TE mode and the magnetic lines of flux in TM mode are perpendicular to the axis of the waveguide. As long as the inside of the waveguide is kept spotless & dry, either mode can give low loss & high efficiency.

To work appropriately, a waveguide should have a specific least diameter comparative with the wavelength of the signal. On the off chance that the waveguide is excessively restricted or the frequency is excessively low (the wavelength is extensively long), the electromagnetic fields can't proliferate. At any frequency over the cutoff (the least frequency at which the waveguide is sufficiently enormous), the feed line will function admirably, albeit certain working attributes differ contingent upon the quantity of wavelengths in the cross section[39].

2.2 Terahertz Waveguide

It is fundamental to create waveguides with minimal transmission loss and minimal dispersion to extend the scope of THz applications. Accordingly, dielectric guides (widely utilized for optical waves) and hollow metallic waveguides (utilized for millimeter waves) display transmission losses of ~5-100 dB/m at THz frequencies.

2.3 THz Wave Propagation

The way in which waves travel is known as wave propagation. We are able to recognize the difference between longitudinal waves and transverse waves with respect to the direction of oscillation relative to the propagation direction. For electromagnetic waves, propagation may happen in a vacuum as well as in a material medium.

2.4 Media of Guided Transmission

Media that gives a conduit from one device to another device is known as bounded or guided transmission media. It also includes Fiber-Optic Cable, Twisted-Pair Cable & Coaxial Cable. A signal that is coming through any of these media is coordinated & accommodated by the physical structure of the medium.

2.5 Background of THz Waveguide

2.5.1 Auston Switch

An Auston switch is an optically gated antenna, which is additionally known as a photoconductive switch. It is normally utilized within the generation and detection of pulsed terahertz radiation. It is named after David H. Auston who was a physicist. He first built up the technology at Bell Labs during the 1960s. An Auston switch comprises of a transmission line antenna with a hole that's bridged by a semiconductor. For terahertz era, a DC bias voltage is connected over the antenna. Light is focused on the gap when it comes from pulsed laser with femto second pulses; it energizes charge carriers, which are subsequently accelerated by the bias voltage in the semiconductor's conduction band. The induced acceleration from the photocurrent makes the charge carriers to radiate in terahertz frequencies, creating a pulse lasting a few picoseconds. To be utilized as a terahertz detector, the switch includes the equal geometry however without the bias voltage. As an alternative, the incident terahertz pulse itself provides the bias field for the charge carrier in the course of the interval when the switch is actuated by utilizing the (much shorter) laser pulse. The induced photocurrent would then be able to be amplified and estimated. To outline whole range of the terahertz pulse, variation of the time delay among the generation & detection of femtosecond pulses can be possible[40].

2.5.2 Microstrip

Microstrip is a sort of electrical transmission line, which can be fabricated using printed circuit board technology. It is used to transmit microwave-frequency signals. It includes a conducting strip segregated from a ground plane by a dielectric layer known as the substrate. Numerous microwave component can be formed from microstrip for example antennas, couplers, filters, power dividers etc. with the whole gadget existing as the design of metallization on the substrate. Microstrip is in this way considerably less costly than conventional waveguide technology, in addition to being far lighter and more minimized structure. ITT laboratories created Microstrip as a contender to stripline (1st distributed by Grieg and Engelmann during December 1952 IRE proceedings). Microstrips have some disservices contrasted to the waveguide such as larger losses and minimized power handling capability. Likewise, in contrast to waveguide, microstrip isn't encased, besides it is vulnerable to inadvertent radiation and cross-talk. For the most minimal expense, microstrip devices might be built on an ordinary FR-4 (standard PCB) substrate.

Anyway, it is frequently discovered that the dielectric losses in FR-4 are excessively large at microwave frequencies, and that the dielectric constant is not adequately firmly controlled[41].

Hence, an alumina substrate is ordinarily utilized. Microstrip transmission lines are additionally built into solid microwave coordinated circuits on a more modest scope.

2.5.3 Circular Metallic Waveguide

A circular waveguide comprises of a hollow metallic cylinder with an inner radius R (see Figure 2.1). Within the inner air-filled volume of the cylinder, electromagnetic waves can proliferate above mode-explicit cut-off frequencies $f_{c, mn}$. By utilizing cylindrical coordinates and Bessel functions, solutions of Maxwell's equations can be discovered. The solutions can be separated into TM& TE modes as in the case of a rectangular waveguide. The various modes are represented by integer numbers m and n .

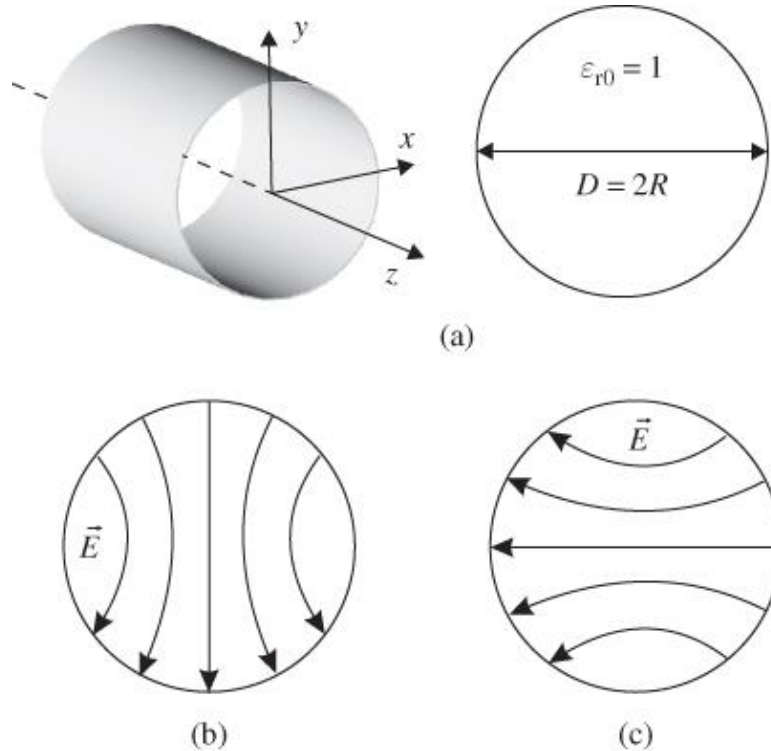


Figure 2.1: (a) Geometry of a circular waveguide and (b,c) horizontal and vertical orientation of the electric field (Fundamental mode TE_{11})[42].

TE_{11} is the wave mode along with the least cut-off frequency (fundamental mode). Figure 2.1 (b-c) represents the electric field distribution in a cross-section area. There is no special heading direction for the orientation of the electric field since the cross-section is a circle. A vertical field orientation and a horizontal field orientation is shown in Figure 2.1(b) & 2.1(c) accordingly. The orientation relies upon the excitation of the mode in practical operation. To transmit two free

information streams at the same time we can utilize orthogonal polarized waves of the principal wave mode.

2.5.4 Hollow Core Fiber:

A widely used optical fiber is hollow-core fiber. It navigates light typically inside a hollow zone, so that as it were a negligible bit of the optical power proliferates within the solid fiber material (commonly a glass). As per the usual physical system for managing light in a fiber, this ought be impossible: typically, the fiber core's refractive index must be greater than the surrounding cladding material. Nonetheless, based on a photonic band gap an alternate managing system can be utilized, as can be acknowledged in a photonic crystal fiber along with a specific structure. These types of fibers are likewise known as photonic bandgap fibers. The title air-guiding fibers is less precise, since it is actually not the air, which gives the guidance[43].

2.5.5 Plastic Sub Wavelength Fibers:

Plastic sub wavelength fibers appeared for their relatively minor losses. In any case, there is a drawback for the sub-wavelength fibers that the vast majority of the field radiates outside the waveguide core, consequently bringing about solid coupling to nature.

For development, Nagel et al. revealed the expansion of a sub wavelength hole inside a strong core, which rises the guided field all around air hole and consequently lessening the ingestion losses. Nevertheless, the damage because of the material is still severe.

2.5.6 Hollow Core Bragg Fibers (HC-BF):

The multilayered cladding of an HC-BF can restrict light with frequency to the band gap range. In a HC-BF, light from all incidence angles and all polarizations could be very much caught in the core. The transverse cross-area of a HC-BF with an ordinary cladding is shown in Figure 2.2 (a). A multilayered cladding composed of alternating dielectric layers with high and low refractive indices surrounds a hollow core with the diameter of d_c ; their thicknesses is represented by d_h and d_l , respectively (with the exception of the innermost and outermost high-index layers). n_h and n_l represents their refractive indices respectively. N means the number of period. It is noticed that for disposing surface modes both thicknesses of the innermost and outermost high-index layers are just $d_h/2$. Refractive index of outermost thick layer is usually equal to n_l where the outermost thick layer is a protective cladding. A transverse resonant behavior rises because of the defect mode, when a defect layer (marked by yellow) is brought into the conventional 1D periodic cladding is appeared in Figure 2.2. Accordingly, we can utilize this type of HC-BF as a band-rejection filter, of which the performance strongly relies upon on the parameters of defect layers (for example the area of N_d , the refractive index of n_d and the thickness of d_d) [44].

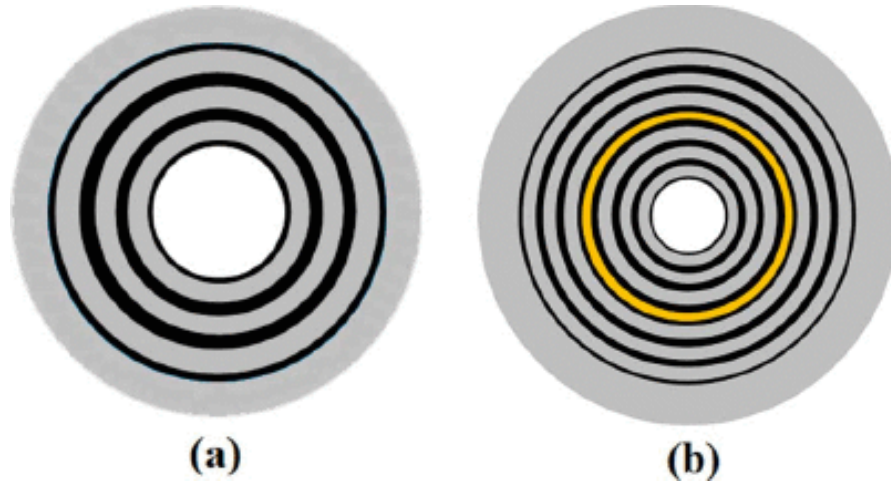


Figure 2.2: Transverse cross-section of HC-BFs with (a) a conventional cladding & (b) with a defect layer. Black and gray, respectively mark the high- and low-index layers. The defect layer is marked by yellow[44].

2.5.7 Photonic Crystal Fiber

A type of optical fiber named Photonic-crystal fiber (PCF), which is dependent on the photonic crystal's properties. In 1996, the University of Bath, UK conducted the first investigation[45]. Light in hollow cores or with confinement feature isn't feasible due to its ability restrict in conventional optical fiber. There are many applications that PCF is presently finding such as, nonlinear devices, high-power transmission, fiber-optic communications, fiber lasers exceedingly precise gas sensors & other areas. Progressively specific classifications of PCF incorporate holey fiber (PCFs utilizing air holes in their cross-sections), photonic-bandgap fiber (PCFs that restrict light by band gap effects), Bragg fiber (photonic-bandgap fiber shaped by concentric rings of multilayer film), and hole-assisted fiber (PCFs guiding light by a conventional higher-index core adjusted by the existence of air holes). Photonic crystal fibers might be viewed as a sub-group of an increasingly common class of micro structured optical fibers, where lights are navigated by basic adjustments & not just by refractive index contrasts.

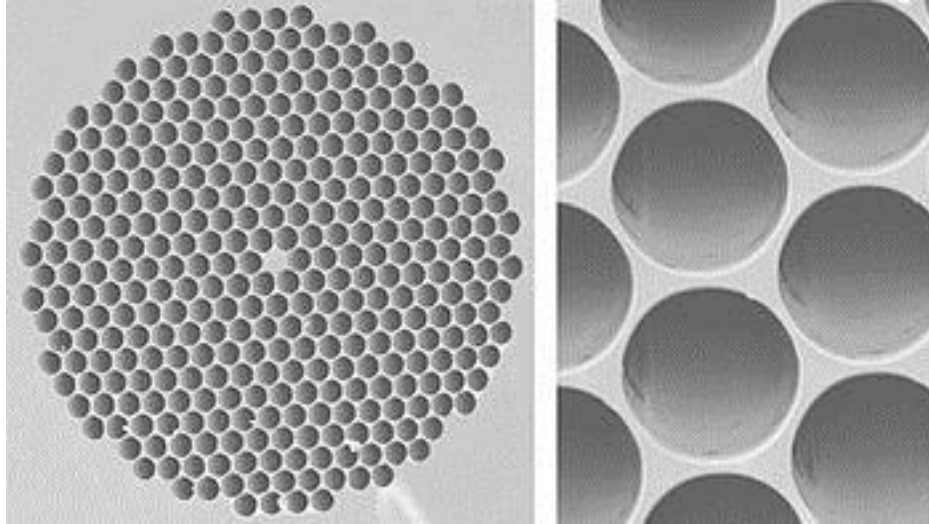


Figure 2.3: Photonic-Crystal Fiber (PCF)[46]

2.5.8 Honey Comb Band Gap Fibers

In Figure 2.4 the honeycomb band gap fiber plans are appeared. All the holes bear a similar diameter shortly "d" in the porous-core fiber. The core is made by evacuating seven honeycomb cells in the hollow-core fiber. The fiber is viewed as made of Topas with a steady refractive record of 1.526. The structure is picked to have a pitch of $A = 250 \mu\text{m}$ and hole to-pitch proportion of $d/A=0.55$, as this leads to a key band gap close to 1 THz. The band gap of the cladding unit cell is determined utilizing the MIT Photonic-Bands package (MPB).

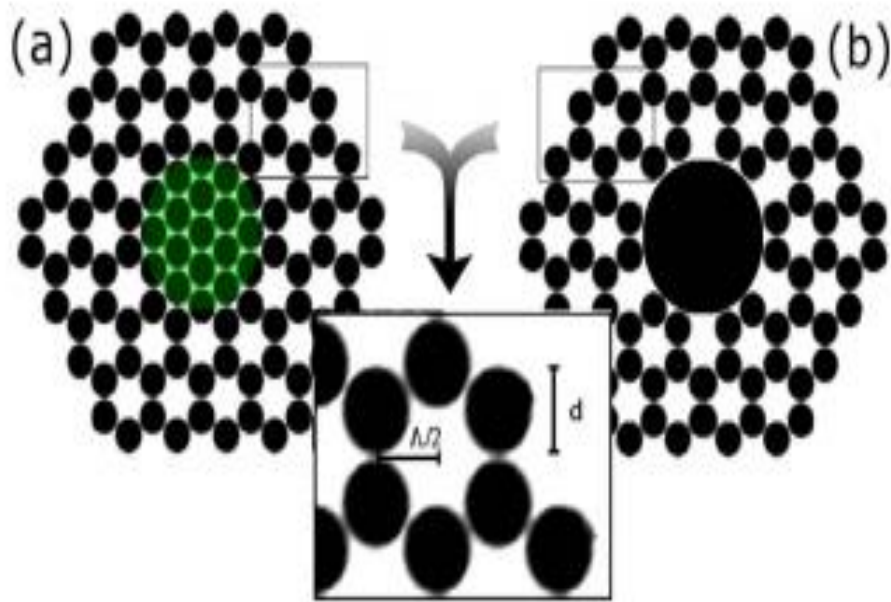


Figure 2.4: (Color online) Honeycomb fiber along with (a) a seven-hole porous core & (b) a seven-cell hollow core. Dark region shows air[47]

2.6 Conclusion:

From the above description, it gives a clear idea about the development of waveguide and their structure. The major outcome of this chapter is to interpret the evolution process of fiber and gain brief information about them. The main focus of this thesis is to develop or design a (Photonic Crystal Fiber) PCF based THz waveguide for data transmission from understanding the features of previous development and implement the same design of PCF for liquid sensing.

Chapter 3

Photonic Crystal Fiber and Application of THz Wave

Fiber optic cable is formulated with a cladding & a core of constant refractive index distinction. As a consequence of the property of light named refraction, core transmits light and this is possible because of distinction among the refractive indexes of the core & cladding. These refracted lights convey much greater loss in the time of propagation over expanded distances, therefore necessitates amplifiers and repeaters for expanded distance communications.

On the other hand, In PCF, producing a much vigorous waveguide to photons than conventional fiber optics, light is captured within the core. Instead of glass, the polymer implicated in PCF bestows the convenience of a more malleable fiber that can allow affordable & facile installation. Depending on the requisite attributes of the propagated light, miscellaneous photonic crystals according to multifarious photonic lattices are fabricated.

3.1 Classification:

Photonic crystal fibers are commonly distinguished in between two momentous classes:

- Index-Guiding Fibers: Similar to customary fibers, they have a rigid core. Lights are restricted in this core by deploying the adjusted total internal reflection process.
- Photonic Bandgap (Air Guiding) Fibers: Have a core of low-index element (swelled core) and periodic micro shaped components. The core regions have a lesser refractive index compared to the contiguous photonic crystal cladding. The lights are conducted by an operation that varies from a total internal reflection in which it utilizes the existence of the photonic bandgap (PBG).

3.2 Construction of PCF

Photonic crystal fiber is categorized among three prime types contingent on the fabrication techniques. They are one-dimensional, two-dimensional, and three-dimensional photonic crystal fibers[48].

3.2.1. One-Dimensional Photonic Crystal Fiber

The dielectric is periodic in a single-direction in one-dimensional photonic crystal fiber. Alternating ledges of the component are accrued together to form the band gap in a single direction. Bragg mirror is one of the common examples of one-dimensional photonic crystal fiber, which is generally exploited in the optical switch, dielectric mirror etc.

3.2.2. Two-Dimensional Photonic Crystal Fiber

By drilling dents towards the ledge, two-dimensional photonic crystal fibers are formed which are utilized in nonlinear appliances. Initially, it was founded in 1996 by Thomas Krauss. The two dimensional periodic alteration shape is known as photonic crystal fiber. Triangular and square lattice PCF formation have been deployed.

3.2.3. Three-Dimensional Photonic Crystal Fiber

By ricking 2D ledges on the apex of each other & by drilling them at several angles, three-dimensional photonic crystal fiber is manufactured. Three-dimensional consequences are generally found in miscellaneous structures such as Diamond structure, Woodpile structure & Y ablonovite structure.

3.3 Development of Photonic Crystal Fiber

In the early 1990s, the photonic crystal fiber is established. To this day many scientists have been contributed in the sector of photonic crystal fiber. An inspection of photonic crystal fiber advancements are demonstrated in Table 3.1.

Table 3.1: An Overview of PCF evolutions

Year	Development
1978	Introduction of Bragg fiber[49]
1992	Invention of the photonic crystal fiber along with air core[50]
1996	Development of photonic coated single-mode fiber[51]
1997	Endlessly single mode PCF[52]
1999	PCF along with photonic bandgap & air core[53]
2000	Extremely birefringent [54]
2000	PCF generated Super continuum[55]
2001	Bragg fiber's fabrication [56]
2001	PCF laser along with double cladding[57]
2002	PCF along with ultra-flattened dispersion[58]
2003	Bragg fiber along with silica & air core [59]
2004	Chalcogenide photonic crystal fiber [60]
2005	Kagome lattice PCF[61]
2006	Hybrid PCF[62]
2007	New technique for manufacturing polymer template for photonic crystals named

	Silicon double inversion [63]
2009	Hollow-core based photonic bandgap fiber [64]
2013	Double cladding based seven core photonic crystals [65]
2014	PCF along with Nano displacement sensors [66]
2015	Innovation of the design of equiangular PCF[67]
2016	Ultraflat Broadband Supercontinuum PCF[68]
2017	Liquid-infiltrated PCF sensor [37]
2018	Spectroscopic Chemical Identification PCF sensor [38]
2019	Surface Plasma resonance(SPR) based PCF [69]
2020	Different refractometric PCF chemical sensor[70]

3.4 Advantages of Photonic Crystal Fiber:

The model of PCFs are very malleable. Over typical optical fibers, there are numerous conveniences of photonic crystal fiber. Some of them are shown below:

1. It imparts a singlemode operation for a concise operating wavelength.
2. High Birefringence.
3. Dispersion is manageable.
4. Only one polarization in single-mode.
5. For comprehensive fiber stay single mode
6. Effectual mode area and nonlinearity.

3.5 Definition, Generation and Detection of THz band

This was due to a scarcity of detectors and compatible origins. Developments in the semiconductor technology in the last 15 years have revealed numerous modern opportunities for Terahertz research. Terahertz radiation has a convenience regarding most other ionizing imaging modalities which generally employed in this day, for instance, MRI, PET, X-ray, CT scans and planar x-rays. One more convenience concerning these modalities & ultrasound is its efficiency to attain idiosyncratic spectral information that can effectively be employed to discriminate within tissue categories. As it has a comprehensive wavelength, Terahertz imaging likewise has

the similarity of inadequate dispersing than Infra-Red. At the point when sub-frequency strategies are not in conduction, for a recurrence of 1 THz, one of the limitations of Terahertz radiation in imaging is its resolution of 0.3 mm. By conducting at higher-level of frequencies or by other methods, for instance, performing in the optical approaching field the resolution can be enhanced. Terahertz images proffer the probability of producing information from profound compositions than presently attainable to the pathologist from branded slides and therefore tumor margin definition is one feasible application. Employing the amplitude & phase data garnered from reflection & transmission, axially and three-dimensional images can be created.

The two forms of Terahertz imaging & spectroscopy are Reflection and Transmission, barely alluding to whether the finder or detector is installed abaft or in frontwards of the form being imaged respectively. Transmission is very expedient in ascertaining elementary tissue characteristics videlicet absorption coefficient and the refractive index. A spectrum produced within the time domain by transmission THz-TDS or imaging, which may then be applied to acquire a period of flight, exploitation images or can be transformed to a spectrum within the frequency domain. When selecting a process, Tissue size is a matter that must be required to be deliberated i.e. if the model is too stocky, the transmission may be disrupted. Having capability *in vivo* utilization, the operation of transmissions is fundamentally *in vitro* with reflection. For instance, reflection also has the potentiality to identify early caries & *in vivo* imaging, it is a credible choice[71],[72],[73],[74].

3.5.1 Generation of Terahertz Radiation

By lasers, electronics and non-linear optics Terahertz radiation is emanated. These generated Terahertz radiations of miscellaneous wavelength either pulsed or continuous wave (CW). Electronic origins involve super-lattice electronic appliances and Backward Wave Oscillators (BWO). These are the propagations of high-frequency electronics, for example exclusively conducts at the microwave edge of the Terahertz section. Photonic origins comprise Dipole Antennas, lasers, Photoconductive, as well as appliances employing mixer of optics. This photonic origin has been ubiquitous into medical implementations. For Terahertz range propagation, the two most extensively applied techniques are optical rectification and secondly the obsolete photoconductive emitters. Both of these are founded on utterly short-pulses from the titanium-sapphire lasers[75].

Now, Photoconductive emitters will be explicated. In a biased semiconductor (photoconductive antenna) the titanium sapphire laser with a photon energy of 800 nm (superior to the semiconductor's band-gap) produces carrier of electron-hole. Usually, the semiconductor implicated is LT-GaAs. The bias (of 1 kV for amplified Ti: Sapphire lasers or around 40 V for Titanium-sapphire lasers) stimulates the carriers which cause the emergence of an electromagnetic pulse as contemplated by the Equations of Maxwell. This is graphically exhibited in Figure 3.1.

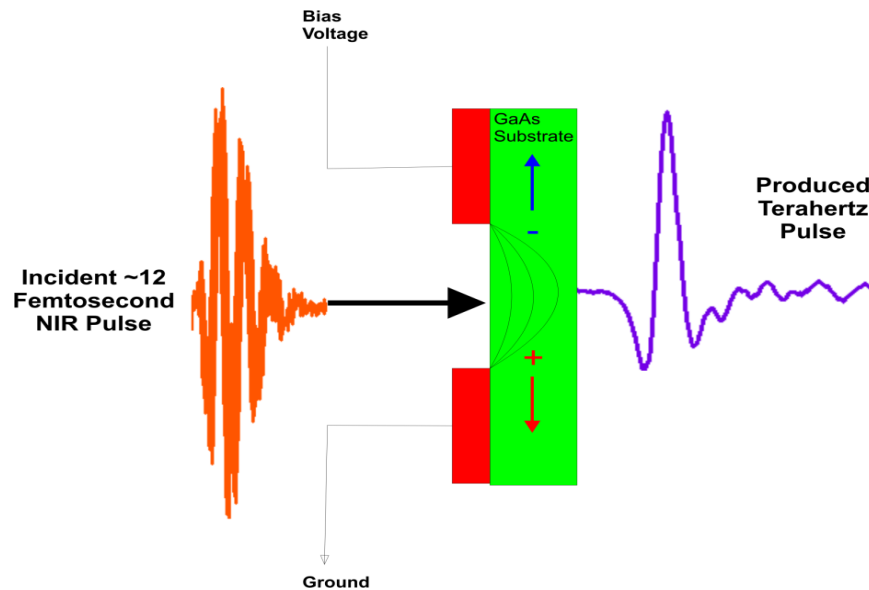


Figure 3.1: Photoconductive switch using for Terahertz range generation[76].

The Terahertz pulses are on account of momentary screening of the predisposition region by photo-impelling charge. A bandwidth up to 5 THz can be generated by this kind of generator, which can usually be employed with an oscillator sole process. The restrictions of this provenance are the pulse width of the excitation laser along with the response time of the semiconductor element implicated. The femtosecond Terahertz emitted pulse is collimated by the silicon hyper-hemispherical lens or crystalline quartz along with an off-axis parabolic mirror. Photoconductive emitters produce Terahertz pulse which have power ledges approximately in the series of nano-watts, with the apex power being series of higher magnitudes. The pulse's bandwidth is predominantly restricted by how expeditiously the charge-carrier can stimulate rather than the period of the laser-pulse[77].

As aforecited, optical indemnification predominantly exploits an amplified titanium-sapphire lasers and an ultra-short laser pulse, the acute pulse is an event over a nonlinear channel; a diaphanous crystalline component for instance Gallium Phosphide (GaP), Gallium Arsenide (GaAs), Zinc Telluride (ZnTe), Gallium Selenide (GaSe) or Indium Phosphide (InP). The crystal

is electrically polarized instantaneously at elevated optical severities. Laser's unison of diverse frequency constituents generates a beating polarization. This alteration in electrical polarization ejects the radiation of Terahertz. The viscosity of the crystal as well as the period of the laser pulse, exploitation, and discrepancy of propagation velocity among the Terahertz pulse within the crystal & Laser, everything moderates the pulse band-width. This approach qualifies the produced frequencies and they can be stimulated to higher than 40 THz. With magnified lasers, production by Optical Rectification is an accessible option. Optical indemnification confides on the nonlinearity in the electric impressibility of components which is also the sole operation audited at the time when the components are pumped under their band gaps.

Another mechanism of Terahertz emissions is Transient currents that eventuate in the inexistence of an exotic biasing region on account of transitory current in the semiconductor periphery. These could be from ripple production (from periphery depletion regions) or a transitory Photo-Dember region emerging from distinctions in diffusion rates among holes and photo produced electrons. Semiconductors such as InP and GaAs, when stimulated with 790 nm those are forecasted to generate Terahertz radiation predominantly through periphery regions of depletion, where the Photo-Dember effect is the operation in InAs.

Many other different techniques of production comprise planar antennas or pin diodes, lithium niobate based origins (high spectral resolution with low powers), free-electron lasers, synchrotrons, transceivers (identical receiver and transmitter formed on photo-conductive antennas) laser-created plasmas & extensive orifice antennas for magnified lasers. An elaborated statement of those corporal theories & functions is conferred in. Each of these has its internal conveniences and drawbacks for instance in synchrotron origins.

Due to their elevated power, exorbitant cost, and enormous volume the application of synchrotron sources seem inadequate presently. Independent electron lasers and Synchrotrons can produce concise pulses of far-infrared radiation, ordinarily on the sequence of 5-10 picoseconds. The typical sources employed in medical applications are almost 1 mW, nevertheless, the application of these provides the powers of 20 W of Terahertz radiations. The convenience of this source is elevated power and extensive tunability. Nonetheless, extensive power is less recommended than small power with superior SNR.

The photo-mixing of two continuous waves (CW) frequency lasers of miscellaneous frequencies (with the identical polarization) allowed the emergence of incessant-wave terahertz radiation. Photo-mixing are harmonious over 300 GHz to 3 THz along with an attainable spectral resolution is almost 1 MHz, which are the major amenities of it. Moreover, method for instance photo-mixing, formed on the photoconductive instrument which is comparatively reasonable, indicates in this field evermore generation is prospective[78].

The generation of Terahertz radiation uses Quantum Cascade Lasers which are a reasonably modern technology (1994) and has been conferred in this study. In 2000, the construction of terahertz lasers has formerly been done with technologies videlicet the p-Germanium oscillator. Although, as it does not function in CW mode & merely works at a less temperature, to be exact 2 K, this was dissatisfactory. These modern cascade lasers formed by GaAs-Al. In CW mode, GaAs hetero structures generate power output of ten milliwatts. In exchange for the weighty femtosecond, this mode exploited optical pumping laser, which denotes it can be transportable. The advantages of this mode comprise the inconsiderable size and vigorous signal to noise ratio. However, to grant usage in the short Terahertz field, (smaller than its current 2 THz limit) exploration into cooling is required. These would be the norm at medical scrutinizing implementations as the tumor to usual tissue comparison which is superior in minor Terahertz frequencies.

3.5.2 Detection Methodologies

Photoconductive receivers, sampling of open space electro optic, single-shot detection, and bolometric computation are all favourable detection techniques. The leading obstruction to track out T-rays are black-body radiation at standard temperature. These have been surpassing by cooling, which is done by the application of accessories videlicet helium cooled bolo-meters. To immanent temperature Cooled bolo-meters are desensitized and records merely the heating outcome of the Terahertz radiation. The bolometer records barely perpetration amplitude however, signals can be obtained by conducting a pump-probe set-up. In pulsed Terahertz processes, the pump-probe method is employed which will be considered afterward. These are those methods, which formed on optical rectification emitters, electro-optic detectors and photoconductive antennae [69].

In pulsed Terahertz modes Photo-conductive dipole antenna's (PDAs) could be applied for detecting the Terahertz radiation by retaining the pump along with probe beams event over it. The photo-conductive antenna has been conferred above for inception but also applied for identification as well.

Optical rectification based Electro Optic detection depends on the sensitivities and the non-linearity in crystal detector. For anisotropic components a birefringence could be inaugurated with a Terahertz electric field into the crystal. To the Terahertz-electric region, the inaugurated birefringence is at ratio. Applying a quadrant wave plate, an Electro-Optic detector, differential photodiode brace, and Wollaston prism this may be ascertained.

For implementations in surveillance, space and medicine a modern detection technique has been advanced. To impart auspicious outcome towards range scanning, this method applied amalgamated MMIC/HEB receivers based on the consolidation of InP monolithic microwave

integrated circuit (MMIC) intermediate-frequency (IF) amplifiers along with quasi-optically coupled phonon-cooled (NbN) hot electron bolometric (HEB) mixers.

3.6 Application of THz wave

3.6.1 Breast Cancer:

The objective is to diverge cancer completely while diminishing the quantity of vigorous tissue harmed, with operative treatment for cancers. Clinically it is necessary to be capable of precisely identify the edges of tumors throughout surgery, preserving usual tissue along with diminishing the amount of another surgical method. Presently, there isn't any attainable technology to complete this in substantive timeframe, as nowadays the exercises are to employ under-active palpation of tissue dispelled in a surgical procedure (which imparts outcome various days afterwards the surgery) & Magnetic Resonance Imaging (MRI) or radiography to identify tumor margin. To diverge the cancer, fail to catch employing these tumor margin, applying radiography methods 10% to 15% of entire surgeries demand another second surgery. An underneath, the reactive probe has been investigated and planned to do only this in substantive time[79]. To be capable to figure tumors it has effectively justified and spectacle distinction betwixt tumor along with conventional tissue such as vivo. The outcomes of one image of these mentioned scenario is exhibited in the Figure 3.2.

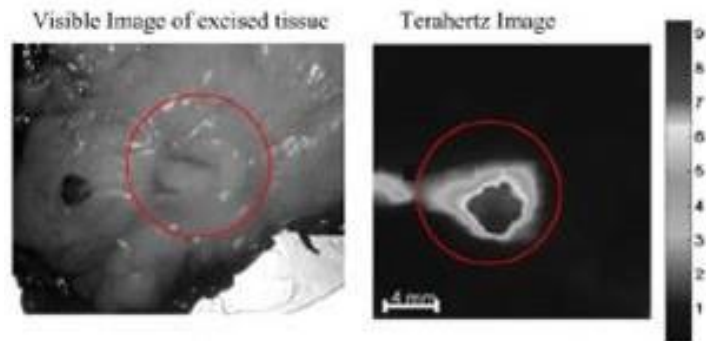


Figure 3.2: A 52 year old patient's Mastectomy, who has invasive lobular carcinoma[80].

This should be marked that; these outcomes are specimens of a 37 patient group and are enacting ex vivo. The Terahertz imaging may likely be susceptible to associate in interpreting tumor edges, along that it also imparts reports about what echelon of aggression. If this is veritable and Terahertz radiation can depict the distinction among micro-metastases and vigorous tissue then these could signify surgeons ought to be susceptible to figure along with the elementary node and check whether the concierge node is cancerous in the course of surgery. This would amend patient endeavor as the duration of surgery could be waned and once fewer surgeries would eventuate.

Correspondingly further research recently discovered that, Terahertz Pulsed Imaging (TPI) can be applied to signify the distinctions among usual tissue & insalubrious tissue by imaging along with Terahertz radiation & distinguish the outcomes with the conventional histological staining method employed. This consequence found that, the contradiction was manifest record till then it reserve into the percolation depth of 1 cm (on an average) in this action. In Figure below images demonstrated those, with the Terahertz image in the right and the histological micrograph exhibited in the left. This should be marked that, E_{\min} is used to show the impulse function for cancerous tissue & E_{\max} is used to show the impulse function for usual obese breast tissue. The contradiction betwixt cancerous tissue and salubrious breast tissue is ideal at 0.5 THz & lower.

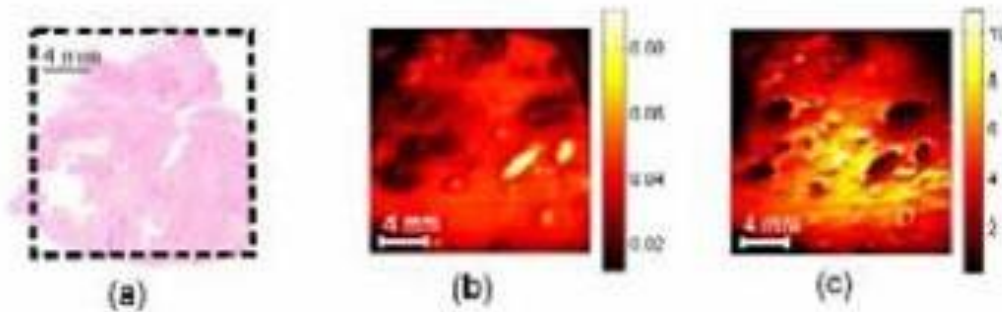


Figure 3.3: Lobular carcinoma (a) image from photomicrograph. (b) Terahertz image of E_{\min} parameter. (c) Terahertz image of E_{\min}/E_{\max} parameter[81].

This enacting investigation recommends that, this TPI is ideal adjusted to skin cancer because of its inadequate percolation depth.

3.6.2 Skin Tumor

There are major three principal skin cancer types; squamous cell carcinoma, basal cell carcinoma and melanoma, both squamous cell carcinoma & basal cell carcinoma are acquainted as non-melanoma skin cancer. In Australia, most customarily eventuating cancer is non-melanoma skin cancer and almost 374000 cases identified in a year. With Australia retaining the maximum rate in the world, the most usual cancers in Australia is also melanoma. The present technique is to scrutinize cancer optically or if in suspicion thereafter a biopsy is attained then cancer dispelled. By cryotherapy, cauterage (burning) or curettage (scraping) conventional cancers are eliminated in surgery. However, with conventionally 1-2 mm of adjoining tissue along with it, melanomas are dispelled by surgery. The draining lymph nodes are also exonerated surgically if they are also invaded. For stout melanomas other vaccines are applied or after surgery interferon is appointed. Chemotherapy or other feasible drugs are employed if the disease is pervasive. To alleviate indications, Radiotherapy can also be applied in palliative care [82].

In today, for skin cancer, the most efficacious provision are MOH's (which is also conversant as chemosurgery and Dr. Frederic Mohs constructed it) that demands a trained surgeon diverge the

tumor in ledges reducing the volume of usual tissue expelled & therefore reducing deformity whilst also minimizing the probability of re-accrual. However, this method is time swallowing and costly. This is because to permit tumor margin measurement and same-day termination of the imperfections, histology examinations are rendered throughout the surgery. The competency to evaluate the approach of subclinical propagation and signify the histological subordinate type of the tumor preoperatively, may facilitate MMS in a single ledge abruption, for all but the most comprehensive tumors, saving time, money, & patient uneasiness. For this objective (pre-operative evaluation) collectively ultrasound and many imaging modalities are being deliberated, optical imaging methods, multispectral exploration and eventually Terahertz imaging. To surpass for this motive each probability has its private idiosyncratic challenges for instance, ultrasound could show tumor in vivo, however, the deficiency of the inferiority to differentiate among transited & salubrious tissue. Every method described here especially Multispectral exploration and optical imaging, all want depth in percolation. Thus, the Terahertz imaging method imparts a substitute.

3.6.3 Dental

For the early detection of caries, TPI (Terahertz Pulsed Imaging) may be used. Outcomes have demonstrated that Terahertz Pulse Imaging provides a distinction proportion betwixt salubrious tissue & bears of 2:1 where the current identification modes are not as fair. For instance, radiography imparts a 2% alteration on the distinction among infected & vigorous tissue. The potentiality resides in clinical operation for a modality, non-invasive, non-ionising for the identification of lurid's caries. Terahertz Pulse Imaging could allow a point scanning (corresponding to an ultrasound) or could be raster scanning (many point caught or Cscan) offering a 3-D depth report concerning the sample without separating it to get profundity report[83].

Terahertz Pulsed Imaging have been applied at segments of teeth of a human & has exhibited to be capable to detect both enamel-dentine junction & the regular caries lesions on entire teeth. Bovine teeth researches have been also accomplished for example in, which have contrast to the gold-standard for ascertaining lesion depth of inorganic fall on enamel Transmission Microradiography (TMR) to TPI. Terahertz Pulsed Imaging's potentiality to calculate lesion depth is associated with Transmission Microradiography by a scaling producer of 0.46 with a 16 μm y-intercept & a coefficient of estimation which is 0.995. These signifies that, demineralization might be involved in refractive-index. Transmission Microradiography demands the teeth is to be reaped in segments before the microradiography on the contrary reflection Terahertz Pulsed Imaging does not. This should be marked that for conveying identification transmission-imaging have been controlled as very costly. The dominant restriction anticipates is whether a reflection arrangement is feasible to approach this a foretime identification such as into a mouth is the protest to have adequate place for probe of the Terahertz.

3.6.4 Detection of Impurities in the Pharmaceutical Industry

The pharmaceutical product production is an exceptionally observed method that demands proper efficiency enactments. By constitutive agencies, the entire group is spoiled if the ultimate product fails to accomplish the usual set. This encourage working on batch-processing methods in the pharmaceutical industries. Typically, pharmaceutical companies produce a complete product and then conduct laboratories to explore a ratio of the group to justify the efficiency of their product. In a non-destructive form, Terahertz radiation can acquire details on corporal formations and chemicals and is susceptible to achieve this in real-time. This exhibits capability for the industry of medicine production, as it is susceptible to exceptionally identify the composition & characteristics of the specimen to examine, for instance, the manufacturability, dissolution range, durability, bioavailability, sanctification, solubility, and other acting properties of the drug. In the course of production, rigid pharmaceutical components may appear into coalescence with water or other contaminations in the time of action, which can have an impact on product implementation. The idiosyncratic physico-chemical features of a product THz Spectroscopy can measure, being capable of exceptionally differentiating one product from another which gives attribute details [84]. Because of the potentiality to differentiate the appointed chemical elements accomplishment Terahertz Spectroscopy could be employed in pharmaceutical product patenting. Terahertz Spectroscopy could calculate the idiosyncratic physicochemical characteristics of a manufactured product, and being capable to especially differentiate the origin of the products from one to another one which gives attribute details. Because of the competency to differentiate the definite chemical constituents, THz Spectroscopy could be employed in pharmaceutical product patenting.

3.6.5 Security

Terahertz radiation can perforate plastics and fabrics, so it can be used in surveillance, for instance, safety examine to expose latent weapons on a person casually. This is of individual consideration because many components of concern have idiosyncratic spectra-fingerprints at the THz range. This proffers the probability to associate spectral determination with imaging. By being intended to a very particular limit of objects and components, inactive identification of terahertz subscriptions ignores the corporal secrecy responsibilities of other identification. At airports or other safety-critical spaces dangerous non-metallic elements like plastic ammunitions or ceramic knives now can be tracked out with terahertz beams. This is probably because T-rays can get over the clothes, but cannot do so via the outward skin (because of the water volume).

3.6.6 Communication

Wireless communications apply in terahertz frequencies is facing a stream of recognition in current times, with the need for comprehensive bandwidths and upper bit rates. Different wireless communication based on THz methods, which has carrier frequency equal to 0.6THz & data rates of transmission up to 100Gbps has been analyzed & advanced[85],[86],[87],[88].

However, implementations of these THz communication methods are still restricted because of innate challenges asserted by the open space propagation (FSP) modality, like potent reliance on atmospheric situations, a fast discrepancy of the terahertz beams particularly in the lower carrier frequency, also line-of-sight characteristic of the links. Especially, because of auto-diffraction & terahertz comparatively lengthy wavelength almost equal to 1mm, determining minimum divergent terahertz beams needs an application of extensive beam diameter & concentrating optics which could be as extensive as different ten of centimetre in diameter at even concise communication-links of different ten of meter. In addition, wireless communications' entry to partly blocked regions can be uncertain because of potent directionality of the THz beams, so, demanding extra THz movement resolution for dependable communications.

Concurrently, waveguides and low-loss terahertz fibers proffer proper resolutions to some of the restrictions produced by the open space THz propagation and can have their self-eligible implementations in THz communications. There are some obvious benefits of applying fibers and THz waveguides. Especially, as light stretches through sealed terahertz fiber, the impact of the wind pressure situations at the communication-link attributes are reduced. Moreover, terahertz fiber is of small diameters & flexible hence, granting entry to in another way physically prevented regions. Finally, the THz fiber dimension is typically coordinate to the wavelength of light, so allowing concise different -mm in diameter communication links with a tiny footprint and low signal outflow outside of the fibers, which is of individual interest for the ultra-high bandwidth on-chip interlinks. During past years, different terahertz fiber with minimum transmission loss ($<0.01\text{cm}^{-1}$) has been introduced & displayed. Normally, such waveguide increases the portion of the guided power at the low loss gas[89],[90],[91]. Between those models, one normally separates sub-wavelength terahertz fiber that guide applying the process of total internal reflection (TIR) & hollow core fiber, which guide applying either anti-resonant reflection (ARROW) or photonic band-gap structure.

3.6.7 Sensor

THz based PCF sensing implementations are multipurpose and broadly applied in the present days. Biochemical, biological, and physical sensors are applied for various features. Physical sensor may be curvature, displacement, temperature, pressure, refractive indices, torsion, electrical field & vibration sensors. Environment, food monitoring, glucose monitoring, food processing sensors are newly added in this field. Every structure of THz based PCF sensors have it's idiosyncratic parameters but the sensitivity varies from one to another. Biosensors execute a modern aperture for several promising implementations along with antibody-antigen collaboration, biological sample tracking, medical diagnosis, food quality control, bio imaging, organic-chemical sensing, environment monitoring. Bio sensor usually applies the equation of Sellmeier to reckon the effective refractive-index shortly n , and λ is the wavelength we considered here. Biosensor's sensitivity relies at the refractive indices & alteration of wavelength. Peak wavelength's ratio alternates to the refractive-index is acquainted similar as

the sensitivity. Evanescent sensor widely relies on their refractive indices, relative sensitivity coefficient & effective refractive-index of air holes. The percentage also varies from one to another due to the EM field differs.

A chemical (liquid and gas) sensor which is highly sensitive also have a tremendous role to play to the industrial process particularly for observing combustible & toxic chemicals (such as toxic liquids or gases) to surpass the safety matters. So that, this has become the main challenges, to severe the production of gas sensors & liquid. These days, scientists are remaining much worried about the advancement of PCF sensors based on THz for safety monitoring issues & environmental. PCF gas sensors and liquid in the transitory fields provide unique and better sensitivity due to PCF's core right away linked with the component to be resolved [92].

3.7 Conclusion

Finally it can be concluded that THz wave has significant application in a wide range of sectors. In this thesis THz wave has been implemented for waveguide and sensing application for developing communication sector. A design of PCF has been demonstrated, which is applicable for both waveguide and sensing application.

Chapter 4

Losses and Factors of THz waveguide and Sensor Designing

There are several factors that should be key concerns for THz wave guide and sensor designing such as Mode power propagation, Effective area, Effective material loss (EML), Waveguide dispersion, Confinement Loss (CL), Sensitivity etc. The above mentioned parameters are described below.

4.1 Effective Material Loss

In an optical fiber, absorption of signal is a genuine loss component. Absorption into optical fibers occurs for various reasons such as the presence of defects within the atomic structure of the fiber material, a few fundamental inherent intrinsic material properties and a couple of outward material properties. Imperfection in the atomic structure can occur due to the lack of oxygen and the absence of specific molecules. Absorption may be incited by diffusion of hydrogen molecules. Be that as it may, the contribution from imperfections at fiber optic assimilation loss is moderately little. One of the fundamental fiber material properties is the inherent intrinsic absorption. In terms of imperfections& impurities free material, at that point whole absorption is because of intrinsic absorption. Silica fibers have exceptionally low natural fabric absorption. Here the vibration of silicon-oxygen bonds causes absorption. Intrinsic absorption is caused by the electromagnetic field of the optical signal & the interaction among these bonds. Extrinsic absorption prompted by the impurity's presence in the fiber component. Which are brought about by the electronic change of metal impurity particle starting with one energy-level to another. Hydroxy particles presence within the fiber is also responsible for extrinsic absorption [93].

$$\alpha_{eff} = \sqrt{\frac{\epsilon_0}{\mu_0}} \left(\frac{\int_{mat} n_{mat} |E|^2 \alpha_{mat} dA}{\left| \int_{all} S_z dA \right|} \right) \quad 4.1$$

Where μ_0 = Permeability and ϵ_0 = Permittivity of vacuum. S_z = The pointing vector that represents amount of power flow and direction for electromagnetic wave. The pointing vector's z component ($S_z = \frac{1}{2}(E \times H^*) \cdot z$), and here H and E are considered to be the magnetic and electric field accordingly. α_{mat} = Bulk material absorption loss.. Figure 5.3 portrays the EML's characteristics as a work of core diameter along with distinctive core porosities. From this figure, for a similar porosity values there is a huge difference in EML when the core diameter changes.

It is a lossy system identified with fiber's fabrication procedure & material composition, and result in the dissemination of transmitted optical power's portion as waveguide's heat. The light absorption process might be intrinsic (brought about by at least one significant segments of glass) or extrinsic (brought about by impurities inside the glass).

4.2 Mode Power Propagation

The measure of helpful power spreading through various areas of the fiber also known as core power fraction can be determined by [94],

$$\eta' = \frac{\int_x S_z dA}{\int_{all} S_z dA} \quad 4.2$$

Where η' represents mode power fraction & X represents the area of interests respectively. Denominator part of the above equation is integrated against the whole area of PCF and numerator part of the above equation is integrated against the region of Interest. A standard PCF can be designed by a process, where it is essential to pass the maximum effective power through the core air holes. Larger D_{core} increments the core power-fraction, however, this also increments the EML. Then again, as D_{core} diminishes EML as well as the core power fraction are also diminishing. These are opposing conditions and it is needed to choose an ideal state of larger core power-fraction & lower EML. In various center porosities, attributes of center power portion as an element of core's diameter where it tends to be detected that, measure of core power enhances along with the expansion of core diameter.

4.3 Confinement Loss

Another vital parameter is Confinement loss, which is treated for PCF plan. It relies beginning with the core porosity & the quantity of air hole utilized at cladding. Which can be calculated by taking the complex refractive index's imaginary part. The confinement loss could be determined by [95],

$$L_c = \left(\frac{4\pi f}{c}\right) \text{Im}(n_{eff}), cm^{-1} \quad 4.3$$

In the above equation, c denotes speed of light in vacuum, the frequency of the guiding light is denoted by f, and $\text{Im}(n_{eff})$ represents the refractive index's imaginary part. The confinement loss is a function of frequency where it is seen that as the frequency increments, the confinement loss gets downsized.

4.4 Waveguide Dispersion

The phase velocity of a wave relies upon its frequency known as dispersion in optics. The normal property of media may be called dispersive media. Sometimes for specificity, the term named chromatic dispersion is utilized. In spite of the fact that the terms are utilized on the optics field to describe electromagnetic waves & light, diffraction in a similar purpose could be used to any kind of wave movement, for example, acoustic dispersion on within the case of seismic waves and sound.

Waveguides are profoundly dispersive because of their geometry (as opposed to simply from the material piece of them). Optical fiber is a kind of waveguide for the frequency of optics (light) broadly utilized in present-day broadcast communications frameworks. Information's rate could be shipped in a single fiber is constrained by beat broadening because of chromatic dispersion between other marvels [96].

Generally, in terms of a waveguide mode with a propagation constant β have an angular frequency $\omega(\beta)$. Therefore, the electromagnetic areas inside the direction of propagation shortly z oscillates proportional to $e^{i(\beta z - \omega t)}$, the group velocity dispersion parameter D is characterized by[97]

$$\beta_2 = \frac{2}{c} \frac{dn_{eff}}{d\omega} + \frac{\omega}{c} \frac{d^2 n_{eff}}{d\omega^2} \quad 4.4$$

Within the case of multimode optical fiber, supposed modular diffraction will likewise prompt broadening of the pulse. Indeed, pulse broadening could also happen in even in single mode fiber, due to polarization mode dispersion (where as there are still two polarization mode). This isn't the cases of chromatic diffraction because they aren't subordinate on the wave-length or band-width of the pulse proliferated.

4.5 Effective Area

The proposed fiber's effective area (F) can be determined by[64]

$$A_{eff} = \frac{[\int I(r)rdr]^2}{[\int I^2(r)dr]^2} \quad 4.5$$

In the above equation; $I(r) = |E_t|^2$ is characterized as the distribution of the transverse electric field intensity in the cross-area of the fibers. The A_{eff} as a work of frequency, from where this is watched whereas the frequency increments from 0.9 THz the A_{eff} reduces. It is a direct result of

all the more light spread for $f > 1$ THz. This is likewise seen that, where at working parameter, the determined A_{eff} is particularly practically identical[98].

4.6 V- Parameter

The normalized frequency in optical fiber [99], V (also called the V number), is denoted by

$$v = \frac{2\pi r f}{c} \sqrt{n_{co} - n_{cl}} \leq 2.405 \quad 4.6$$

V- Parameter ought to be fulfilled to function in single-mode condition. r indicates the radius of core and f indicates the frequency. Here, n_{co} and n_{cl} represents the refractive index of the core & cladding accordingly. The perfect esteem of n_{cl} is nearly unity though the viable esteem of n_{cl} ought to not be unity. The purpose of that is cladding comprises of air as well as Topas too. In useful structure, the V-parameter ought to be more noteworthy than unity.

4.7 Sensitivity

Updated Beer Lambert Law should be utilized to calculate the sensing capability of the introduced design. Sensing capability is also known as relative sensitivity, which is determined by the interaction among the material used in the core & the guided light through the core[100]. The following equation shows the above mention situation,

$$I(f) = I_0(f) \exp[-r\alpha_m l_c] \quad 4.7$$

In the above equation, $I(f)$ and $I_0(f)$ represents the intensities of light & absence of analyte in the core accordingly. Coefficient of sensitivity is represented by R and the peak of sensitivity is also determined by using r . Material absorption co-efficient is represented by α_m . When light passes in the core its decrement of intensity can be calculated by α_m . The frequency of light and length of fiber is presented by f and l_c accordingly. The co-efficient of relative sensitivity r can be expressed by the following equation[36]

$$r = \frac{n_r}{Re[n_{eff}]} k \quad 4.8$$

In the above equation, refractive index of analyte & effective modal index in the core is expressed by n_r and n_{eff} accordingly. In denominator the effective modal index's real part is utilized and k denotes total power fraction inside the core which is given below

$$k = \frac{\int_{sample} R_e(E_m H_n - E_n H_m) dx dy}{\int_{total} R_e(E_m H_n - E_n H_m) dx dy} \times 100 \quad 4.9$$

4.8 Origination of Finite Element Method (FEM)

(PDEs) partial differential equations can solve the problems of the laws of physics, which are space and time dependent. As these geometries and problems have a vast majority, only analytical methods cannot solve these PDEs. So, we have to build an approximation of the equations. Basically, these equations are built upon different types of discretization. By using this method, the PDEs are being approximated with numerical model equations. Now these equations can be solved by numerical methods. Now, an approximation of the real solution to the PDEs are as same as the solution to the numerical model equations. On the other hand, to evaluate these type of approximations, the finite element method (FEM) is used[101].

For an example, u is a function that is the dependent variable in a PDE (i.e., temperature, electric potential, pressure, etc.). u can be approximated by another function u_h using linear combinations of basis functions according to the following expressions[102]:

$$u \approx u_h \quad 4.10$$

and

$$u_h = \sum_i u_i \psi_i \quad 4.11$$

Here, ψ_i indicates the basic functions and u_i indicates the coefficients of the functions that approximate u with u_h .

The finite element method offers great freedom while selecting discretization and it is a great benefits for the users, to discretize space and the basis functions both elements may be used. It is a theory that is well developed. The close relation between the numerical formulation and the weak formulation of the PDE problem is the main reason behind this. In short, this theory can provide important error calculations, or bound for the error, when we use computer to solve the numerical model equations.

Looking back at the history of FEM, the usefulness of the method was first recognized at the start of the 1940s by Richard Courant, a German-American mathematician. While Courant recognized its application to a range of problems, it took several decades before the approach was applied generally in fields outside of structural mechanics, becoming what it is today.

4.8.1 PDE and the principle of physics

The language of mathematics is expressed by the laws of physics. For example, conservation laws like the law of conservation of energy, conservation of mass, and conservation of momentum would all be able to be communicated as partial differential equations (PDEs). Constitutive relations may likewise be utilized to communicate these laws regarding variables such as temperature, density, velocity, electric potential, and other dependent variables.

Differential equations include expressions. These expressions determine a small change in a dependent variable with respect to a change in an independent variable (x, y, z, t). The derivative of the dependent variable is referred by this small change with respect to the independent variable.

Say there is a solid with time-varying temperature yet unimportant varieties in space. For this situation, the equation for conservation of internal (thermal) energy may bring about an equation for the difference of temperature, with an exceptionally little change in time, because of a heat source g.

$$\rho C_p \frac{dT}{dt} = g(T, t) \tag{4.9}$$

Here, ρ expresses the density and C_p expresses the heat capacity. T denotes temperature as the dependent variable and t denotes time as the independent variable. A heat source is described by the function that changes with temperature and time. Eq. 4.9 expresses that assuming there is an adjustment in temperature in time, and then this must be adjusted (or caused) by the heat source. The eq. is a differential eq. communicated regarding the derivatives of one independent variable (t). Such differential equations are known as ordinary differential equations (ODEs).

4.8.2 Different Elements

For the basic functions and the test functions, the same set of functions is used by the Galerkin method. However, there are numerous ways (infinitely many, in theory) of characterizing the basic functions (i.e., the elements in a Galerkin finite element formulation) for this method. Now we will survey some of the most well-known components. For linear functions in 2D and 3D, the most well-known components are outlined in the figure below. The linear basic functions, as characterized in a triangular mesh that structures triangular linear components, are depicted in the following figure. The basic functions are defined as functions of the positions of the nodes (x and y in 2D and x, y, and z in 3D).

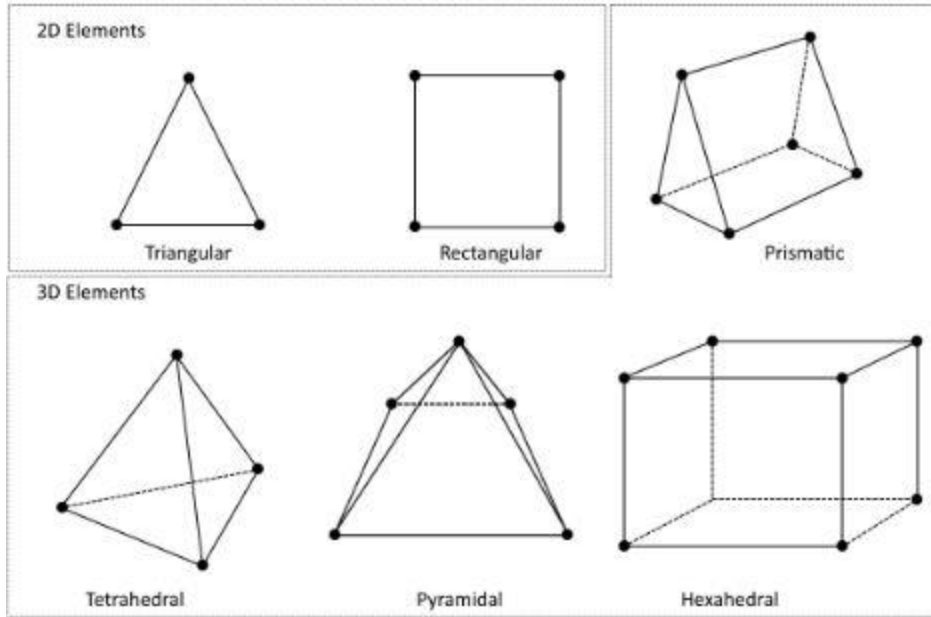


Figure 4.1: Node placement and geometry for 2D and 3D linear elements[103].

4.8.3 Finite Element Analysis (FEA) Software

For reducing the number of prototypes and experiments, the finite element analysis (FEA) software is utilized. When designing, optimizing, or controlling a device or process these prototypes and experiments must be run. This does not really mean that organizations and research institutes save money by embracing FEA. They do, in any case, get greater advancement for their dollar, which may bring about acquiring a competitive edge against the opposition. Hence, it could be sensible to build innovative work assets for FEA.

FEA model has been found useful in predicting real-life properties when it is established. The understanding and intuition is produced by the FEA to fundamentally improve a design and operation of a device or process. At this stage, the last degree of improvements can be hard to get with intuition only. It is given by the optimization methods and automatic control. For describing automatic control and incorporating, most modern FEA software features strategies such as descriptions in mathematical and numerical models. Optimization strategies are typically included in the solution process, which is additionally described in detail below.

The presentation of high fidelity models have likewise added to an accelerated understanding. This has started new ideas, very new designs, and operation schemes that would have been covered up or in any case unimaginable without demonstrating. In this manner, FEA is an integral tool for research and innovative work departments in organizations and establishments that work in exceptionally serious business sectors. Over time, the utilization of FEA software has extended from bigger organizations and establishments that help instructing engineers to smaller organizations in a wide range of industries and institutions with a wide assortment of disciplines.

4.8.4 Working Principle of software

The Finite Element Method (FEM) discretizes the mathematical models. This results in corresponding numerical models. The discretized equations and the results are solved and tested respectively, hence the title finite element analysis.

The laws of physics are described by language of mathematics. That is for space and time-dependent descriptions. This results in partial differential equations (PDEs). The dependent variables, such as structural displacements, velocity fields, temperature fields, and electric potential fields represents the result to the PDEs. The result is described in space and time, along the independent factors x , y , z , and t .

For a given framework, the reason of these descriptions is found in the investigation of the result to the PDEs that outcome in understanding a studied framework and the capacity to make expectations about it. To understand, predict, optimize, and control the model or operation of a device or process FEA is used.

4.8.5 Mathematical Model and Numerical Model

A mathematical model of a framework can be expressed by one or various PDEs that characterize the applicable laws along with boundary and initial conditions. Some additional conditions are imposed on the result and on a section of the modelled domain by the boundary conditions (e.g., surfaces, edges, or points). For the same model, various dissimilar boundary conditions can be utilized. The state of the framework in the starting point of a time-varying event is defined by the initial conditions.

4.9 Well-Posed Mathematical Problems

If a mathematical scheme is accurately defined, it may also be well posed. A mathematical scheme is well posed if it has a distinctive solution that relies on the problem data (i.e., source terms, constraint values, fluxes and initial values). If the model is not well posed, this will be manifest in the numerical scheme and will cause problems in the solution process.

Being well posed can be seen as the scheme's minimal requirement to be utilized for numerical simulations, such as in FEA.

From a theoretical point of view, usually it is very hard to determine if a realistic nonlinear 3D model is well posed or not this is why, greatly simplified models are used in primary analysis. The conclusions drawn from these simplified schemes are used to determine how more realistic models behave. Even a well-posed model can be very sensitive to changes in the model data. Such models are sensitive and not well conditioned.

Latest numerical methods for solving PDEs have revolutionized in applied mathematics. The reason is that analytical solutions to mathematical schemes can only be found in very rare cases,

such as in simple geometries and certain combinations of equations. While these cases are important from a theoretical point of view, often they are of little use to the engineer. Numerical methods do not have this limitation, so they can handle complicated geometries and nonlinear problems. Other computational problems exist for numerical methods, but the applicability to new models and geometries is not one of them.

Numerical methods can give an approximation of the solution to a well-posed mathematical scheme. Most numerical methods are based on a quantization of the modelled domain and the described dependent variables. Element methods volume and the finite difference are the most commonly utilized methods for this quantization. As the name reveals, the finite element method (FEM) is used in finite element analysis.

The quantization of a mathematical scheme results in a numerical model for the described system, where the numerical model is a discrete approximation of the mathematical model. The error initiated by using the numerical model instead of the mathematical model is referred to as the truncation error.

The truncation error is defined as the difference between the mathematical model and solution to the numerical. If the numerical model is consistent and stable, then the truncation error approaches zero, as the element sizes approach zero (i.e., the numerical solutions converge to the solution to the mathematical model). The truncation error then converges at a fixed rate, measured by the order of accuracy. Consistency is equivalent to a positive order of accuracy.

The starting point of the finite element system is the weak formulation of the mathematical scheme. This form can be attained from the point wise PDEs (also called the strong form) by introducing test functions, multiplying the PDEs with these test functions and then integrating them over the modelled domain. This process can be optionally combined with integration by parts. For each test function, the integral relation must hold. To be consistent with the PDEs, there must be infinitely many test functions that must be general enough. Therefore, infinitely many integral relations must hold, whereas the point wise PDEs must hold for each point in the schemed domain.

The finite element method initiates test functions that are defined through a computational mesh. For each computational cell, or mesh element, a number of test functions are locally defined. Moreover, as part of the finite element method, shape functions are defined. These are utilized to present the candidate solution. For time-dependent problems, the finite element process is often only utilized for the spatial quantization. In this case, the system of equations, attained after the finite element quantization, is a method of ordinary differential equations (ODEs). This process may, in turn, be quantization with a finite difference method or other similar methods.

4.10 Process of FEM

For historical reasons, traditional finite element analysis refers to schemes based around structural mechanics. Since the popularity of modelling multi physics applications has increased, and because of the fact that the finite element method is broadly utilized for fluid flow and electromagnetic simulations, the term “finite element analysis” has also become more accepted in other engineering and science sectors. No matter what the application areas, the processes included in finite element analysis are the identical.

Below is a summary of the actual workflow, from geometry to scheme documentation.

4.10.1 Geometry

Finite element analysis requires that the model geometry is “water tight”. Computer aided design (CAD) geometries are not always employed for analysis. This implies that, for example, something that is a volume in the actual world can be explained by a set of loosely connected 3D surfaces in a CAD drawing. In finite element analysis, these surfaces have to actually form a real volume.

Even if a set of 3D surfaces in a CAD drawing do form a volume, some surfaces may be slender and some edges may be unaccountably short in relation to the size of the geometry. This results in an undesirable concentration of elements at the offending geometrical features.

4.10.2 Materials

The fundamental laws in a mathematical scheme include physical properties of the materials. The properties may rely on the modelled variables (the "dependent variables"). For example, in an analysis of mechanical, thermal expansion, and thermal properties often rely on the temperature.

In practice, this includes determining the accurate validity intervals for the material properties and the correct reference point. Additionally, various materials have to be attributed to the different parts of the geometry.

4.10.3 Domain Settings

In structural mechanics, the mathematical scheme may be defined by the selected loads, materials, and constraints on the methods. Usually boundary conditions, the materials, initial conditions and domain equations, define the mathematical scheme.

4.10.4 Mesh

The definition of materials, domain settings, geometry, boundary conditions, loads, initial conditions, and constraints can be carried out without discretization. However, in much older FEA software, this is still done for the discretized scheme.

The numerical model completes once the mesh is created. Various phenomena and analyses need varied mesh settings. Such as, in wave propagation problems, for example, modeling elastic waves in electromagnetic waves or structural mechanics in radio frequency analysis, the size of the largest element has to be substantially smaller than the wavelength in order to solve the problem.

4.10.5 Solution

If creating the mesh is considered a complicated task, then setting and selecting the solvers and attaining a solution to the equations (which constitute the numerical model) in a reasonable computational time is an even more complicated task. The difficulty is comprised with a variety of challenges.

First of all, the discretized scheme can be very large in terms of algebraic equations. A 3D model can easily have several million degrees of freedom. A central portion of the solution procedure for numerical schemes originating from the finite element system is to resolve a large linear system of algebraic equations. Eigenvalue, Nonlinear, parametric and time-dependent problems are treated with iterative systems, where a sequence of large linear systems is resolved.

Large linear systems are, generally, difficult to solve efficiently. Black box methods exist, but they are often too expensive for realistic schemes. Examples are direct solvers, relied on general-purpose iterative methods.

To find a successful and near-optimal alternative, some sort of features of the underlying system has to be exploited. For multiphysics problems, such a structure might not exist or may be complicated to identify. In such cases, it can be effective to split the problem into its physics constituents for which it is known how to exploit the structure. To accelerate the iterative solution procedure linear systems, modern FEA packages use geometric or algebraic multigrid methods.

The nonlinearity of models is another source of problems for FEA solvers. Newton methods utilize local derivative information to search for better solution candidates, which is only reliable if the current estimate of the solution is close enough to the real numerical solution. In practice, the initial guess for the solution is not every time close enough and the Newton method is usually not sufficient to use in such cases. Different simplifications, or relaxations of the problem may be fruitful. Instead of the main problem, a simpler nearby problem may be resolved to give a solution. Such as, one may neglect certain nonlinearities to attain a linear problem that can be resolved easily. Segregated and continuation solvers are developed for these purposes.

The third class of complications encountered by FEA solvers includes the fact that the numerical scheme might not be stable or, for other reasons don't give a good approximation to the mathematical scheme. In these situations, the solution process might be much more complicated than for a more benign and well-behaved numerical scheme. It may be difficult to find out and

understand the reason for this problem. In many cases, the remedy can modify the model in some way other than through the solver settings. A better adapted mesh is often an important ingredient in scheme behavior improvement.

4.10.6 Results

In older FEA packages, the plots and derived values to be analyzed had to be defined before the solution was ran. Omission of some main definitions means that the solution has to be carried out once again from the beginning. The definition of the expressions and derived values to be analyzed in post processing is, therefore, considered a part of preprocessing.

Modern FEA packages allow for the definition of expressions and derived values on the fly, after the solution has been counted. In these packages, the definition of expressions and derived values is part and parcel of post processing to drill down on scheme predictions.

4.11 Electromagnetic Waves in Media

Maxwell's equation has following forms shown below in a medium without free charge which is characterized by a magnetic permeability, electric permittivity and electric conductivity.

Equation Name	Differential Form	Comment
Maxwell-Ampere's Law	$\nabla \times H = \sigma E + \varepsilon \frac{\partial(E)}{\partial t}$	A magnetic field is generated by the change in an electric field.
Faraday's law	$\nabla \times E = -\frac{\partial(\mu H)}{\partial t}$	An electric field is generated due to the rate of change in an electric field.
Gauss's Law	$\nabla \cdot (\varepsilon E) = 0$	It is assumed that, there is no free electric charge.
Gauss's Magnetic Law	$\nabla \cdot (\mu H) = 0$	There are no free magnetic charges.

4.12 Efficient solution of Maxwell's equations for optical fibers

Let consider for a fiber with the refractive index $n(r)$, we will solve the Maxwell's equations analytically. The following Maxwell's equations take form in a source-free region where fields have the time dependence $\exp(+j\omega t)$ [105].

$$\nabla \times E = -j\omega\mu_0 H \quad 4.9$$

$$\nabla \times H = j\omega n^2 \varepsilon_0 E \quad 4.10$$

$$\nabla \cdot (n^2 E) = 0 \quad 4.11$$

In Eq. 4.9 and 4.10 by applying curl operators, we can eliminate H to give

$$\nabla \times \nabla \times E = n^2 k^2 E \quad 4.12$$

We can assume the functional forms $E_r = e_r \cos(m\phi) \exp(-j\beta z)$, $E_z = e_z \cos(m\phi) \exp(-j\beta z)$ and $E_\phi = e_\phi \sin(m\phi) \exp(-j\beta z)$ & defined $Q_1 \equiv d(\ln n)/dr$ and $Q_2 \equiv dQ_1/dr$, Now the Eq. 4.11 becomes

$$e_z = [de_r/dr + (1/r + 2Q_1)e_r + (m/r)e_\phi] / (j\beta) \quad 4.13$$

Now, e_z is can be determined by e_r and e_ϕ ; and Eq. 4.12 takes the form shown below

$$[d^2/dr^2 + (1/r + 2Q_1)d/dr + n^2 k^2 - \beta^2 - (m^2 + 1)/r^2 + 2Q_2]e_r = (2m/r^2)e_\phi \quad 4.14$$

$$[d^2/dr^2 + (1/r)d/dr + n^2 k^2 - \beta^2 - (m^2 + 1)/r^2]e_\phi = (2m/r^2)(1 + rQ_1)e_r \quad 4.15$$

The right-hand side of Eq. 4.13 satisfied identically with the equation for e_z . Let's assume that $m \neq 0$, and redefined the dependent variables as: $e_\pm \equiv e_r \pm e_\phi$, so that $e_r = (e_+ + e_-)/2$ & $e_\phi = (e_+ - e_-)/2$

Now, we will define the operators as below:

$$D_1^\pm = d^2/dr^2 + (1/r)d/dr + n^2 k^2 - \beta^2 - (m^2 \pm 1)/r^2, D_2^\pm = Q_1(d/dr \pm m/r) + Q_2 \quad 4.16$$

The remained coupled equation can be illustrated as below:

$$D_1^- e_- + D_2^+ (e_+ + e_-) = 0 \quad 4.17$$

$$D_1^+ e_+ + D_2^- (e_+ + e_-) = 0 \quad 4.18$$

The D_2 's vanishes in regions of constant index and e_- , e_+ satisfied Bessel equations. For the numerical integration's preparation, finally a system of four first-order equations is formed by transforming the two coupled second-order equations[106], where two of the four defined new variables as: $e_- \equiv de_- / dr$ & $e_+ \equiv de_+ / dr$.

In a medium with continuous physical properties, Electromagnetic fields and their derivatives are also continuous. To be specific, where $n(r)$ and its derivatives are also continuous, as well as e_- , e_+ and their derivatives also. Practically, $n(r)$ and its first two derivatives can be guaranteed as continuous everywhere. To ensure the continuity of e_- , e_+ , e_-' , and e_+' everywhere, the limited-continuity condition is found to be sufficient enough.

In a region of constant index in the cladding where an artificial boundary is used, the fields and all their derivatives are found continuous (For the measured profiles also, a constant value is assigned for the index which is beyond some sufficiently large radius). The integration is done up to a radius r_{\max} the differential equations which is at least incrementally beyond the beginning of the constant-index region. The proper solution of Eqs. 4.17 and 4.18 are the Bessel functions which are well behaved at the boundary and at infinity in a condition of $r \geq r_{\max}$, therefore, we find the following equations below:

$$e_-(r_{\max}) = d_{m-1} K_{m-1}(\alpha_2 r_{\max}) \quad 4.19$$

$$e_-'(r_{\max}) = d_{m-1} \alpha_2 K_{m-1}'(\alpha_2 r_{\max}) \quad 4.20$$

Along that, all minuses replaced by pluses in two similar relations. Bessel function's prime denotes differentiation w. r. t. the entire argument, the d's are constants, & $\alpha_2 \equiv (\beta^2 - n_2^2 k^2)^{1/2}$, the cladding's constant index of refraction is represented by n_2 . When we divide Eq. 4.19 by Eq. 4.20 we attain the following equation,

$$e_- \alpha_2 K_{m-1}' - e_-' K_{m-1} = 0 \quad 4.21$$

In a similar way,

$$e_+ \alpha_2 K_{m+1}' - e_+' K_{m+1} = 0 \quad 4.22$$

At a boundary of r_{\min} , integration is started. With an index of n_1 on the axis integration is started, the index is assumed to be n_1 from the axis out to say, $0.02 \mu\text{m}$ & r_{\min} is set to a lower value. Let's with a constant index of an idealized profile from the axis out to $4.00 \mu\text{m}$, r_{\min} set as $3.99 \mu\text{m}$ to

reduce the integrating time. For either case, if $n_1^2 k^2 > \beta^2$, initial conditions for integration can be written as below:

$$c_{m-1} J_{m-1}(\alpha_1 r_{\min}) = e_-(r_{\min}) \quad 4.23$$

$$c_{m-1} \alpha_1 J_{m-1}'(\alpha_1 r_{\min}) = e_-'(r_{\min}) \quad 4.24$$

The pluses used to replace minuses in similar relations, where $\alpha_1 \equiv \sqrt{(n_1^2 k^2 - \beta^2)}$ (If $n_1^2 k^2 < \beta^2$, the J 's should be replaced by I Bessel functions.). The constants, either C_{m-1} or C_{m+1} , is chosen arbitrarily; the other is iterated.

For the specialization of fundamental mode, let's set $m = 1$, $C_0 = 1$, and $C_2 \ll C_0$. For a sufficiently long wavelength and with these choices, the only solution that exists known as fundamental mode.

4.13 Conclusion

From above description it is clear that without maintaining the above mentioned factors, design of THz waveguide and sensor should not be acceptable. Because for efficient THz waveguide and sensor designing lower effective material loss or material absorption loss, lower confinement loss (CL), higher core power fraction, comparable effective area, maximum sensitivity should be maintained. Besides finite element method (FEM) for numerical investigation has been discussed.

Chapter 5

Design I: Proposed Sectorized Circular THz Waveguide for transmission

In this chapter, a suspended core cladding structured photonic crystal fiber (PCF) has been proposed for efficient THz wave propagation. Guiding properties of developed PCF are investigated through the Comsol Multiphysics with the finite element method. Due to the strategic geometrical optimization, it renders improved performances in the most of the crucial cases. It exhibits ultra-low effective material loss of 0.022 cm^{-1} at 0.9 THz, besides, near-zero flatten dispersion is observed in the wide THz spectrum. Moreover, to ensure the suitability of proposed PCF, other significant guiding properties such as confinement loss, effective area, and v-parameter. are observed in the same THz frequency. Furthermore, fabrication feasibilities in the existing manufacturing platform are also discussed in detail.

THz wave propagation theoretically refers to the frequency range of 0.1 to 10 THz. It has long range of applications in medical imaging[107], wireless communication[88], security[108], drug testing[109], sensing[110], biotechnology[111]. It creates a link between infrared frequency band and microwave and support the transmission between optical and electrical frequency[112]. Also, THz wave origination and revelation methods have been picked up immense ubiquity for its noteworthy down to earth applications. Be that as it may, because of the absence of low-loss transmitting medium, the majority of the THz frameworks rely upon free space for its wave proliferation. In this way, it encounters some unfortunate issues, for example, intense arrangement, beneficiary transmitter arrangement, path loss and questionable retention loss which are impacted by the idea of the environment and hard to coordination with different parts. To conquer these troubles, different sorts of waveguides were previously announced. Negligible material loss is considered for dry air. Considering this fact some waveguides were designed with sub-wavelength air holes in the center[89]. Nonetheless, the majority of the transmitted light passed outside the center which caused high material dispossession. Hollow- core Bragg fibers were likewise presented which lamentably had undesirable attenuated band properties[113]. Afterward, polystyrene foam was presented yet it had the detriment of a lot bigger size[114].

These days, PCF are generally famous as it gives the designer to control its attributes just by altering the intermittent air hole adjustment. Nonetheless, they need to confront a lot of losses for the issue of solid material [17]. To accomplish further improvement, porous core was presented rather than solid material in the center. As of late, numerous specialists have revealed different strands dependent on porous core and among them Uthman *et al.*[19] announced a hexagonal structure in both cladding and core. They utilized Teflon as the backdrop material which demonstrated an EML of 0.12 cm^{-1} . They did not demonstrate some significant properties for

THz applications like core power fraction and dispersion. Next Kaijage et al.[20] proposed a porous core octagonal PCF which showed an EML of 0.076cm^{-1} . They too disregarded to dissect the properties of dispersion and core power fraction. Hasan *et al.* proposed a circular PCF showed an EML of 0.056cm^{-1} [21]. They didn't provide any information about refractive index and V-parameter. Raonaqul *et al.*[16] announced a pivoted hexagonal structure at the center and standard hexagonal structure in the cladding with an EML of 0.066cm^{-1} and moderate core power fraction of 40% but their EML was also high. Rana *et al.*[115] proposed a PCF with octagonal structure in both cladding and core. They demonstrated an EML of 0.058cm^{-1} yet neglected to notice the dispersion property. Saiful *et al.* [116] proposed a hexagonal PCF with reduced EML of 0.053cm^{-1} but the variation of dispersion was $1.20 \pm 0.25\text{ps/THz/cm}$. Besides they didn't explain anything about V-parameter. Hasanuzzaman *et al.*[24] proposed a novel PCF incorporating hexagonal core and kagome lattice with an EML of 0.034cm^{-1} with a negligible confinement loss. They also achieved a zero flattened dispersion although the fabrication of kagome structure is more challenging compared to circular structure. Another square lattice porous core photonic crystal fiber was also processed in [25] with an EML of 0.076cm^{-1} and confinement loss of 10^{-3}cm^{-1} . They didn't explain anything about effective area and mode index. The above-mentioned works suggested a great scope for PCF improvement by considering the fact of confinement loss, EML, effective area, core power fraction, V- parameter etc.

In this chapter a sectored circular core and cladding structured PCF has been proposed which offers a very low EML of 0.022cm^{-1} . Beside this other performance parameters such as confinement loss, effective area, flattened dispersion, core power fraction, V- parameter, and effective mode index have been discussed in details.

5.1 Design

In this chapter an optimized low loss PCF has been numerically analyzed and successfully designed. A sectored roundabout structure of center is proposed. The cladding region follows the same sectored circular design also. Figure 5.1 describes clearly the cross-sectional view of core-cladding region. Topas is used as a background material for both cladding and core region of designed fiber because of its low material absorption loss with a consistent refractive list inside a wide range of frequency, lower fluctuation with the variation of refractive index and least scattering than Silica, Teflon or Poly methyl methacrylate (PMMA) and they contain higher absorption loss[116]. Grooved region of the proposed design has been filled with air. The vast majority of the earlier proposed structure, explored around $3000\mu\text{m}$ of all out PCF diameter across with around $300\mu\text{m}$ center size[116],[117]. To compete our result with the existing PCF we tune our PCF core cladding structure nearly existing works and finally optimal case is identified. In our proposed design the diameter of the core is noted as D_{Core} . For optimal case the value of D_{Core} is $350\mu\text{m}$. In both core and cladding region the area is sectored by three rectangles at 120° . In cladding region the length of each rectangle is noted by L . The value of L is considered $825\mu\text{m}$ as optimum. The width of this rectangle is noted as W . For core region the

optimal length and width of each rectangle is considered as $175 \mu\text{m}$ and $10\mu\text{m}$ respectively. The optimal value of outer cladding for the designed fiber is $1200 \mu\text{m}$. By comparing with other researches [118],[119],[120] and doing trial and error we have achieved the above mentioned optimal value.

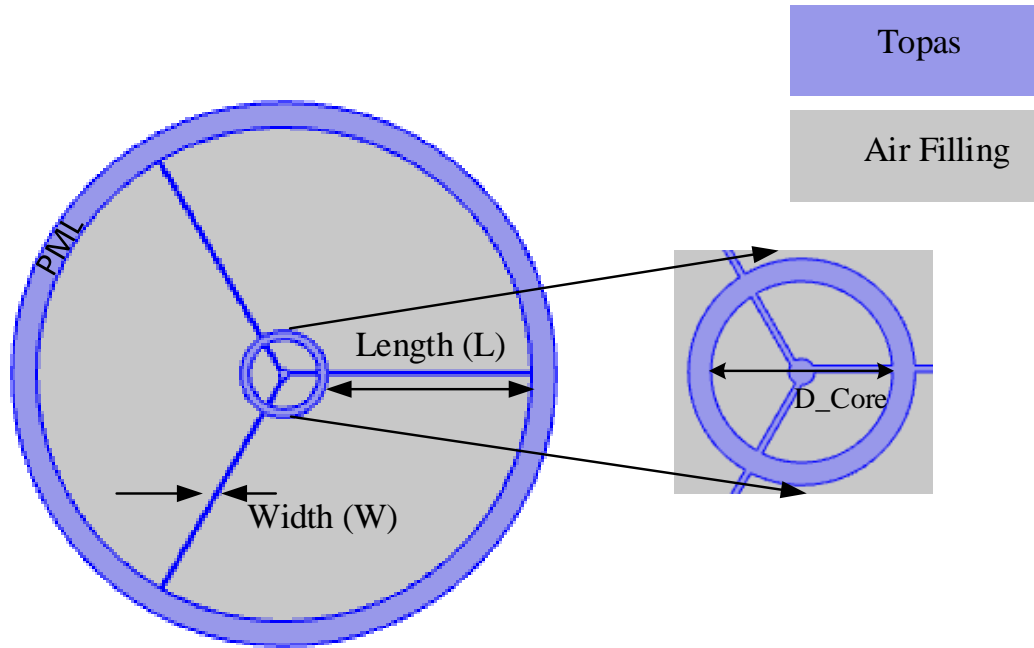


Figure 5.1: Illustration of the cross-sectional details of core-cladding region with enlarged core

Since a circular boundary can reduce the unexpected electromagnetic radiation, a circular shaped perfectly matched layer (PML) is added with the thickness of 10% of total fiber radius.

5.2 Numerical Analysis

Finite Element Method (FEM) is an important tool for investigating electromagnetic characterization. Comsol software version 5.3a based on Finite Element Method (FEM) has been used to evaluate the different properties of proposed THz waveguide. One of the popular and effective computational procedure is FEM for modeling of electromagnetic wave propagation & interaction with surrounding components. Many wave propagation properties such as dispersion, losses, electromagnetic field distributions and modeness can be obtained by FEM method in terms of frequency & spatial position. By using numerical analysis tools FEM able to solve the mechanics, coupled physics and chemistry as well as biological crux rather than determination of propagation characteristics only[121],[122]. Several steps required to complete our proposed FEM model.

Step 1: Introductory step for FEM model is model geometry selection. Parameters required in this step is the simulation domain definition. The spatial range selection limits of the simulation will be one, two or three dimensional. In our research, two-dimensional mode was used. Spatial extents might be divided into smaller domain in the simulation section, which is known as subdomain.

Step 2: Assigning physical properties is the 2nd step. For each subdomain material properties such as magnetic permeability, dielectric permittivity, refractive index should be defined. Topas is used as a bulk material in our proposed design whose refractive index was 1.53.

Step 3: This step involves assigning boundary & initial condition. For defining a boundary surface such as continual boundary, these conditions are used. For waveguide simulation purpose, an electric field source has been assigned as a boundary.

Step 4: The next step of FEM modeling method is known as mesh analysis, which is defined as the discretization of the simulation domain. Here the spatial area is divided into several discrete elements. Subdomains which created the simulation domain are much bigger then these discrete elements.

Step 5: The final process of FEM model is the system PDEs solutions which required to calculate the electromagnetic field distribution. Computational time required for solving system PDEs depend on the mesh elements, volume of simulation and type of electromagnetic phenomena.

The flow chat shown in Fig. 5.2 briefly expressed the entire FEM process.

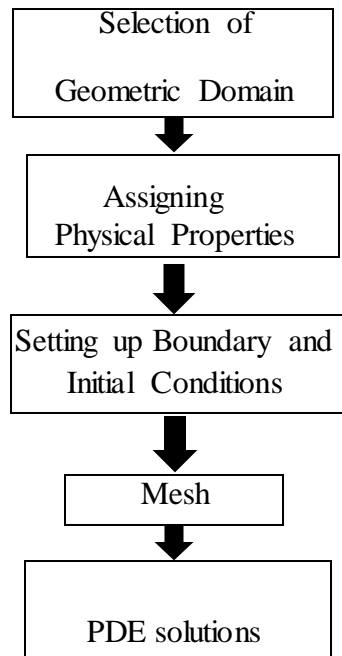


Fig. 5.2: Steps required to complete a finite element analysis

All parameters of the proposed PCF have been determined at the optimal frequency $f = 0.9$ THz and 90% core porosity. Core porosity is the ratio of total air area in the core region to total area of the core.

Fundamental electromagnetic field of mode for different values of porosity is shown in the following figure 5.3. It shows tight confinement of light which is necessary for THz propagation on the other hand negligible interaction of light is identified in cladding.

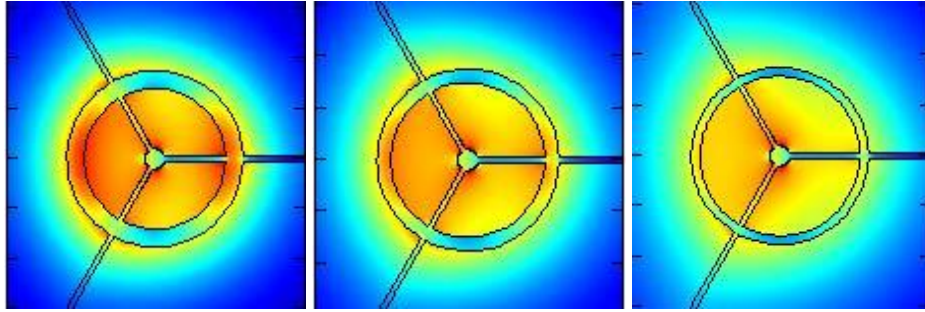


Figure 5.3: Fundamental electric field of mode for different values of porosity (a) 80% (b) 85% (c) 90%

Widely used polymer materials are very absorbent and as a result it is a challenge in designing a wave guide for THz frequency bands. This absorption is called EML or material absorption loss. Efficiency of a PCF depends on the amount of light which will propagate through the air lattices in the core. If the material absorbs more light, then the loss of PCF is higher. As a result, the efficiency of PCF reduces. So the EML should be reduced as much as possible. It can be calculated by the equation of EML which is depicted in equation no 4.1 in chapter 4.

Figure 5.4 shows the response of EML of the proposed fiber with the variation of frequency at different core diameters. From figure 5.4 it is observed that EML is increasing linearly with frequency which satisfies the theoretical consequence of EML calculation from the following empirical equation. The following equation is a developed equation which is copied from reference on [123],[124].

$$\alpha(\nu) = \nu^2 + 0.63\nu - 0.13 [dB / cm] \quad 5.1$$

Where ν denotes the operating frequency.

The reason behind that EML is proportional to electromagnetic wave frequency[120]. Besides it can be said that when frequency increases, light is tightly confined in the core section which increases the interaction of light with background material and as a result EML increases. Again increasing the core diameter also causes interaction between the propagating electromagnetic field and the background material, which increases the EML. At the optimal design parameter numerical value of EML is observed in our proposed design is 0.022 cm^{-1} , which is

commensurable with the prior proposed PCF geometry for the same application[116],[24],[118],[16].

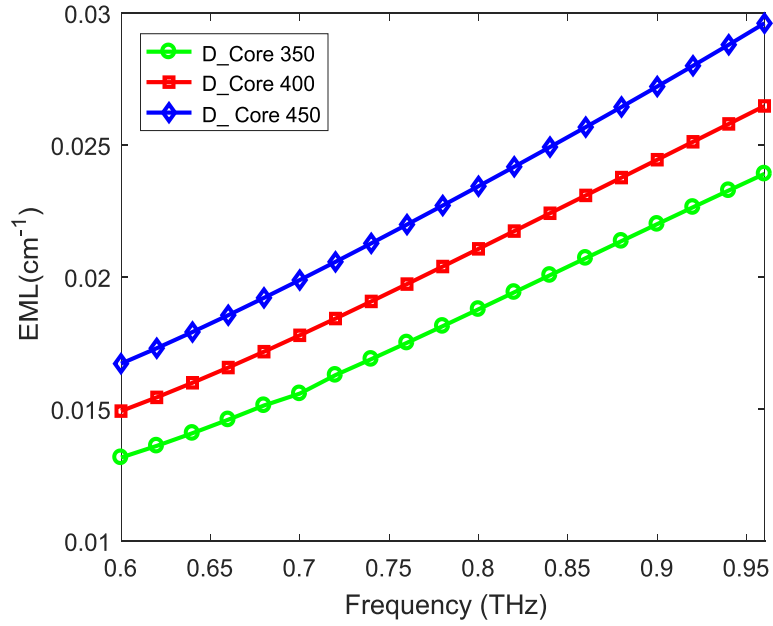


Figure 5.4: Effect of frequency on EML at different core diameter

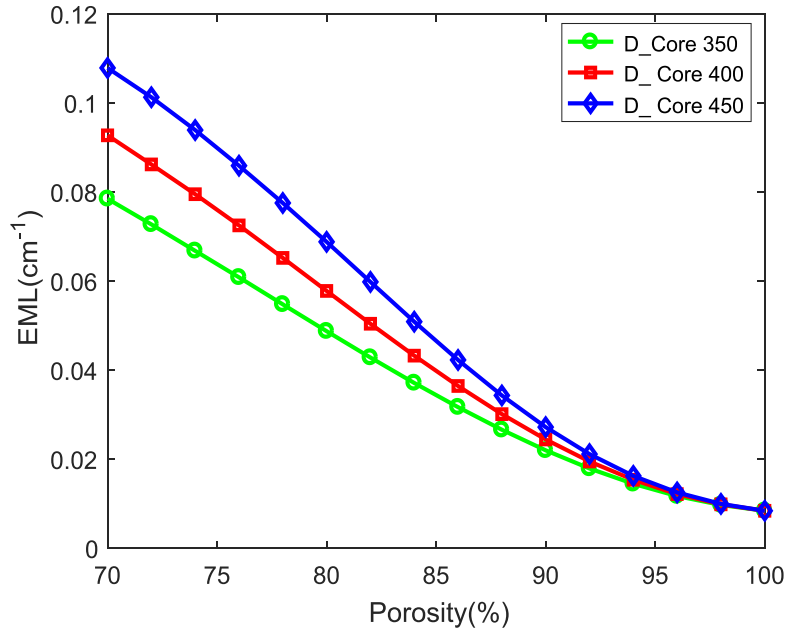


Figure 5.5: Effect of porosity on EML at different core diameter (D_Core).

Figure 5.5 demonstrates that the estimation of EML downsizes with expanding porosity. The explanation is that the volume of solid material into the center declines with the augmentation of porosity and at the point when porosity is extended then light cooperation with background material will decrease. From figure 5.5 it is likewise seen that when the estimation of center breadth is scaled up then the estimation of EML will likewise increment. The reason behind that is, in the event that the estimation of center breadth is expanded, at that point the territory of background material ought to be expanded. If the territory of background material is expanded then light interaction with background material will increase and that's why the effective material loss will increase.

Power fraction is defined as the percentage of dissipated light power into the porous core fiber. A high core power fraction is essential for maintaining efficient transmission for THz waves. Equation of core power fraction is depicted in chapter 4 in equation no 4.2. The mode power propagation by the air core corresponding to frequency for diverse core diameter is delineated in Fig. 5.6. This figure depicts that the air core power fraction enhances with the boost of frequency. Increment of frequency is facilitated for tightened confinement which increases the mode power absorption inside the core region by the air holes.

Figure 5.6 also depicts that the achieved core power fraction is 34% at optimal design parameter. Besides, this figure also depicted that when the value of core diameter is scalped then the core power fraction will also increase. The purpose for that is, if the core diameter increases then the size of air lattice will also increase and more power will be propagated by the air lattices which will increase the core power fraction.

Confinement loss can be considered as an important tool for THz waveguide. Confinement loss is defined as the amount of light that spreads out from the core and mainly depends on the lattice structure of the core and cladding. Due to this loss, a portion of transmitted light goes through the cladding region. Equation of confinement loss is depicted in chapter 4 in equation no 4.3. The relation between the propagation length of THz wave and confinement loss is directly proportional. In the event that the confinement loss is high, at that point the propagation distance ought to be decreased. So confinement loss is necessary to reduce as possible.

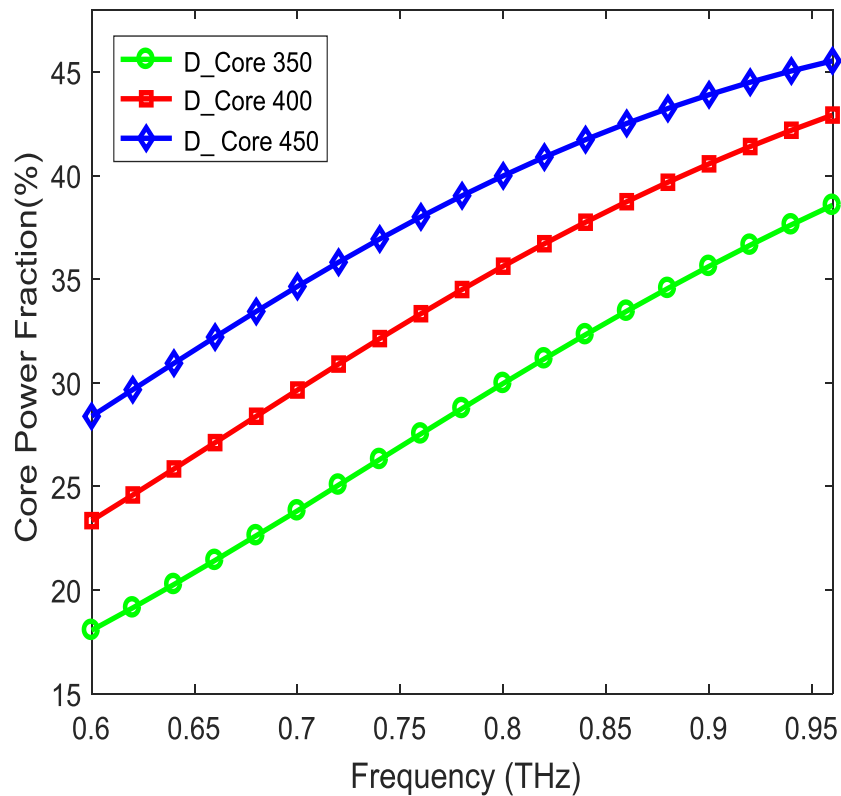


Figure 5.6: Effect of frequency on core power fraction at different core diameter (D_Core).

Figure 5.7 depicts the scenario of confinement loss as a function of frequency. It is observed that the value of confinement loss is decreased with the incremental value of frequency. This is on the grounds that, When frequency escalates, more light starts towards fixed repression inside the core, in outcome of confinement loss diminishes. Besides it is also noticed that confinement loss also decreased with the incremental value of core diameter. The reason behind that with the augmentation of core diameter, all the more light start to go through to the core, which limits the confinement loss. It is a positive sign for proposed PCF structure.

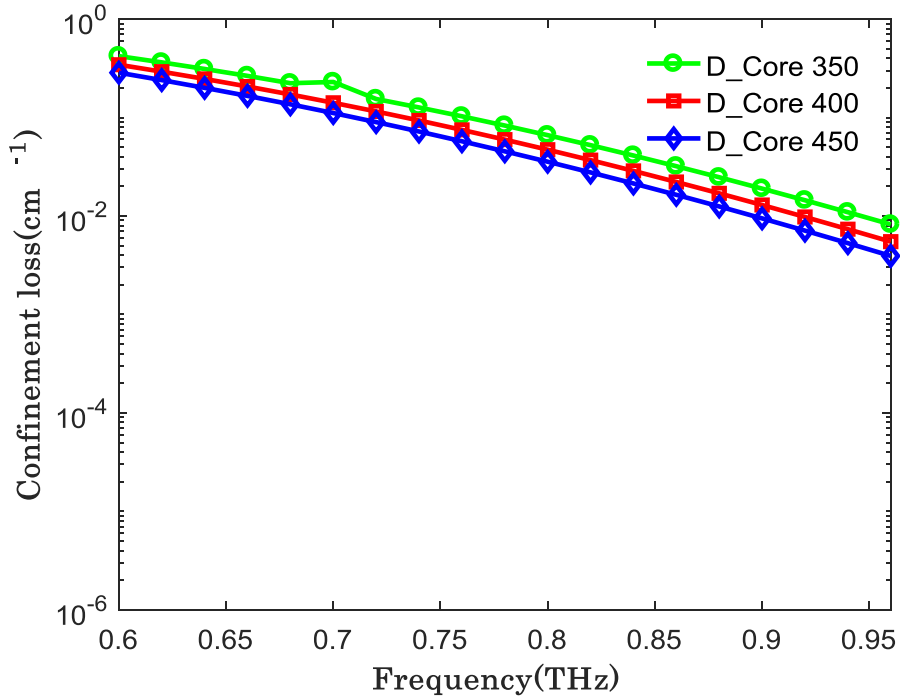


Figure 5.7: Effect of frequency on confinement loss at different core diameters (D_{core}).

For a quality waveguide design, dispersion is another important parameter because if the dispersion is higher, then higher amount of bit error will be happened[125]. So the fluctuation of dispersion is necessary to reduce close to zero. In this proposed structure, Topas has been used a background material whose dispersion is close to negligible[120] and only waveguide dispersion can be considered. Equation of waveguide dispersion is depicted chapter 4 in equation no 4.4.

Figure 5.8 delineates the nature of dispersion variation with respect to frequency. It shows that a flattened dispersion is obtained from the frequency range of 0.7 to 0.9 THz with a variation of $0.7321 \pm 0.162 \text{ ps/THz/cm}$. The explanation for this, the waveguide dispersion relies upon the refractive index of center and cladding. Distinctive refractive index of center and cladding upgrade the dispersion. In this proposed PCF, air has been utilized in both center and cladding which help to level the dispersion. From this proposed PCF achieved value of dispersion is highly comparable with previously proposed geometry for similar application [116][16].

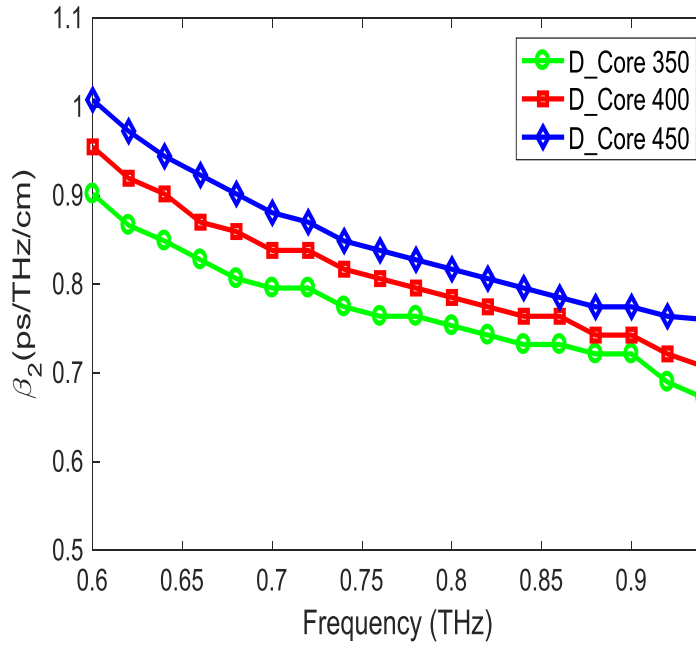


Figure 5.8: Effect of frequency on dispersion at different core diameter (D_{core}).

The area in which light started interacting is defined as effective area. Enormous estimation of effective area is significant for communication mechanism on the grounds that wide effective mode area limits the disabilities emerging by the distinctive nonlinear impacts. Expanding the separation between the air holes in the cladding segment and using little air holes in cladding large effective area can be achieved. Equation of effective area is depicted in chapter 4 in equation no 4.5.

Figure 5.9 depicts the scenario of effective area as a function of operating frequency. Obviously the effective area is decreasing with the gradual changes of frequency. On the grounds that with the accrument of frequency the mode power firmly restricted in the center segment which decreases the region of effective area in the tested frequency range of 0.6THz to 0.95THz. Designed PCF has provided a moderate value of effective area. At optimal frequency, value of effective area is $3 \times 10^{-7} \text{ m}^2$ which is comparable.

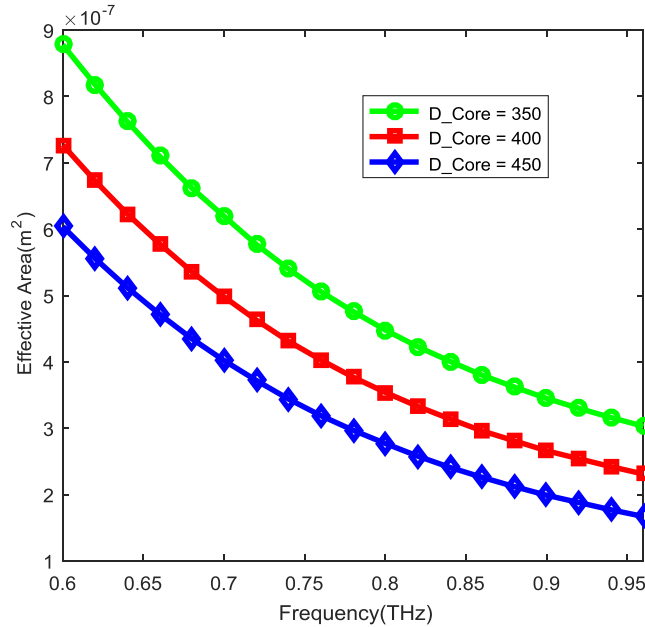


Figure 5.9: Effect of frequency on Effective area at optimal core diameter.

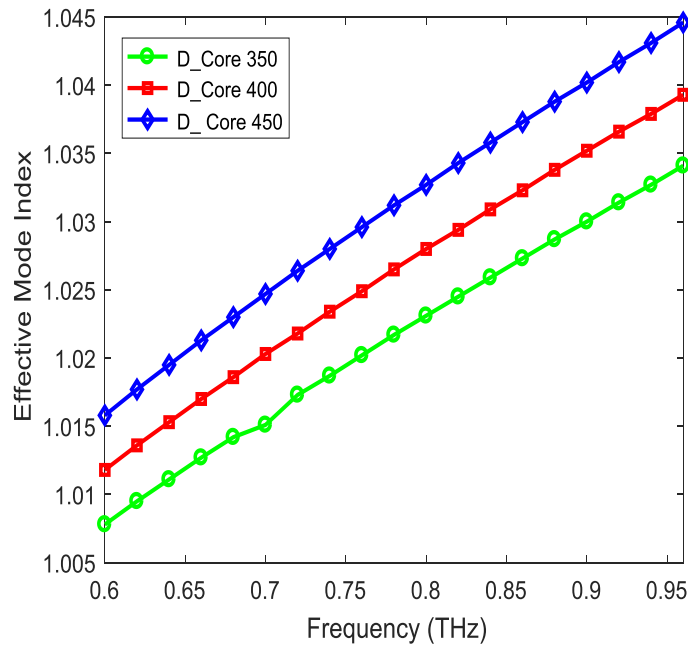


Figure 5.10: Characteristics of Effective Mode Index for proposed photonic crystal fiber.

Because of symmetrical arrangement in the core and cladding air holes, the designed fiber shows the same confinement for both polarization mode. In our investigation we only consider X-polarization mode. Figure 5.10 depicts that Effective Mode Index (EMI) increases with frequency. The main reason for this type of characteristics is the transmission mechanism of light into the core. Light travels into the core and is being confined by internal reflection system. The

explanation for the reflection of light is that the incident angle of light is greater than the critical angle when it travels from higher denser medium to lower denser medium. That's why light is being tightly confined in the central point of the core. As a result when the value of frequency is boosted, then the value of EMI (Effective Mode Index) will also upturns.

For protracted distance THz Communication Single Mode Fiber (SMF) qualities are fundamental. The mode characteristics can be calculated V-Parameter which is depicted in chapter 4 in equation no 4.6. The ideal value for refractive index of cladding is nearly unity though it's should not be unity[30],[31],[32]. The explanation for that is cladding not only consists of air but also Topas. On the off chance that $V \leq 2.405$ at that point the fiber acts as a single mode fiber (SMF) something else the fiber considered as multimode fiber (MMF) [126].

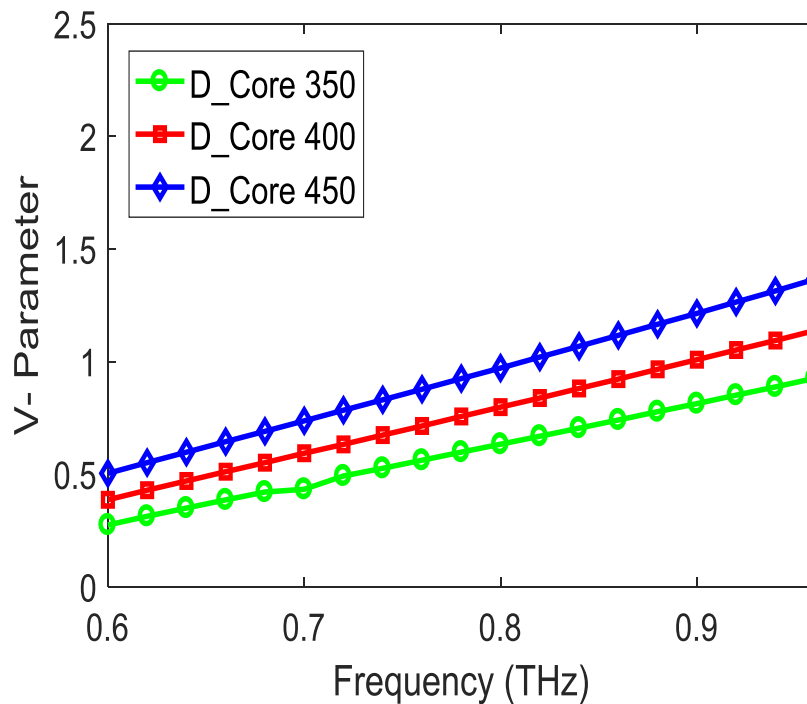


Figure 5.11. V-Parameter as a function of frequency at different core diameters.

Figure 5.10 depicts the scenario of V-parameter at different core diameters. It is observed that the value of V-Parameter is increasing sharply with the incremental value of frequency. It has been watched that with the incremental value of frequency originates expressive boost of index distinction between effective indices of cladding and core therefore V parameter is heightened[25]. At optimal design condition our value of V-Parameter is 0.75, which satisfy the condition for single mode operation. Finally a characteristics comparison table of previous

design and proposed design is shown in Table1. Table 1 exhibits the illustration between our designed structure of PCF and already proposed diverse PCF structure considering effective material loss and design layout. It will be mentioned that our designed PCF structure shows better results in the most of the crucial cases.

Table 5.1: Comparison between existing and proposed design.

References	Frequency (THz)	EML (cm^{-1})	Design Structure	
			Core	Cladding
[116]	1	0.053	Hexagonal	Circular
[24]	1	0.035	Hexagonal	Kagome
[124]	1	0.04	Hybrid	Octagonal
[16]	1	0.066	Circular	Hexagonal
[20]	1	0.07	Circular	Octagonal
[34]	1	0.06	Elliptical	Slotted
[25]	1	0.076	Square	Isosceles square
Proposed PCF THz Waveguide	0.90	0.022	Sectored Circular	Sectored Circular

5.3 Feasibility assessment of fabrication

It is essential to think about the constructive execution of PCF. There are different approaches to fabricate it. The most normally utilized techniques are drilling, capillary stacking, extrusion, stack and draw, sol-gel and 3D-printing [118]. Different lattice structures have been fabricated by Max Plank Institute[127]. Practically several categories of design can be manufactured by the extrusion strategy demonstrated by Kiang et al [128]. As our suggested design of PCF is circular and it comprises a number of grooved air lattices, 3D-printing technique is suitable for it [129].

5.4 Conclusion

In this chapter a circular manner PCF design has been proposed and investigated for THz wave propagation. At optimal design parameters proposed design shows a lower EML of 0.022cm^{-1} , confinement loss of the order of 10^{-1}cm^{-1} , core power fraction of 34% and flattened dispersion.

The proposed design structure can be fabricated easily because of the design simplicity and ongoing technologies. So considering the above mentioned properties it can be concluded that if the proposed fiber is utilized properly with recent technology then it will open a new era of long distance transmission for THz wave.

Chapter 6

Design II: Proposed Sectored Circular THz Sensor

In this chapter a topas based novel sectored circular photonic crystal fiber (PCF) is proposed for liquid analyte sensing in THz frequency range. Cladding holes of the proposed geometry are filled with air and core holes having different analytes of various refractive indices. In this paper Comsol V5.3a software is utilized for numerical simulation by implementing the finite element method (FEM). Obtained results demonstrate that at an operating frequency of 1.5 THz, the average sensitivity is 92.14 % and the confinement loss is $2.308 \times 10^{-9} \text{cm}^{-1}$. Moreover, the proposed the proposed PCF also display a moderate effective area and a lower material absorption loss at optimal design condition. In addition the fabrication feasibility for considered design methodology is discussed in details. Due to the simplicity of design and comparable performances, designed sensor is highly applicable as a biochemical sensor in various industrial applications.

As of late huge advancement has been done for researching and structuring the remarkable properties of PCF. The overall structure of a PCF contains a number of microscopic air lattices[130]. Light will have to pass by two methods inside the core of a PCF. One is mechanism of photonic band gap, which is applicable for photonic band gap fibers and another one is internal reflection mechanism, which is applicable for index guiding fiber[131]. By utilizing a PCF drawbacks of a local optical fiber can be alleviated owing to its substantial favorable features for example minimum confinement loss[132], maximum birefringence[133], maximum sensitivity[134], high effective area[135]. To achieve superior performance, geometrical properties of a PCF i.e. structure and dimension of air lattices in cladding and core can be altered. Consequently, instead of the local optical fiber the PCF has been receiving an attention from a significant number of researchers for a wide range of implementations, which mostly cover spectroscopy[97], medical diagnosis[136], biomedical imaging[137], optical communication, sensing etc. For sensing application, PCF yields prominent characteristics of robustness and design flexibility. Sensitivity can be characterized by changing the geometrical parameter in the design for example, porosity, core diameter[138]. Sensor can make a major contribution for detecting hazardous chemicals which are responsible for industrial endangerment. Besides they are immune to crucial environmental situation, cheap and small in size. PCF based sensors have a large number of applications in environmental[138], biomedical[139] and industrial[140] sectors for detecting toxic substances. In industrial sectors PCF sensors can be used for bioprocess controlling and production monitoring. Sensor can play a significant role for detecting harmful chemicals which are responsible for industrial hazards. Quality of air in the environment can be maintained by using gas sensors[141]. These can detect

harmful greenhouse gases such as CO₂, CH₄ and NO₂, which are exhausted from vehicles and industries[141]. Medical functions for example biomedical imaging, drug detection, bacteria detection, protein sensing and cancer cell detection PCF based sensor can be used[142]. Another sensing application where PCF based sensor are used which includes humidity sensor [143], temperature sensor[144], biosensor[145].

A wide number of studies have been conducted which demonstrate a variety of sensors based on different PCF designs. Lee et al.[146] designed a photonic crystal fiber sensor in 2000 which was used for detecting ionic strength and pH. Biochemical and physical sensors were proposed and investigated by pinto et al.[92] in 2012. H olyaee et al. [142] proposed a PCF gas sensor with an improved sensitivity of 10% and minimum confinement loss by varying the diameter of holes of cladding. In 2015 Adegil et al. [116] proposed a PCF structure with a vertically and a horizontally suspended air lattices and improved sensitivity 25% and reduced confinement loss of 10⁻⁴ dB/m but any description about material absorption loss wasn't provided. Morshed et al.[147] proposed a micro structured PCF gas sensor with an improved sensitivity of 42.27% and reduced confinement loss of 4.78× 10⁻⁶ dB/m at $\lambda = 1.33 \mu\text{m}$ but material absorption loss and birefringence was not analyzed in that design. In 2016 Arif et al. [148] designed a hexagonal PCF sensor with a sensitivity of 55.83%. The analyte for that sensor was ethanol. Asaduzzaman et al. [149] designed an elliptical air holes and asymmetrical core based PCF sensor with a sensitivity of 53.07% and birefringence of 6.9×10⁻³ at the wavelength of 1.33 μm . Islam et al.[150] designed a spiral PCF sensor with a sensitivity of 57.16% in 2017. But any information about effective material loss (EML) wasn't analyzed. Paul et al.[151] unveiled an alcohol sensor with octagonal cladding and porous core PCF which attained a lower confinement loss of 4.99×10⁻⁹ dB/m and a sensitivity of 69.09%. However effective area, material absorption loss weren't investigated. K. Ahmed et al. modeled a hybrid photonic crystal fiber for chemical sensing applications. The sensitivity of the reported design was 49.17% for ethanol[152]. B. K. Paul et al. modeled a circular air lattice PCF with 64.19 % relative sensitivity and confinement loss of 2.07×10⁻⁵ dB/m, which was attained at the wavelength of 1.48 μm [153]. Recently, Sultana et al. [36] demonstrated a Zeonex based PCF for ethanol sensing. At 1 THz frequency this design achieved 7.79×10⁻¹² cm⁻¹ confinement loss and a sensitivity of 68.87%.

In this chapter a sectored circular core-cladding structured PCF has been introduced for different refractometric sensing in the THz spectrum. The proposed sensor shows lower confinement loss, average sensitivity of 92.14% and moderate effective area at optimal design condition.

6.1 Methodology of Design:

In figure- 6.1, the magnified view of the developed PCF sensor is shown to illustrate the cross-sectional details of core-cladding region. The core is sectored by three rectangles at 120° and the cladding region follows the same sectored circular design also. Sectored circular core is preferable over solid core because core is filled with bulk amount of fluid analyte. The cladding region of the designed PCF has three suspended holes in it.

Both cladding and core region of the designed fiber have Topas as their background material and the sectored region of the core has been filled with air. To complete the design of the core, various types of liquid analytes are used according to varying refractive indices in 1.33 to 1.37 range. In the proposed design the diameter of the core is noted as D_{Core} . Most of the previous works evaluate their performance in the range of 280 μm to 400 μm core diameter and for this reason we also investigated our design in the range of 280 to 400 μm [34],[37]. Finally we achieved comparable performance or in some cases better performance at 350 μm . That's why we have considered 350 μm as an optimal. To obtain tight confinement the value of core diameter is varied. Since a circular boundary can reduce the unexpected electromagnetic radiation, a circular shaped perfectly matched layer (PML) is added with the thickness of 10% of total fiber radius. The outer radius of the designed fiber is 1000 μm . In cladding region the length of each rectangle is noted by L . The value of L is 825 μm . The width of this rectangle is noted as strut (S) with the value of 5 μm . For core region the length of each rectangle is 170 μm and width is 5 μm .

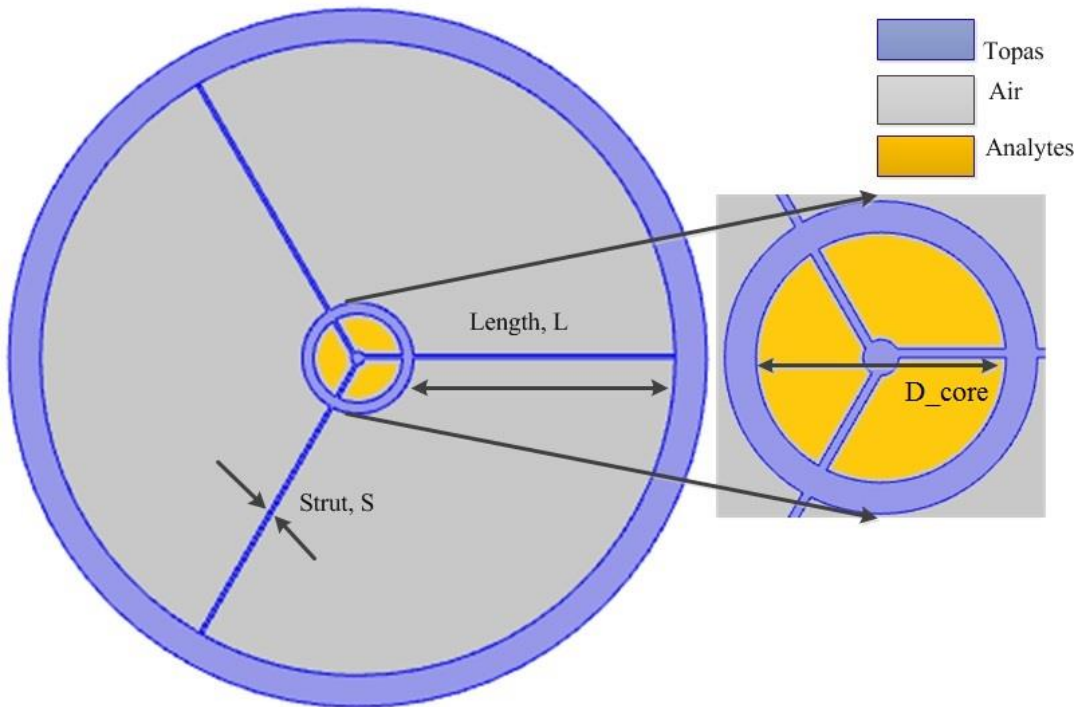


Figure 6.1: Illustration of the cross-sectional details of core-cladding region with enlarged core.

6.2 Simulation Results:

To characterize our proposed design we have carried out multiple simulation on Full vector finite element method (FEM) based COMSOL multi physics V5.3a software [124]. Different analytes with a variety of refractive indices are inlayed in the core of the demonstrated PCF sensor. Refractive indices (μ) are varied from 1.33 to 1.37. Different guiding properties namely sensitivity, confinement loss, material absorption loss are evaluated for a wide range of

frequencies from 1 to 2 THz. Moreover effects of varying strut width on various guiding features are also analyzed. Electric field distributions for different refractive indices are displayed in fig- 2 for X polarization mode.

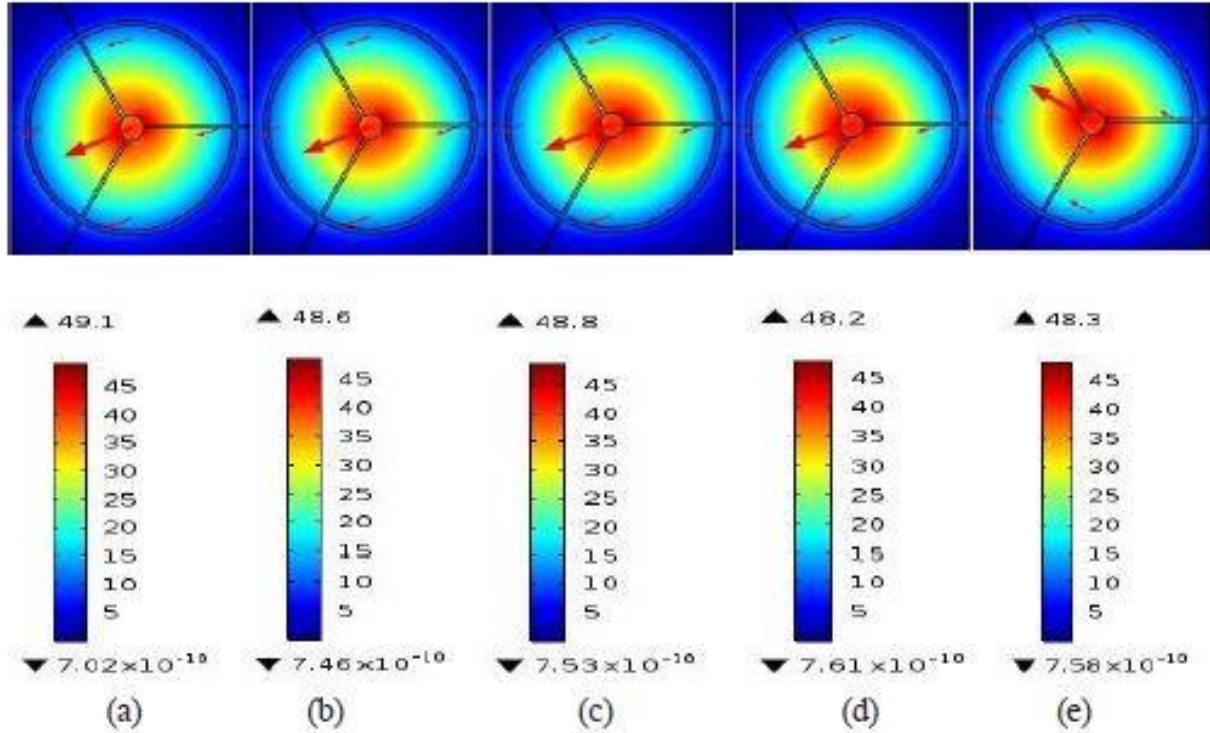


Figure 6.2: Electric field distribution of designed PCF at different refractive indices

(a) $\mu = 1.33$, (b) $\mu = 1.34$, (c) $\mu = 1.35$, (d) $\mu = 1.36$, and (e) $\mu = 1.37$

Due to the stronger interaction of the evanescent field with the sensed material, the above figures clearly indicate that the light is tightly confined in the core. That's why leakage losses will be negligible and the sensitivity will high. The figure depicts that the light confinement in the core of a PCF is better for those analytes whose refractive index is higher than other. This shows that the designed sensor is better for that type of chemical sensing whose refractive index is high.

One of the most powerful numerical method for developing & designing photonic components and devices is known as full vectorial Finite Element Method (FEM) with the perfectly match layer (PML) has been utilized in this study[154],[155],[156]. FEM method has already been discussed in chapter 5 under section no 5.2. All the optical propagation properties could be calculated in a single run by applying the PML as boundary conditions, which is a useful technique to evaluate propagation characteristic of leaky modes in PCFs[157][158]. The modal analysis conducted on the cross-section in the x-y plane of the PCF as the direction of wave propagation in the z-plane.

The Maxwell's equation in terms of the anisotropic PML boundary condition [157] could be expressed as:

$$\nabla \times ([s]^{-1} \nabla \times E - k_0^2 n^2 [s] E) = 0 \quad 6.1$$

In the above equation, the electric field vector is expressed using E , the wave number in the vacuum is expressed in $k_0 (= \frac{2\pi}{\lambda})$, the refractive index of the domain is expressed using n , PML matrix is expressed using $[s]$, an inverse matrix of $[s]$ is expressed using $[s]^{-1}$ and the operating wavelength is expressed by λ .

To comprehend the benefits of the proposed PCF for detecting applications of sensing and its interpretation, it is profoundly imperative to assess the sensitivity K and co-efficient of relative sensitivity r , which are demonstrated by the adjusted Beer Lambert Law, mentioned in chapter 4 in equation no 4.7. Equation of co-efficient for relative sensitivity r and sensitivity K are also expressed in chapter 4 in equation no 4.8 and 4.9 respectively.

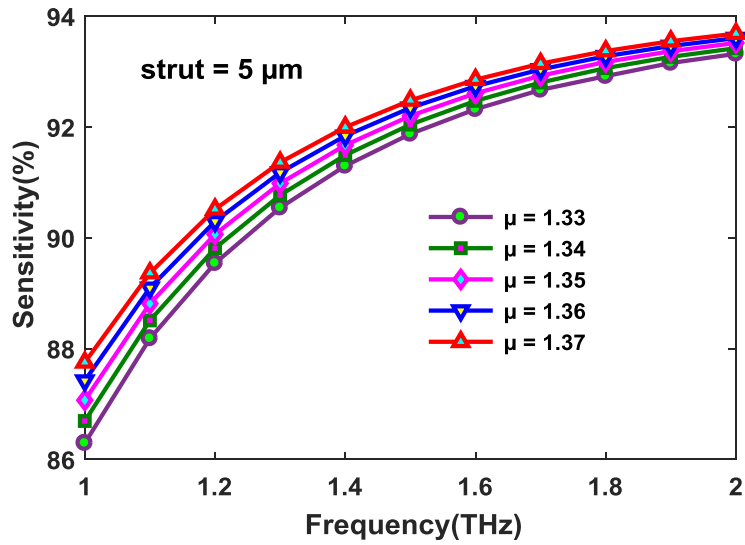


Figure 6.3: Effect of frequency on the sensitivity at strut 5μm

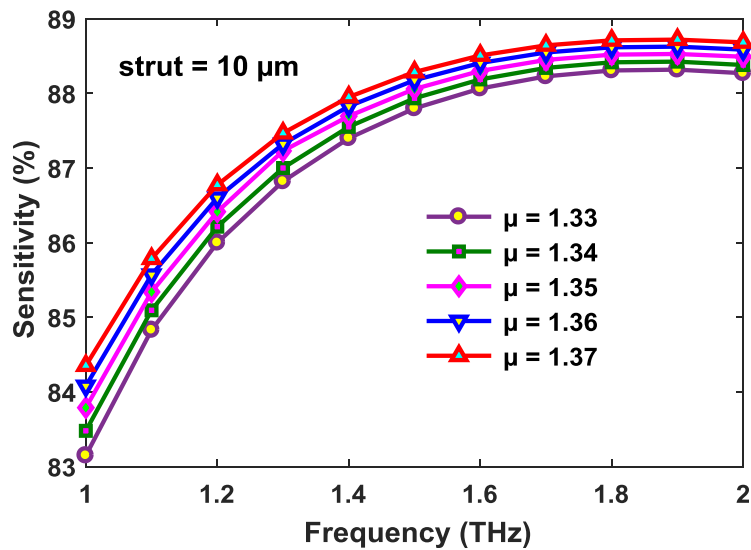


Figure 6.4: Effect of frequency on the sensitivity at strut 10μm

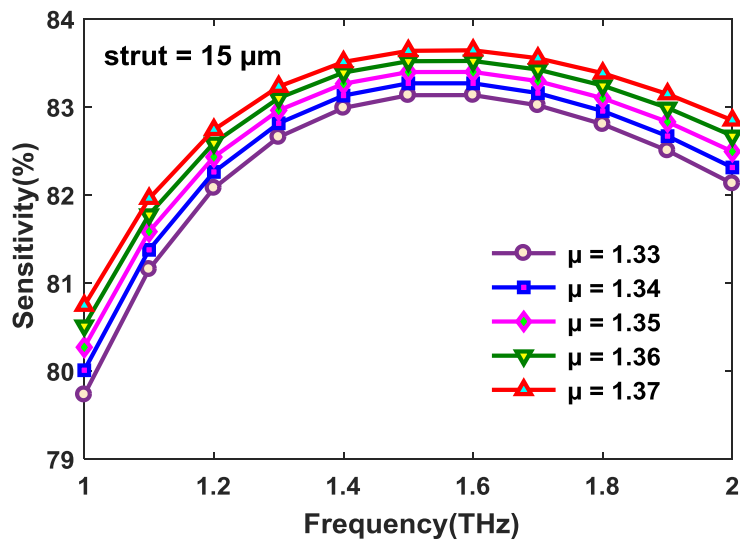


Figure 6.5: Effect of frequency on the sensitivity at strut 15μm

Figure 6.3, 6.4 and 6.5 show the scenario of sensitivity against frequency for different chemical analytes at strut width 5μm, 10 μm and 15 μm accordingly. At first it is noticed from the above figures that, sensitivity increases sharply with the incremental value of frequency. This can be clarified by the reality both the core power fraction and the refractive mode index increment with frequency. The expansion in center core power fraction is more prevailing at minimum frequencies and as a result sensitivity increases. At higher frequencies notwithstanding, the center core power fraction nearly arrives at a most extreme worthwhile the effective mode index

keeps on expanding. It is also noticed that when the value of strut width is 15 μm then the value of sensitivity decreases after a certain point of frequency. In figure 6.5 it is observed that sensitivity is decreasing after 1.5THz. This scenario can be interpreted by the fact that when the frequency and strut width is increasing in parallel then sensitivity will reaches it's maximum value but after a certain point of frequency, light interaction with the analyte in the core will be decreased. As a result light will pass or leak from core to cladding. Consequently sensitivity will start to decrease.

Figure 6.3, 6.4 and 6.5 depict the scenario of changing strut size in the proposed design. From the above mentioned figures it is observed that when the width of strut is minimum then the sensitivity is maximum. The reason behind this when strut size is minimum then light interactive area with the analyte in the core is maximum. Consequently core power fraction will be maximum and as a result sensitivity will be maximum. Besides when the size of strut is increasing then the core power fraction is decreased in the core. Considering this issue an optimal width of 5 μm for the proposed PCF sensor have been chosen. As both X and Y polarization shows the same result because of choosing symmetrical geometry for avoiding fabrication complexity, so X- polarization for data analysis has been chosen. For achieving a balance relation between confinement loss, EML and sensitivity, 1.5 THz is chosen as an optimal frequency. Maintaining the above mentioned optimal conditions, achieved relative sensitivity are 91.8%, for $\mu = 1.33$, 92.0%, for $\mu = 1.34$, 92.2%, for $\mu = 1.35$, 92.3% for $\mu = 1.36$, and 92.4% for $\mu = 1.37$. Therefore it is observed that at 1.5 THz frequency the designed sensor shows maximum sensitivity for different liquid analytes which are comparable with [159],[124],[100],[37].

Figure 6.6 depict the scenario of sensitivity with respect to core diameter. From figure 6.6 it is noticed that when the value of core diameter is scaled up then sensitivity is increasing steadily. The reason behind that is, when the value of core diameter is increased then maximum area of core will be covered by analytes and then maximum power will be absorbed by analytes in the core region. That's why maximum sensitivity will be achieved. The proposed design shows 92.14% average sensitivity at optimal design condition.

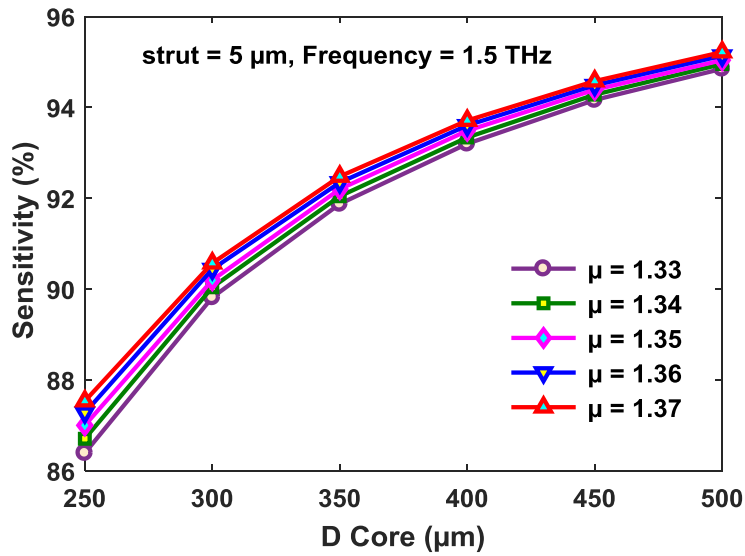


Figure 6.6: Sensitivity with respect to core diameter (D Core) at strut 5 μm

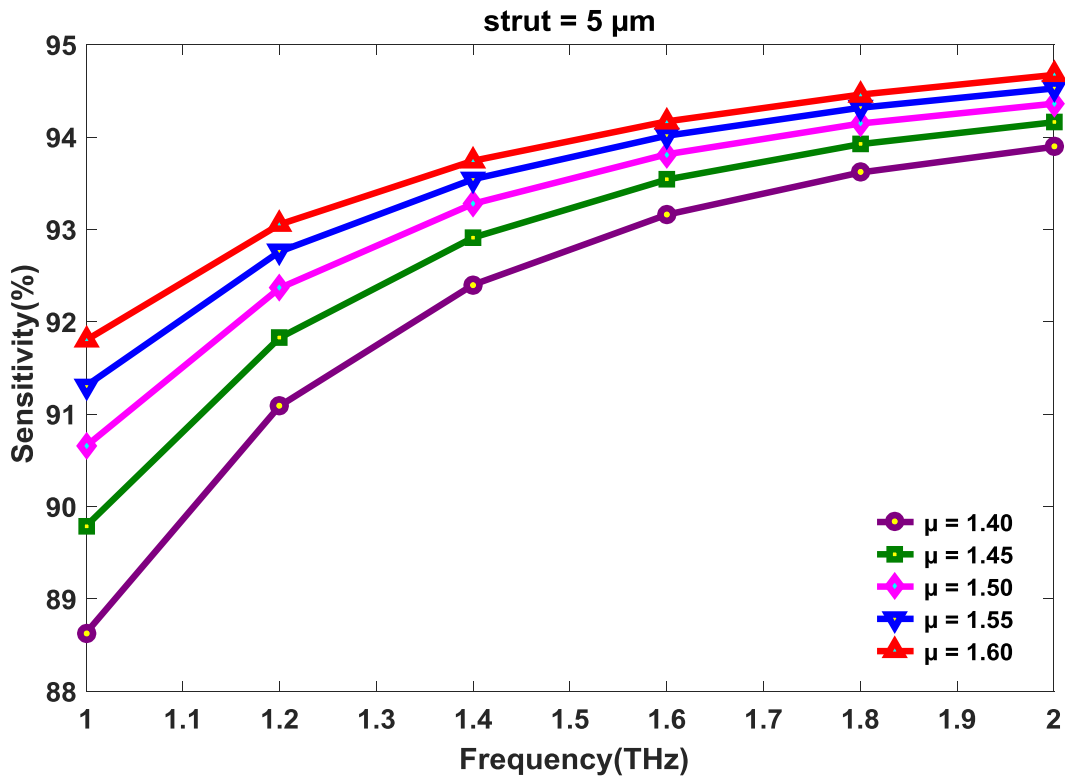


Figure 6.7: Sensitivity with respect to frequency at strut 5 μm for a bigger range of value of μ

Figure 6.7 depict the scenario of sensitivity with respect to frequency for a bigger range of value of μ . From above figure it is observed that scenario of sensitivity with respect to frequency is

similar to figure 6.3, figure 6.4 and figure 6.5. It is also noticed that range of sensitivity is increased with the incremental value refractive index.

Although due to the leakage of the power, confinement loss happens in the cladding region, the capability to trap significant portion of power in core region is still a salient feature of the proposed PCF. The strength of propagated signal is attenuated by the confinement loss in THz waveguide. Equation of confinement loss is depicted in equation 4.3 in chapter 4.

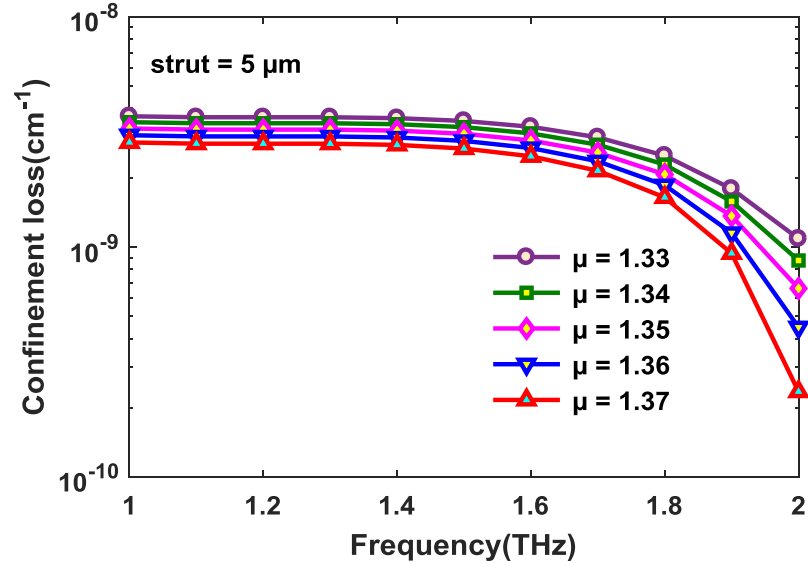


Figure 6.8: Effect of frequency on the confinement loss at strut 5μm

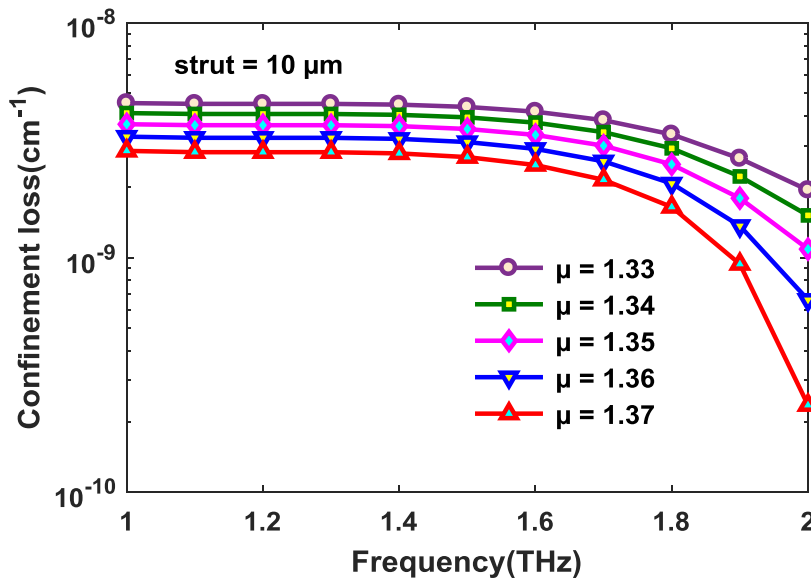


Figure 6.9: Effect of frequency on the confinement loss at strut 10μm

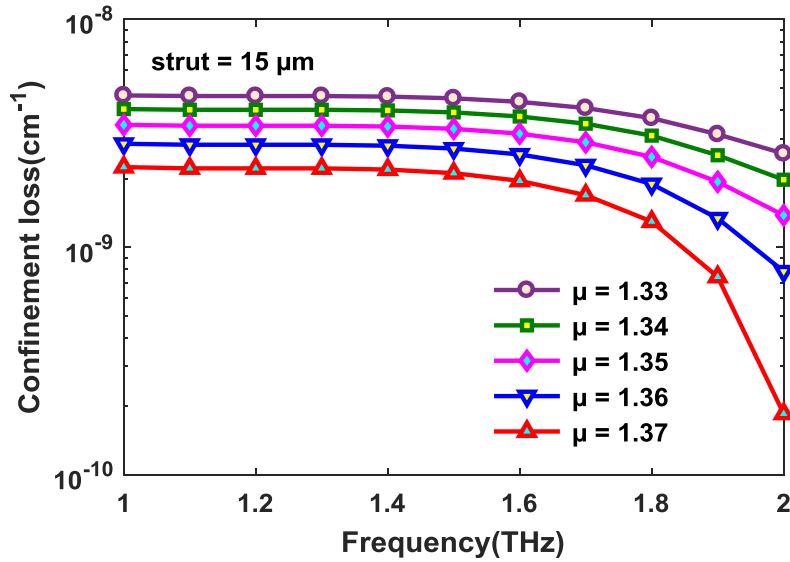


Figure 6.10: Effect of frequency on the confinement loss at strut 15 μm

Figure 6.8, 6.9 and 6.10 illustrate the effect of frequency on the confinement loss for various liquid analytes. From the above figures we can depict that with the increase of frequency the value of confinement loss decreases steadily. The explanation for this characteristic is that the leakage of light will be reduced with the incremental value of frequency and as a result confinement of light will be tighter with higher frequency. That's why confinement loss is reduced. Considering an optimal design parameter of 5 μm strut width and 1.5THz operating frequency, achieved lower confinement losses are $2.88 \times 10^{-9} \text{cm}^{-1}$, $2.69 \times 10^{-9} \text{cm}^{-1}$, $2.502 \times 10^{-9} \text{cm}^{-1}$, and $2.308 \times 10^{-9} \text{cm}^{-1}$, $2.11 \times 10^{-9} \text{cm}^{-1}$ for different refractive indices of 1.33, 1.34, 1.35, 1.36 and 1.37 respectively.

In PCF sensor one of the most salient parameter is Effective material loss (EML). The guided mode of light goes through some undesired losses in the inner portion of fiber. The cause of this loss is the use of light absorbent polymer materials. That's why effective material loss is introduced in this fiber. Equation of material absorption loss or EML is depicted in equation 4.1 in chapter 4.

Fig. 6.11, 6.12 and 6.13 depict that the behavior of EML responses similarly with the frequency. In these figures we have shown the EML with respect to frequency for different strut width of 5 μm , 10 μm and 15 μm respectively. This relation satisfies the empirical formulation of EML which is depicted in equation 4.1 in chapter 4.

Higher the frequency is, the propagating wave will be more tightly confined in the core section which will lead to more interaction between light and background material. As a result EML increases with frequency. It can be concluded from the following figures that with the incremental value of frequency, the value of EML is also increasing besides a larger width of

strut shows a value of higher EML. At optimal design parameter achieved EML are 0.009598cm^{-1} , 0.009620cm^{-1} , 0.009624cm^{-1} , 0.009658cm^{-1} , 0.009694cm^{-1} for $\mu = 1.33, 1.34, 1.35, 1.36, 1.37$ respectively. From above mentioned parameter it is observed that EML is low when $\mu = 1.33$ and EML is high when $\mu = 1.37$. The reason behind this when refractive index is low then light will not be more compact in the core and it will go through cladding, that's why EML will be lower than other analytes besides when refractive index is high then light will be more compact in the core and as a result EML is high.

Figure 6.14 depict the scenario of EML with the incremental core diameter (D Core). From figure 6.14 it is observed that the relation between core diameter and EML is proportional with each other because if the core diameter is increased then the area of background material will increase. As a result light interaction with background material will increase. That's why effective material loss will escalate.

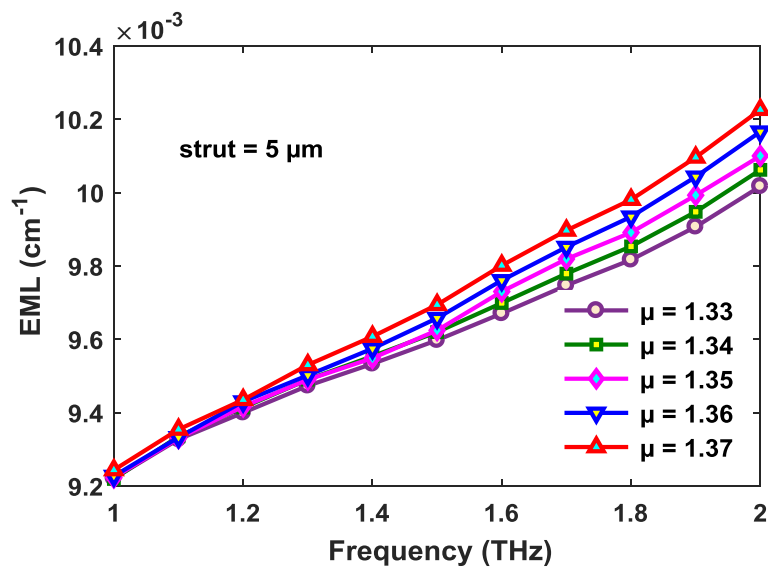


Figure 6.11: Effect of frequency on EML at strut $5 \mu\text{m}$

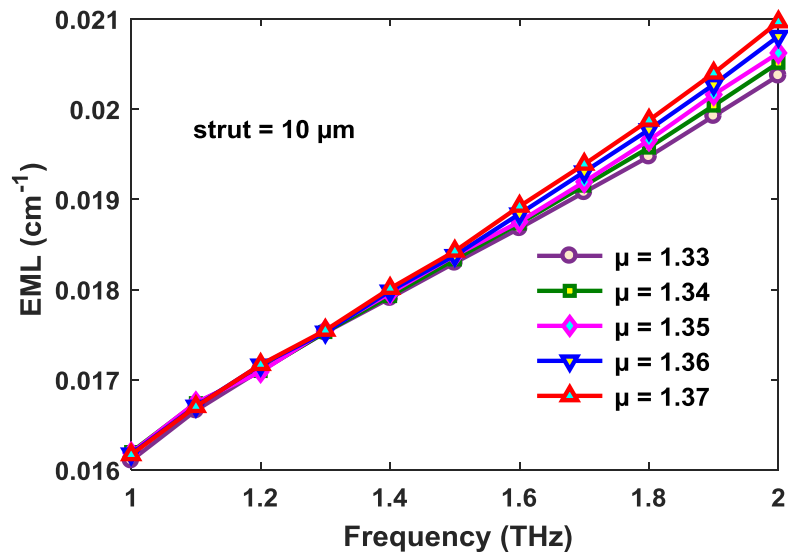


Figure 6.12: Effect of frequency on EML at strut 10 μm

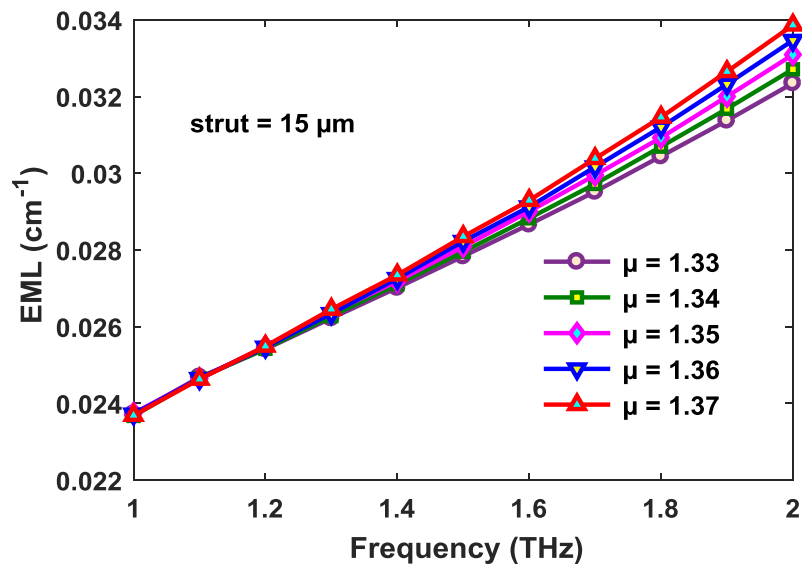


Figure 6.13: Effect of frequency on EML at strut 15 μm

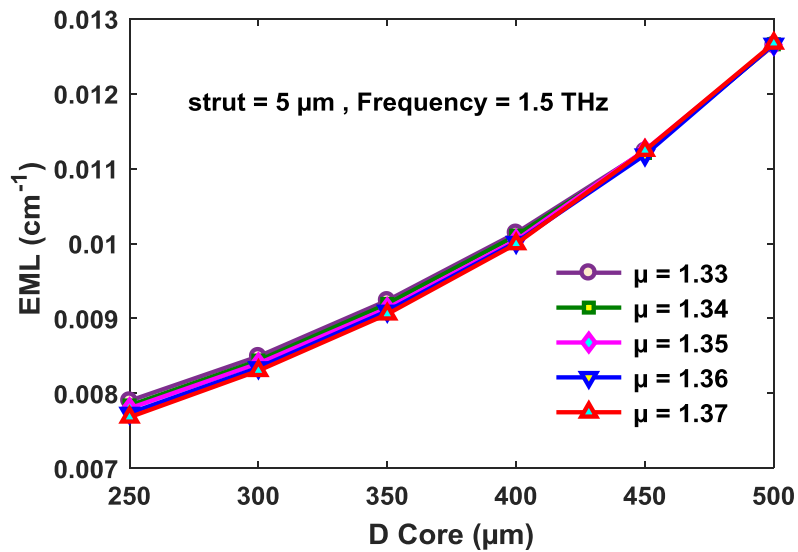


Figure 6.14: EML with respect to core diameter (D Core) at strut 5 μm

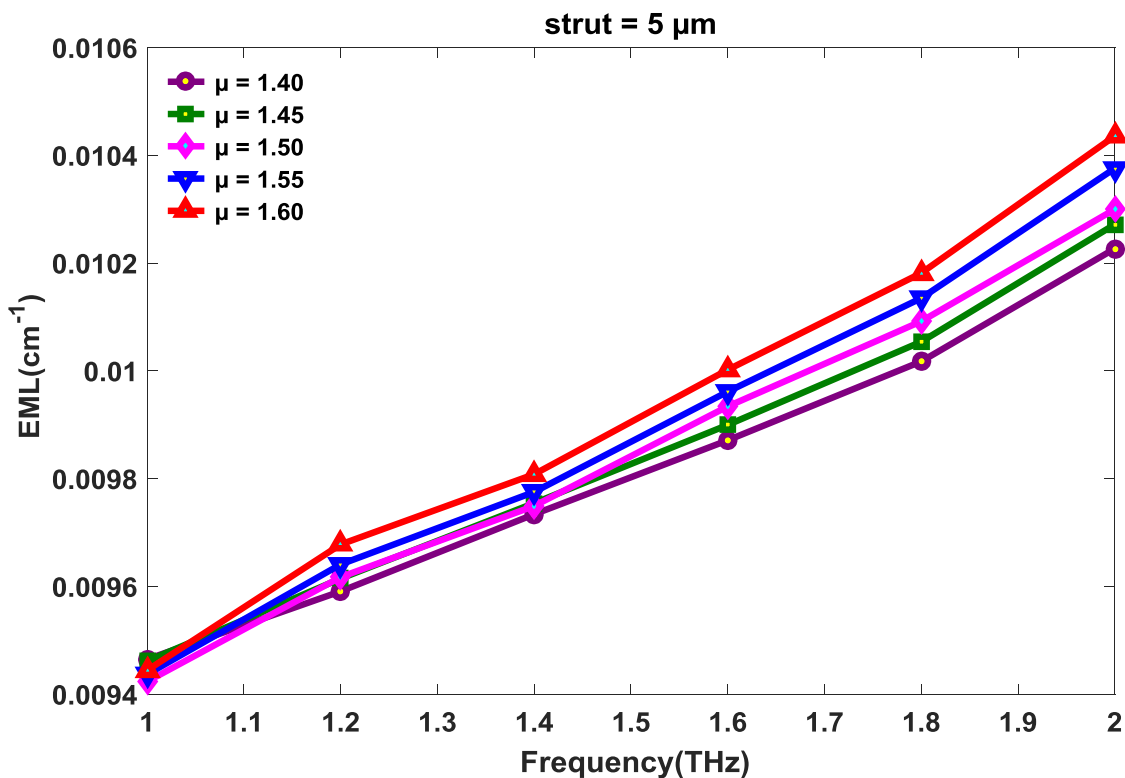


Figure 6.15: EML with respect to frequency at strut 5 μm for a bigger range of value of μ

Fig. 6.15 depicts the behavior of EML responses with respect to frequency. In the above figure it is shown that the EML with respect to frequency for strut width of 5 μm behaves like figure 6.11. This relation satisfies the empirical formulation of EML which is depicted in equation 4.1 in

chapter 4. The characteristics of figure 6.15 is similar to the figure no 6.12, 6.13 and 6.14 respectively.

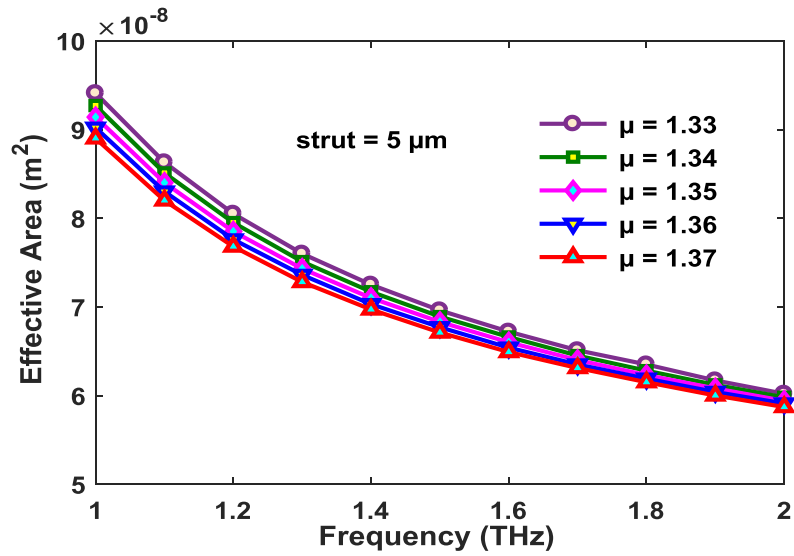


Figure 6.16: Effect of frequency on effective area at strut 5 μm

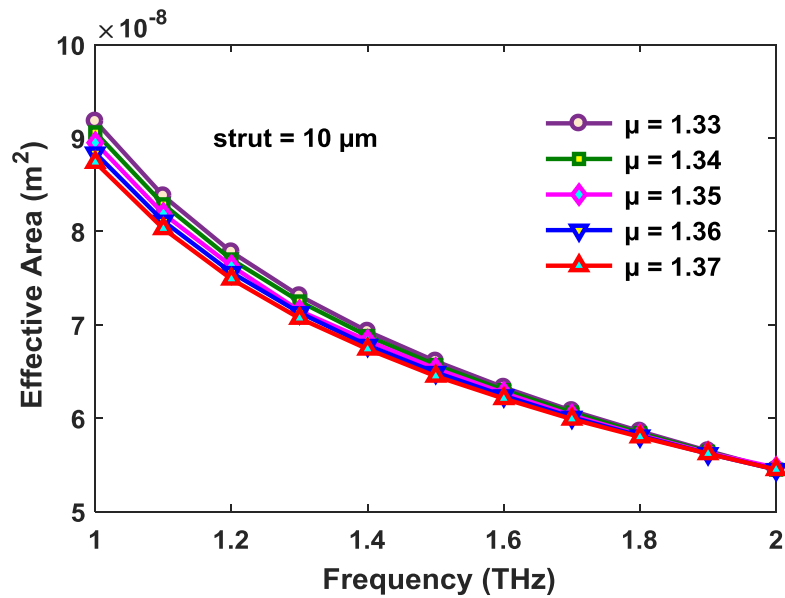


Figure 6.17: Effect of frequency on effective area at strut 10 μm

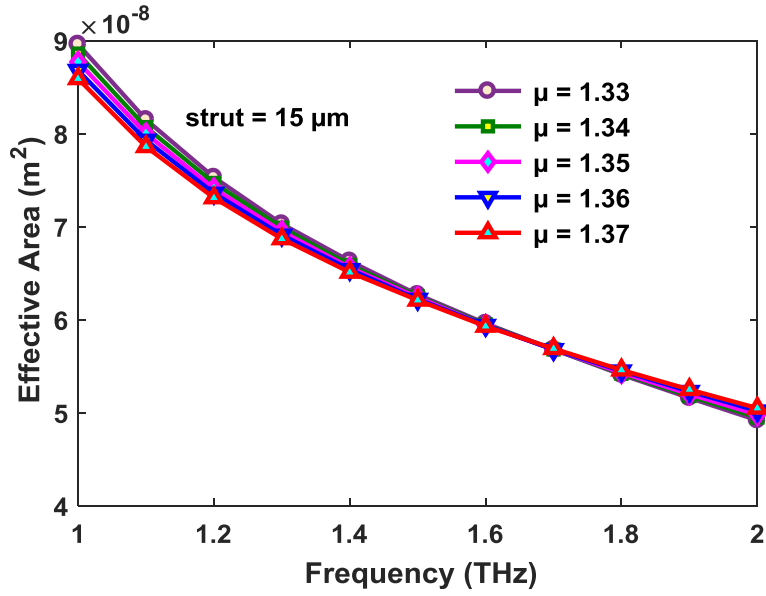


Figure 6.18: Effect of frequency on effective area at strut 15 μ m

Fig. 6.16, 6.17 and 6.18 depict the effect of frequency on effective area at different strut width. From above figures it have been noticed that effective area is decreasing sharply with the incremental value of frequency because light is tightly confined in the core of PCF at higher frequency. The reason behind this, at higher frequency light is tightly confined in the core of PCF. That's why effective area is decreased at higher frequency level. At optimal design parameter an effective area of $6.96 \times 10^{-8} \text{ m}^2$, $6.89 \times 10^{-8} \text{ m}^2$, $6.83 \times 10^{-8} \text{ m}^2$, $6.77 \times 10^{-8} \text{ m}^2$, $6.71 \times 10^{-8} \text{ m}^2$ have been achieved for a refractive index of 1.33, 1.34, 1.35, 1.36 and 1.37 respectively. It is also observed from the above figure that with the increment of strut size, effective area is decreasing. This is because when the when the strut size is increased then the amount of background material in the core will increase and as a result maximum light will pass through the core. It is noted that light always try to pass through the solid path. If maximum amount of light pass through the core then the designed fiber shows tight confinement. As a result effective area is decreased.

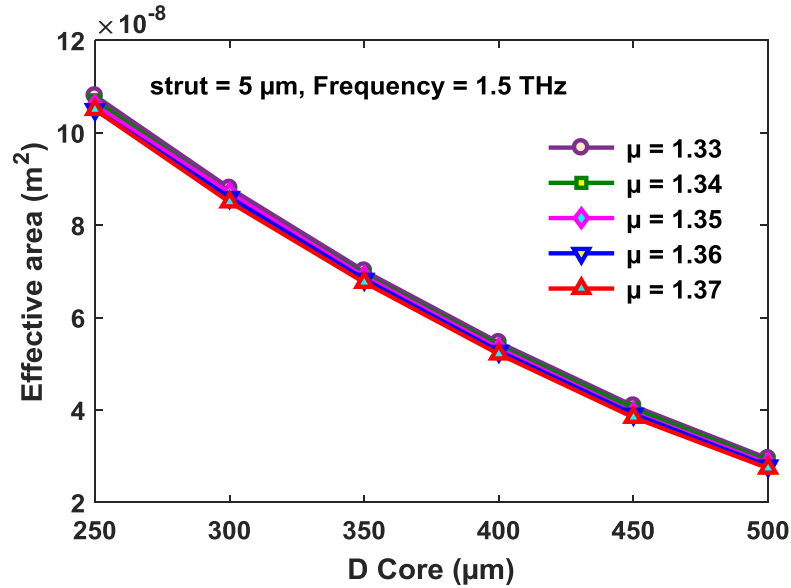


Figure 6.19: Effect of core diameter D Core (μm) on effective area at strut $5\mu\text{m}$

Figure 6.19 depicts the scenario of effective area with the core diameter. From above figure it is noticed that when the value of core diameter is scaled up then effective area is decreasing. The reason behind that is, when the value of core diameter is increased then maximum light will pass through the core region. As a result light shows a tight confinement through the core, that's why the effective area will decrease.

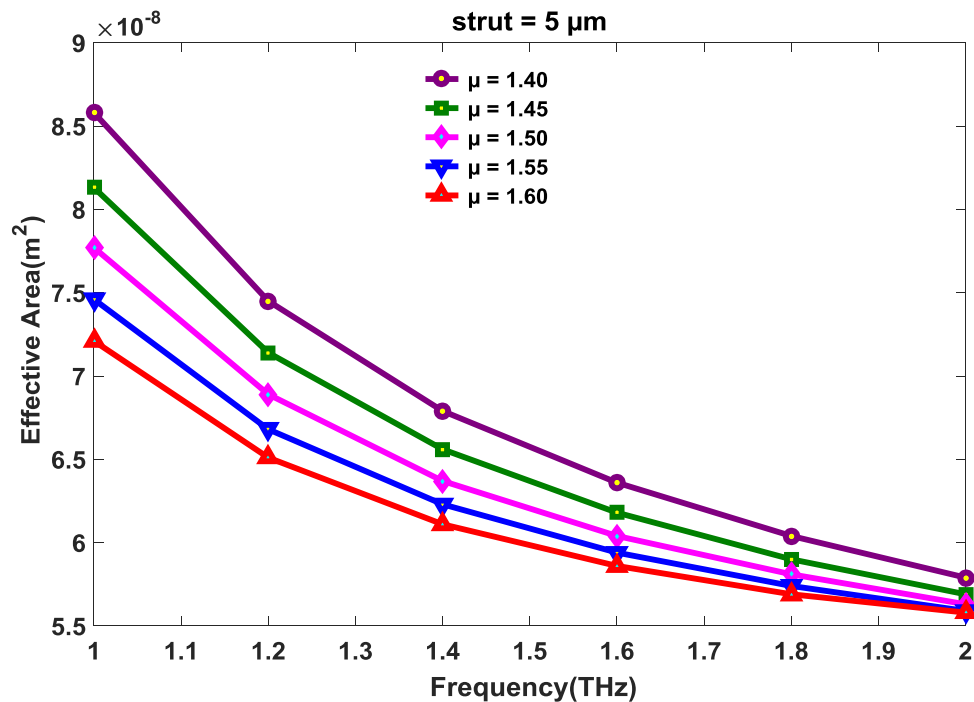


Figure 6.20: Effect of frequency on EML at strut $5\mu\text{m}$ for a bigger range of value of μ

Fig. 6.20 depicts the response of Effective area with respect to frequency. In the above figure it is shown that the effective area with respect to frequency for strut width of $5\mu\text{m}$ behaves like figure 6.16. The characteristics of figure 6.20 is similar to the figure no 6.12, 6.13 and 6.14 respectively.

Numerical aperture is considered another imperative specification of a fiber, which relies upon the contrast between the refractive indices of the cladding and the core. For medical imaging techniques higher order of numerical aperture is very essential factor. The numerical aperture (NA) can be determined by the accompanying condition.

$$NA \approx \left(1 + \frac{\pi A_{eff}}{\lambda^2}\right)^{\frac{1}{2}} \quad 6.2$$

Where λ and A_{eff} denotes the wavelength and modal effective area respectively.

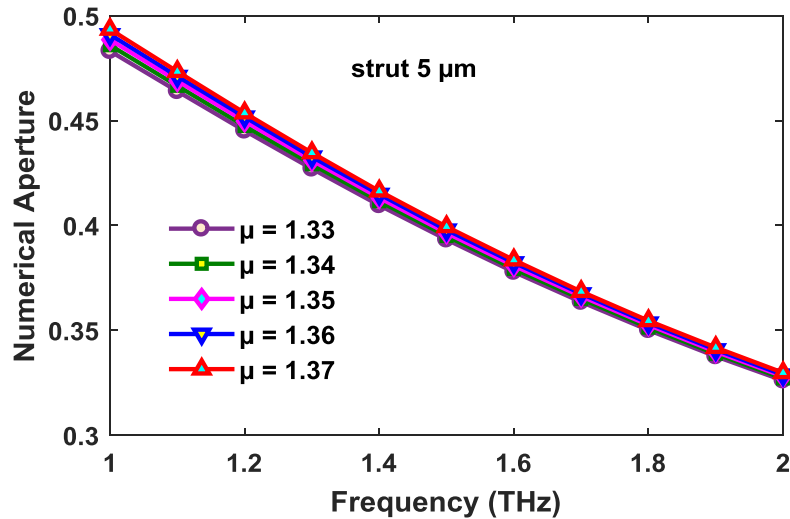


Figure 6.21: Effect of frequency on numerical aperture at strut $5\mu\text{m}$

From figure 6.21 it is noticed that numerical aperture (NA) is decreasing with the gradual estimation of frequency. The determined numerical aperture attributes at considered design parameters are 0.3986, at $\mu = 1.33$, 0.396, at $\mu = 1.34$, 0.397, at $\mu = 1.35$, 0.397, at $\mu = 1.36$, and 0.398, at $\mu = 1.37$.

Beam divergence and spot size can be considered as two imperative parameters for structuring a biosensor. To find out the spot size of proposed PCF sensor an intimate relationship will have to establish between V-parameter and spot size. Marcuse formula has been established to determine the equation of spot size(W_{eff}), which can be expressed by the following equation.

$$W_{eff} = R \times \left(0.65 + \frac{1.619}{V^{\frac{3}{2}}} + \frac{2.789}{V^6} \right) \quad 6.3$$

Where V and R represents the symbol of normalized value of V-parameter and radius of air hole respectively. So as to decide the beam divergence, here is used spot size. Beam divergence of the PCF can be learned utilizing the Gaussian beam theory, which can be expressed by the following theory.

$$\theta = \tan^{-1} \left(\frac{\lambda}{\pi W_{eff}} \right) \quad 6.4$$

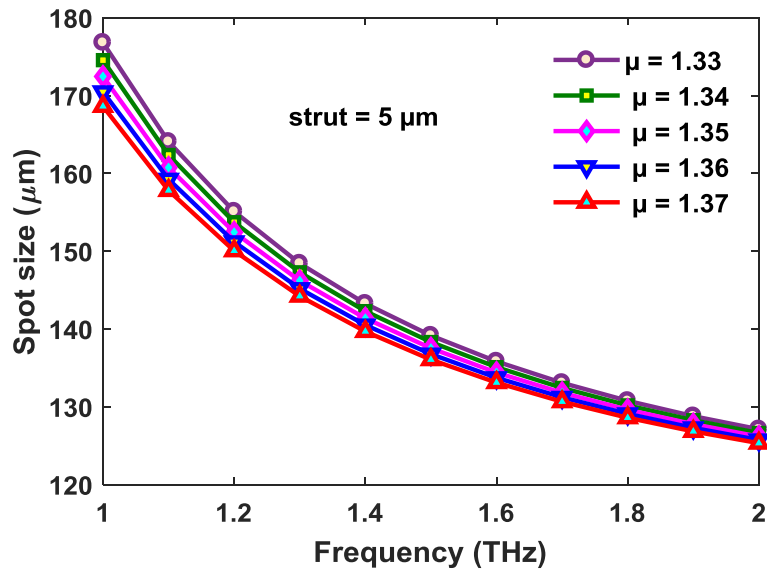


Figure 6.22: Spot size as a function of frequency at strut 5 μm

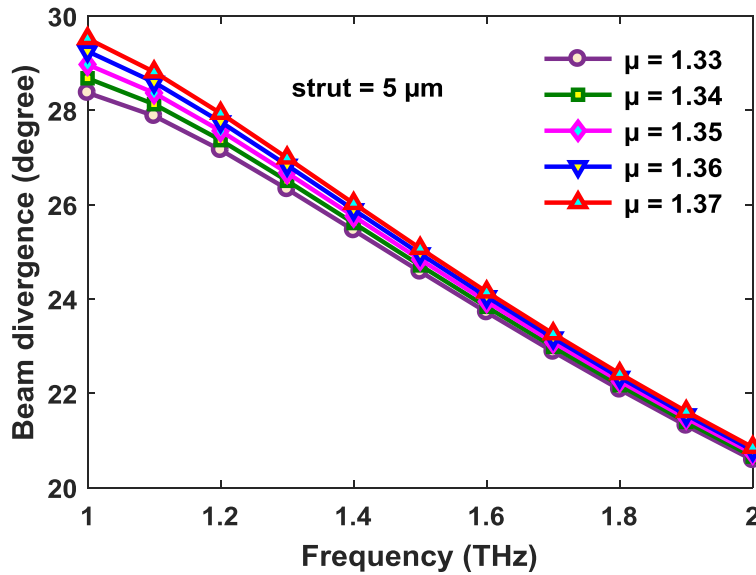


Figure 6.23: Beam divergence as a function of frequency at strut 5 μm

Fig. 6.22 depicts the scenario between frequency and spot size in THz range for different analytes. Fig. 6.22 likewise demonstrates that the higher THz range shows lower spot size reaction. In spite of the fact that it can be seen that for the different refractive indices the subsequent spot size are nearly equal yet really there exists a deviation. Deviation of the spot size for all parts are appeared inside a similar figure. At optimal design condition determined spot sizes are 136.1 μm, 136.8 μm, 137.5 μm, 138.3 μm and 132.5 μm for $\mu = 1.33, 1.34, 1.35, 1.36, 1.37$ respectively. The designed sensor shows higher spot size for all researched analytes at 1.5 THz frequency.

Beam divergence of an optical fiber can be assessed by the amount of light beam which will be passed through the core. It is considered as an important parameter related to splicing, sensing and laser beam focusing. Beam quality can be assessed by observing superior beam divergence. The relationship between beam divergence and frequency are illustrated in fig. 6.20. At optimal design parameter beam divergences are 25.08°, 24.96°, 24.84°, 24.71°, 24.58° for $\mu=1.33, 1.34, 1.35, 1.36$ and 1.37 respectively.

Table 6.1: Performance comparison of the demonstrated design with previously designed sensors

Ref	Analyte	Sensitivity(%)	Lc	EML (cm ⁻¹)	A _{eff} (μm ²)
[143]	n=1.35	55.83	10 ⁻¹⁰ db/m	---	---
[146]	n=1.35	67.66	3.28×10 ⁻¹¹ db/m	-----	---
[154]	n=1.35	61.45	1.41×10 ⁻¹⁰ db/m	----	4.57
[155]	n=1.35	52.22	----	---	---
[156]	n=1.35	85.7	1.7×10 ⁻⁹ cm ⁻¹	---	69800
Proposed Sensor	n=1.33	91.8%	2.88×10 ⁻⁹ cm ⁻¹	0.009694	6.96×10 ⁻²
	n=1.34	92.0%	2.69×10 ⁻⁹ cm ⁻¹	0.009658	6.89×10 ⁻²
	n=1.35	92.2%	2.502×10 ⁻⁹ cm ⁻¹	0.009624	6.83×10 ⁻²
	n=1.36	92.3%	2.308×10 ⁻⁹ cm ⁻¹	0.009620	6.77×10 ⁻²
	n=1.37	92.4%	2.11×10 ⁻⁹ cm ⁻¹	0.009698	6.71×10 ⁻²

Finally a comparison with the existing works are presented in table 6.1. Above mentioned table describes a comparison among other existing sensor and the one we have designed. This table describes that the designed sensor has not only achieved highest sensitivity but also displayed minimum EML and Confinement Loss, and moderate modal effective area also.

6.3 Proposed sensor's experimental setup

The proposed sensor's experimental setup is shown in Fig. 2. At first, a super continuum light source with a spectrum range of 450 nm to 1600 nm launched the incident light. To process this, Super K compact, NKT Photonics™ could be utilized [160]. Afterwards the light is transferred through the polarizer which is accompanied with a polarizer controller. The polarized light then passes through the sensor with the help of a single-mode fiber (SMF-28). The light then transported to an Optical Spectrum Analyzer (AQ6370C, Yokokawa™) using a single-mode fiber [160]. It is become possible to couple the sensor with SMF-28 in a proper manner because of method known as splicing. The splicing could be attained by using Vytran FFS-2000 splicer using the filament fusion methodology, and the SMF & the PCF can be aligned using manual-mode rotational and translational alignment[160]. Another splicing method can be introduced with a coupling efficiency of 84.5% that connects the SMF & the PCF by inserting an etched SMF tip into the PCF [34]. Moreover, many high-efficiency SMF-PCF couplers has been introduced by the researchers that could be utilized in our experiment as well[161],[162]. So, an SMF with a coupling efficiency range of 80–90% could be connected to our proposed sensor. To facilitate the liquid analyte inlet & outlet an analyte channel is implanted at a suitable position

which shown in Fig. 6.24. A programmable micro injection pumper (LSP01-1A, Longer Pump™) is used to inject the analyte inside the channel[160]. The used analyte will be stored in waste reservoir, which is connected with the channel's outlet. The resonance wavelength shifted towards higher or lower wavelengths due to the existence of several unknown analytes. These spectrums could be identified using an optical spectrum analyzer. Finally, the inspection of wavelength peak shifts is done by using a computer where the final attained output spectrums are exhibited.

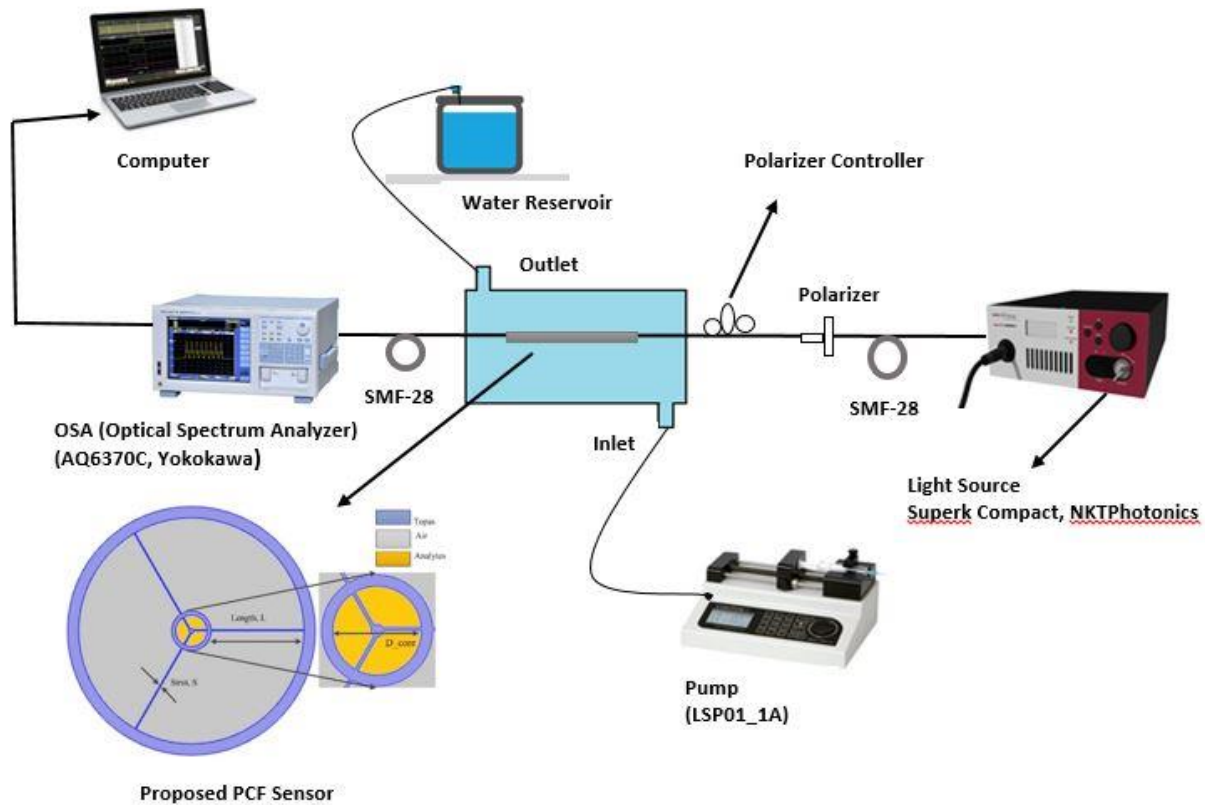


Figure 6.24: Exploratory arrangement schematic of the proffered sensor for experimental sensing applications[163].

6.4 Feasibility Assessment of Fabrication

Fabrication of a proposed design is a key concern for researchers. Different number of fabrication techniques such as Sol-gel, Stack and draw, 3D printing, Capillary stacking etc have already been developed for PCF fabrication[164],[165],[166],[167]. Some process of fabrication are suitable for hexagonal air hole structure, some are for elliptical, circular, rectangular or square shaped cladding and core structured PCF[168]. Besides some process are able to fabricate asymmetrical structured PCF and some are for symmetrical structured PCF. The proposed PCF based sensor is constructed by circular sectored core and cladding. By using extrusion technique, various types of structure have been fabricated by Max Plank Institute. Moreover 3D printing

fabrication technique is capable to fabricate any types of asymmetrical and symmetrical PCF structure[129]. So the proposed design can easily fabricate by using 3D printing and extrusion technique[168],[129],[169].

6.5 Contribution of this research:

In this research a simple PCF waveguide is designed whose core cladding follows the same geometric structure. It is assured that this type of simple geometric structure was not reported previously[19],[170],[171],[172]. All of them uses different types of core-cladding but in our proposed design we have used simple and similar geometric pattern for core-cladding. For waveguide designing porous core is chosen because if porous core is used then light interaction with the background material of core is reduced. When light goes minimum interaction the with background material then EML will be reduced. That's why our designed THz waveguide shows a lower value of EML comparatively with others[34],[14],[173],[174]. Our main objective was to design a THz waveguide but after designing a waveguide we implement the same design for sensing application. After implementing the proposed design in sensing application it shows an average sensitivity of 92.2% for different liquid analytes. In previous research works it is noticed that different researcher have implemented different designs for waveguide and sensing applications[171][175][19][172] but in this research we have implemented the same design for waveguide and sensing applications.

6.6 Conclusion:

A sectored circular porous core PCF is proposed for liquid analytes sensing with various refractive indices at THz frequency range. At optimal design parameter, proposed design shows a high sensitivity of 91.8%,92.0%, 92.2% , 92.34%, 92.48% and low confinement loss of 2.88×10^{-9} per centimeter, 2.69×10^{-9} per centimeter, 2.302×10^{-9} per centimeter, 2.308×10^{-9} per centimeter, 2.11×10^{-9} per centimeter for refractive indices of 1.33, 1.34, 1.35, 1.36, and 1.37 respectively. Besides moderate effective area and lower EML at optimal design condition have been achieved. Existing fabrication techniques are implementable in the proposed design. To end up, it can be concluded that the proposed sensor is capable to detect a wide variety of chemical in the industrial and medical sectors.

Chapter 7

Conclusion and Future work

7.1 Conclusion

In this thesis a sectorized circular core cladding photonic crystal fiber (PCF) based THz waveguide and sensor had been proposed. There were two key concerns of the proposed design. One was to demonstrate a well-guided single THz waveguide but maintaining minimum losses and another one was to characterize different properties of the designed PCF-based THz sensor, for various chemical substances of different refractive indices. Successfully two of the expected goals have been achieved.

For THz waveguide, an optimal condition of 0.9 THz operating frequency, core diameter of 350 μm , and porosity of 90% have been selected. At optimal design condition, low EML (Effective Material Loss) of 0.022 cm^{-1} has been achieved. Moreover, other parameters such as Core power fraction of 35%, Confinement loss of 0.01 cm^{-1} , V-Parameter of 0.75 and nearly flattened dispersion for optimal design were also obtained.

On the other hand, the same design was implemented for sensing application. An optimal condition of 1.5 THz operating frequency and Core diameter of 350 μm has been selected. The frequency range was varied from 1 to 2 THz. For both cases (waveguide and sensing) Topas was selected as a background material. At optimal design condition, an average sensitivity of 92.14 % and an average lower confinement loss of $2.458 \times 10^{-9} \text{cm}^{-1}$ have been achieved. Besides moderate effective area and lower material absorption loss were also achieved. It can be concluded that the proposed designed PCF is highly suitable for practical implementation for both THz waveguide and sensor also.

7.2 Future Work:

In this thesis, various properties of THz waveguide and sensor of the proposed design have been analyzed but there are some features which haven't been analyzed yet. Such as Bending Loss (BL), Total Loss (TL) etc. The above-mentioned factors can be analyzed in the proposed design.

Recently a new field of research named surface plasma resonance (SPR) has been started. The demonstrated design has not been implemented in the field of SPR. The demonstrated design can be improved for implementing in the field of SPR.

In our proposed THz sensor, we have taken the refractive index in the range from 1.33 to 1.37 but this range can be increased to 1.39. Then most of the liquid analytes will be analyzed.

Design of the core can be shifted to 90° so that the range of EML will probably decrease and sensitivity will probably increase.

Background material of the proposed design can be changed to observe the effect of EML, Confinement loss, Sensitivity etc.

In proposed design, the core isn't hollow core. Designed core is sectorial circular core. By designing the proposed PCF as a hollow core, its effect on EML, effective area, dispersion and bending loss can be observed.

The demonstrated design was simulated in THz frequency range but it can be shifted to GHz and MHz frequency range to observe the effect of sensitivity, EML, effective area, numerical aperture throughout the investigation procedure.

In this thesis, THz technology was focused in wave guide and sensing application but it can implement in medical application for breast cancer detection and these effective dielectric estimations might be utilized to decide the cancer cell fixation in the samples. Furthermore, these non-disastrous dielectric estimations at terahertz frequencies might be correlative to low-frequency estimations of cancer cell fixations. Moreover, THz pictures of breast tissue in a relative report with MRI, X-beam, and fluorescence microscopy study are probably going to give correlative data to detect malignant neoplastic disease.

Concerning future viewpoints, terahertz spectroscopy is obviously not fit to be actualized in a clinical apparatus. More work is expected to explain the connection of terahertz radiation with organic tissues at miniature and large scale levels. One of the following stages could be the subjective and quantitative extraction of the various pieces of a tissue, for example, fibrosis and fat. This could be at first evolved with tissue apparition spectroscopy and chemo metric instruments.

Finally, further information is expected of the collaboration of THz radiation with tissue, potentially by breaking down the reaction at the cell level. To accomplish this point, some researchers are dealing with the improvement of near field sensor capable of isolating cells from fibers and the way to execute this new sort of imaging sensor.

References

- [1] D. Abbott and X. C. Zhang, "Scanning the issue: T-ray imaging, sensing, and detection," *Proceedings of the IEEE*, 2007, doi: 10.1109/JPROC.2007.900894.
- [2] W. Withayachumnankul *et al.*, "T-ray sensing and imaging," 2007, doi: 10.1109/JPROC.2007.900325.
- [3] M. M. Awad and R. A. Cheville, "Transmission terahertz waveguide-based imaging below the diffraction limit," *Appl. Phys. Lett.*, 2005, doi: 10.1063/1.1942637.
- [4] D. J. Cook, B. K. Decker, and M. G. Allen, "Quantitative THz spectroscopy of explosive materials," *Opt. InfoBase Conf. Pap.*, p. MA6, Mar. 2005, doi: 10.1364/otst.2005.ma6.
- [5] C. J. Strachan *et al.*, "Using terahertz pulsed spectroscopy to quantify pharmaceutical polymorphism and crystallinity," *J. Pharm. Sci.*, 2005, doi: 10.1002/jps.20281.
- [6] R. M. Woodward, V. P. Wallace, D. D. Arnone, E. H. Linfield, and M. Pepper, "Terahertz Pulsed Imaging of skin cancer in the time and frequency domain," 2003, doi: 10.1023/A:1024409329416.
- [7] D. A. Crawley *et al.*, "Terahertz pulse imaging: A pilot study of potential applications in dentistry," *Caries Res.*, 2003, doi: 10.1159/000072167.
- [8] R. Köhler *et al.*, "Terahertz semiconductor-heterostructure laser," *Nature*, 2002, doi: 10.1038/417156a.
- [9] N. E. Karpowicz, J. Chen, T. Tongue, and X. C. Zhang, "Coherent millimetre wave to mid-infrared measurements with continuous bandwidth reaching 40 THz," *Electron. Lett.*, 2008, doi: 10.1049/el:20080356.
- [10] Q. Wu, M. Litz, and X. C. Zhang, "Broadband detection capability of ZnTe electro-optic field detectors," *Appl. Phys. Lett.*, 1995, doi: 10.1063/1.116356.
- [11] B. Bowden, J. A. Harrington, and O. Mitrofanov, "Silver/polystyrene coated hollow glass waveguides for the transmission of THz radiation," 2007, doi: 10.1364/ol.32.002945.
- [12] M. Goto, A. Quema, H. Takahashi, S. Ono, and N. Sarukura, "Teflon Photonic Crystal Fiber as Terahertz Waveguide," *Japanese J. Appl. Physics, Part 2 Lett.*, 2004, doi: 10.1143/jjap.43.1317.
- [13] K. Nielsen, H. K. Rasmussen, A. J. Adam, P. C. Planken, O. Bang, and P. U. Jepsen, "Bendable, low-loss Topas fibers for the terahertz frequency range," *Opt. Express*, 2009, doi: 10.1364/oe.17.008592.
- [14] M. S. Islam, J. Sultana, A. Dinovitser, B. W. H. Ng, and D. Abbott, "A novel Zeonex based oligoporous-core photonic crystal fiber for polarization preserving terahertz applications," *Opt. Commun.*, 2018, doi: 10.1016/j.optcom.2017.12.061.

- [15] L.-J. Chen, H.-W. Chen, T.-F. Kao, J.-Y. Lu, and C.-K. Sun, "Low-loss subwavelength plastic fiber for terahertz waveguiding," *Opt. Lett.*, 2006, doi: 10.1364/ol.31.000308.
- [16] R. Islam, G. K. M. Hasanuzzaman, M. S. Habib, S. Rana, and M. A. G. Khan, "Low-loss rotated porous core hexagonal single-mode fiber in THz regime," *Opt. Fiber Technol.*, vol. 24, pp. 38–43, Aug. 2015, doi: 10.1016/j.yofte.2015.04.006.
- [17] H. Han, H. Park, M. Cho, and J. Kim, "Terahertz pulse propagation in a plastic photonic crystal fiber," *Appl. Phys. Lett.*, vol. 80, no. 15, pp. 2634–2636, Apr. 2002, doi: 10.1063/1.1468897.
- [18] K. Nielsen, H. K. Rasmussen, P. U. Jepsen, and O. Bang, "Porous-core honeycomb bandgap THz fiber," *Opt. Lett.*, 2011, doi: 10.1364/ol.36.000666.
- [19] M. Uthman, B. M. A. Rahman, N. Kejalakshmy, A. Agrawal, and K. T. V. Grattan, "Design and characterization of low-loss porous-core photonic crystal fiber," *IEEE Photonics J.*, vol. 4, no. 6, pp. 2315–2325, 2012, doi: 10.1109/JPHOT.2012.2231939.
- [20] S. F. Kaijage, Z. Ouyang, and X. Jin, "Porous-core photonic crystal fiber for low loss terahertz wave guiding," *IEEE Photonics Technol. Lett.*, vol. 25, no. 15, pp. 1454–1457, 2013, doi: 10.1109/LPT.2013.2266412.
- [21] M. I. Hasan, S. M. A. Razzak, G. K. M. Hasanuzzaman, and M. S. Habib, "Ultra-low material loss and dispersion flattened fiber for THz transmission," *IEEE Photonics Technol. Lett.*, vol. 26, no. 23, pp. 2372–2375, Dec. 2014, doi: 10.1109/LPT.2014.2356492.
- [22] M. S. Islam *et al.*, "Extremely low material loss and dispersion flattened TOPAS based circular porous fiber for long distance terahertz wave transmission," *Opt. Fiber Technol.*, 2017, doi: 10.1016/j.yofte.2016.11.014.
- [23] M. S. Islam, S. Rana, M. R. Islam, M. Faisal, H. Rahman, and J. Sultana, "Porous core photonic crystal fibre for ultra-low material loss in THz regime," *IET Commun.*, vol. 10, no. 16, pp. 2179–2183, Nov. 2016, doi: 10.1049/iet-com.2016.0227.
- [24] G. K. M. Hasanuzzaman, M. S. Habib, M. A. Hossain, S. M. A. Razzak, and Y. Namihira, "Low Loss Single-Mode Porous-Core Kagome Photonic Crystal Fiber for THz Wave Guidance," *J. Light. Technol. Vol. 33, Issue 19, pp. 4027-4031*, vol. 33, no. 19, pp. 4027–4031, Oct. 2015.
- [25] M. R. Hasan, M. A. Islam, and A. A. Rifat, "A single mode porous-core square lattice photonic crystal fiber for THz wave propagation," *J. Eur. Opt. Soc.*, vol. 12, no. 1, p. 15, Dec. 2016, doi: 10.1186/s41476-016-0017-5.
- [26] M. F. H. Arif, M. J. H. Biddut, K. Ahmed, and S. Asaduzzaman, "Simulation based analysis of formalin detection through photonic crystal fiber," 2016, doi: 10.1109/ICIEV.2016.7760106.
- [27] M. R. Hasan, S. Akter, M. S. Rahman, and K. Ahmed, "Design of a surface plasmon resonance refractive index sensor with high sensitivity," *Opt. Eng.*, 2017, doi:

10.1117/1.oe.56.8.087101.

- [28] H. Thenmozhi, M. S. Mani Rajan, and K. Ahmed, "D-shaped PCF sensor based on SPR for the detection of carcinogenic agents in food and cosmetics," *Optik (Stuttg.)*, 2019, doi: 10.1016/j.ijleo.2018.11.098.
- [29] K. Ahmed *et al.*, "Design of D-shaped elliptical core photonic crystal fiber for blood plasma cell sensing application," *Results Phys.*, 2019, doi: 10.1016/j.rinp.2019.02.026.
- [30] K. Ahmed *et al.*, "Refractive Index-Based Blood Components Sensing in Terahertz Spectrum," *IEEE Sens. J.*, 2019, doi: 10.1109/JSEN.2019.2895166.
- [31] I. S. Amiri *et al.*, "Tri-core photonic crystal fiber based refractive index dual sensor for salinity and temperature detection," *Microw. Opt. Technol. Lett.*, 2019, doi: 10.1002/mop.31612.
- [32] M. A. Jabin, K. Ahmed, M. J. Rana, B. K. Paul, Y. Luo, and D. Vigneswaran, "Titanium-Coated Dual-Core D-Shaped SPR-Based PCF for Hemoglobin Sensing," *Plasmonics*, 2019, doi: 10.1007/s11468-019-00961-6.
- [33] J. Sultana, M. S. Islam, J. Atai, M. R. Islam, and D. Abbott, "Near-zero dispersion flattened, low-loss porous-core waveguide design for terahertz signal transmission," *Opt. Eng.*, 2017, doi: 10.1117/1.oe.56.7.076114.
- [34] M. S. Islam *et al.*, "Zeonex-based asymmetrical terahertz photonic crystal fiber for multichannel communication and polarization maintaining applications," *Appl. Opt.*, 2018, doi: 10.1364/ao.57.000666.
- [35] M. S. Islam, M. Faisal, and S. M. A. Razzak, "Dispersion flattened extremely high-birefringent kagome lattice elliptic core photonic crystal fiber in THz regime," *Opt. Quantum Electron.*, 2019, doi: 10.1007/s11082-019-1744-9.
- [36] J. Sultana, M. S. Islam, K. Ahmed, A. Dinovitser, B. W.-H. Ng, and D. Abbott, "Terahertz detection of alcohol using a photonic crystal fiber sensor," *Appl. Opt.*, 2018, doi: 10.1364/ao.57.002426.
- [37] M. S. Islam *et al.*, "Liquid-infiltrated photonic crystal fiber for sensing purpose: Design and analysis," *Alexandria Eng. J.*, 2018, doi: 10.1016/j.aej.2017.03.015.
- [38] M. S. Islam *et al.*, "A novel approach for spectroscopic chemical identification using photonic crystal fiber in the terahertz regime," *IEEE Sens. J.*, 2018, doi: 10.1109/JSEN.2017.2775642.
- [39] "Waveguide." <https://whatis.techtarget.com/definition/waveguide>.
- [40] "Auston Switch," [Online]. Available: <https://www.revolvy.com/page/Auston-switch>.
- [41] "Microstrip," [Online]. Available: <https://en.wikipedia.org/wiki/Microstrip>.
- [42] "Circular Metallic Waveguide." https://www.oreilly.com/library/view/rf-and-microwave/9781118349571/c04_level1_7.xhtml#c04_fig_anc_0022.

- [43] "Hollow core fibers." https://www.rp-photonics.com/hollow_core_fibers.html.
- [44] I. Explorer, "IEEE Explorer," [Online]. Available: <https://ieeexplore.ieee.org/document/7875632>.
- [45] "Research Gate." [https://www.researchgate.net/publication/238400437_How_do_we_make_sense_of_the_p
rocess_of_legitimising_an_educational_action_research_thesis_for_the_award_of_a_PhD
_degree_A_contribution_to_educational_theory](https://www.researchgate.net/publication/238400437_How_do_we_make_sense_of_the_process_of_legitimising_an_educational_action_research_thesis_for_the_award_of_a_PhD_degree_A_contribution_to_educational_theory).
- [46] "Wikipedia." https://en.wikipedia.org/wiki/Photonic-crystal_fiber.
- [47] S. S. Mishra and V. K. Singh, "Comparative study of fundamental properties of honey comb photonic crystal fiber at 1.55 μ m wavelength," *J. Microwaves, Optoelectron. Electromagn. Appl.*, 2011, doi: 10.1590/S2179-10742011000200005.
- [48] "Techopedia." <https://www.techopedia.com/definition/24948/photonic-crystal-fiber-pcf>.
- [49] K. O. Hill and G. Meltz, "Fiber Bragg grating technology fundamentals and overview," *J. Light. Technol.*, 1997, doi: 10.1109/50.618320.
- [50] M. Szpulak, W. Urbanczyk, T. Martynkien, J. Wojcik, and W. J. Bock, "<title>Temperature sensitivity of photonic crystal holey fibers</title>," 2003, doi: 10.1117/12.497722.
- [51] Y. Colombe, D. H. Slichter, A. C. Wilson, D. Leibfried, and D. J. Wineland, "Single-mode optical fiber for high-power, low-loss UV transmission," *Opt. Express*, 2014, doi: 10.1364/oe.22.019783.
- [52] T. A. Birks, J. C. Knight, and P. S. J. Russell, "Endlessly single-mode photonic crystal fiber," *Opt. Lett.*, 1997, doi: 10.1364/ol.22.000961.
- [53] C. Hensley, D. H. Broaddus, C. B. Schaffer, and A. L. Gaeta, "Photonic band-gap fiber gas cell fabricated using femtosecond micromachining," *Opt. Express*, 2007, doi: 10.1364/oe.15.006690.
- [54] J. Ju, W. Jin, and M. S. Demokan, "Properties of a highly birefringent photonic crystal fiber," *IEEE Photonics Technol. Lett.*, 2003, doi: 10.1109/LPT.2003.818051.
- [55] J. M. Dudley, G. Genty, and S. Coen, "Supercontinuum generation in photonic crystal fiber," *Rev. Mod. Phys.*, 2006, doi: 10.1103/RevModPhys.78.1135.
- [56] R. Suresh, S. C. Tjin, and J. Hao, "Fiber Bragg Grating" in *Advanced Topics in Science and Technology in China*, 2012.
- [57] F. Jansen, F. Stutzki, C. Jauregui, J. Limpert, and A. Tünnermann, "High-power very large mode-area thulium-doped fiber laser," *Opt. Lett.*, 2012, doi: 10.1364/ol.37.004546.
- [58] W. Reeves, J. Knight, P. Russell, and P. Roberts, "Demonstration of ultra-flattened dispersion in photonic crystal fibers," *Opt. Express*, 2002, doi: 10.1364/oe.10.000609.

- [59] G. Vienne *et al.*, “Ultra-large bandwidth hollow-core guiding in all-silica Bragg fibers with nano-supports,” *Opt. Express*, 2004, doi: 10.1364/opex.12.003500.
- [60] P. Russell, “Recent advances in photonic crystal fibres,” 2004, doi: 10.1109/ictcon.2003.1264563.
- [61] J. D. Joannopoulos, S. G. Johnson, J. N. Winn, and R. D. Meade, *Photonic crystals: Molding the flow of light*. 2011.
- [62] C. Markos, J. C. Travers, A. Abdolvand, B. J. Eggleton, and O. Bang, “Hybrid photonic-crystal fiber,” *Rev. Mod. Phys.*, 2017, doi: 10.1103/RevModPhys.89.045003.
- [63] M. Hermatschweiler, A. Ledermann, G. A. Ozin, M. Wegener, and G. Von Freymann, “Fabrication of silicon inverse woodpile photonic crystals,” *Adv. Funct. Mater.*, 2007, doi: 10.1002/adfm.200601074.
- [64] W. Jin, H. F. Xuan, and H. L. Ho, “Sensing with hollow-core photonic bandgap fibers,” *Meas. Sci. Technol.*, 2010, doi: 10.1088/0957-0233/21/9/094014.
- [65] S. Brustlein *et al.*, “Double-clad hollow core photonic crystal fiber for coherent Raman endoscope,” *Opt. Express*, 2011, doi: 10.1364/oe.19.012562.
- [66] L. Duan and Y. Qiu, “Recent advances in organic electroluminescent materials and devices,” *Cailiao Yanjiu Xuebao/Chinese Journal of Materials Research*. 2015, doi: 10.11901/1005.3093.2014.724.
- [67] T. S. Saini, A. Kumar, and R. Kumar Sinha, “Broadband mid-IR supercontinuum generation in As₂Se₃ based chalcogenide photonic crystal fiber: A new design and analysis,” *Opt. Commun.*, 2015, doi: 10.1016/j.optcom.2015.02.049.
- [68] C. Huang *et al.*, “Ultraflat, broadband, and highly coherent supercontinuum generation in all-solid microstructured optical fibers with all-normal dispersion,” *Photonics Res.*, 2018, doi: 10.1364/prj.6.000601.
- [69] M. N. Hossen, M. Ferdous, M. Abdul Khalek, S. Chakma, B. K. Paul, and K. Ahmed, “Design and analysis of biosensor based on surface plasmon resonance,” *Sens. Bio-Sensing Res.*, 2018, doi: 10.1016/j.sbsr.2018.08.003.
- [70] M. R. Islam, M. F. Kabir, K. M. A. Talha, and M. S. Islam, “A novel hollow core terahertz refractometric sensor,” *Sens. Bio-Sensing Res.*, 2019, doi: 10.1016/j.sbsr.2019.100295.
- [71] J. . Chettle, D.R., Fremlin, “Physics in Medicine & Biology,” 1984.
- [72] B. H. Brown, R. H. Smallwood, D. C. Barber, P. V. Lawford, and D. R. Hose, *Medical physics and biomedical engineering*. 2017.
- [73] W. Shi, Q. Fang, X. Zhu, R. A. Norwood, and N. Peyghambarian, “Fiber lasers and their applications [Invited],” *Appl. Opt.*, 2014, doi: 10.1364/ao.53.006554.
- [74] I. Giles, “Fibre optics,” 1983, doi: 10.1088/0305-4624/14/3/408.

- [75] S. Matsuura and H. Ito, "Generation of CW terahertz radiation with photomixing," *Top. Appl. Phys.*, 2005, doi: 10.1007/10828028_6.
- [76] J. Y. Suen, W. Li, Z. D. Taylor, and E. R. Brown, "Characterization and modeling of a terahertz photoconductive switch," *Appl. Phys. Lett.*, 2010, doi: 10.1063/1.3374404.
- [77] P. Davidovits, *Physics in biology and medicine*. 2018.
- [78] R. K. Hobbie and B. J. Roth, *Intermediate physics for medicine and biology, fifth edition*. 2015.
- [79] N. Kukutsu and Y. Kado, "Overview of millimeter and terahertz wave application research," *NTT Technical Review*. 2009.
- [80] E. M. Abreu, P. Pereira, J. C. Marques, and G. Esteves, "Invasive lobular carcinoma: A rare presentation in the male breast," *BMJ Case Rep.*, 2016, doi: 10.1136/bcr-2016-215665.
- [81] A. J. Fitzgerald *et al.*, "Terahertz pulsed imaging of human breast tumors," *Radiology*, 2006, doi: 10.1148/radiol.2392041315.
- [82] "Cancer Council." <https://www.cancer.org.au/cancer-information/types-of-cancer/melanoma>.
- [83] O. Fejerskov, "Changing paradigms in concepts on dental caries: Consequences for oral health care," 2004, doi: 10.1159/000077753.
- [84] N. Pavel, "Medical physics," in *The New Physics*, 2012.
- [85] I. F. Akyildiz, J. M. Jornet, and C. Han, "Terahertz band: Next frontier for wireless communications," *Phys. Commun.*, 2014, doi: 10.1016/j.phycom.2014.01.006.
- [86] T. Nagatsuma *et al.*, "Terahertz wireless communications based on photonics technologies," *Opt. Express*, 2013, doi: 10.1364/oe.21.023736.
- [87] S. Koenig *et al.*, "Wireless sub-THz communication system with high data rate," *Nat. Photonics*, 2013, doi: 10.1038/nphoton.2013.275.
- [88] T. Nagatsuma, G. Ducournau, and C. C. Renaud, "Advances in terahertz communications accelerated by photonics," *Nat. Photonics*, vol. 10, no. 6, pp. 371–379, Jun. 2016, doi: 10.1038/nphoton.2016.65.
- [89] L.-J. Chen, H.-W. Chen, T.-F. Kao, J.-Y. Lu, and C.-K. Sun, "Low-loss subwavelength plastic fiber for terahertz waveguiding," *Opt. Lett.*, vol. 31, no. 3, p. 308, Feb. 2006, doi: 10.1364/ol.31.000308.
- [90] A. Hassani, A. Dupuis, and M. Skorobogatiy, "Low loss porous terahertz fibers containing multiple subwavelength holes," *Appl. Phys. Lett.*, 2008, doi: 10.1063/1.2840164.
- [91] A. Hassani, A. Dupuis, and M. Skorobogatiy, "Porous polymer fibers for low-loss Terahertz guiding," *Opt. Express*, 2008, doi: 10.1364/oe.16.006340.

- [92] A. M. R. Pinto and M. Lopez-Amo, "Photonic crystal fibers for sensing applications," *Journal of Sensors*. 2012, doi: 10.1155/2012/598178.
- [93] J. Arnaud, "Optical waveguide theory," *Optical and Quantum Electronics*. 1980, doi: 10.1007/BF00620035.
- [94] A. Bertoncini and C. Liberale, "3D Printed waveguides based on photonic crystal fiber designs for complex fiber-end photonic devices," *arXiv*. 2020, doi: 10.1364/optica.397281.
- [95] K. Saitoh, N. Florous, and M. Koshiba, "Ultra-flattened chromatic dispersion controllability using a defected-core photonic crystal fiber with low confinement losses," *Opt. Express*, 2005, doi: 10.1364/opex.13.008365.
- [96] S. Ali, N. Ahmed, S. Aljunid, and B. Ahmad, "Hybrid porous core low loss dispersion flattened fiber for THz propagation," *Photonics Nanostructures - Fundam. Appl.*, 2016, doi: 10.1016/j.photonics.2016.09.003.
- [97] S. J. Oh *et al.*, "Measurement depth enhancement in terahertz imaging of biological tissues," *Opt. Express*, 2013, doi: 10.1364/oe.21.021299.
- [98] M. Selim Habib, M. Samiul Habib, S. M. Abdur Razzak, Y. Namihira, M. A. Hossain, and M. A. Goffar Khan, "Broadband dispersion compensation of conventional single mode fibers using microstructure optical fibers," *Optik (Stuttg.)*, 2013, doi: 10.1016/j.ijleo.2012.12.014.
- [99] N. N. Chen, J. Liang, and L. Y. Ren, "High-birefringence, low-loss porous fiber for single-mode terahertz-wave guidance," *Appl. Opt.*, 2013, doi: 10.1364/AO.52.005297.
- [100] S. Chowdhury, S. Sen, K. Ahmed, and S. Asaduzzaman, "Design of highly sensible porous shaped photonic crystal fiber with strong confinement field for optical sensing," *Optik (Stuttg.)*, 2017, doi: 10.1016/j.ijleo.2017.03.123.
- [101] COMSOL, "Introduction to COMSOL Multiphysics 5.3," *Manual*, 2014.
- [102] Comsol, *Multiphysics COMSOL*. 2010.
- [103] COMSOL, *Modeling Guide*. 2010.
- [104] COMSOL Multiphysics, "Optimization Module," *User's Guid.*, 2015.
- [105] S. G. Johnson and J. D. Joannopoulos, "Electromagnetic theory," in *Encyclopedia of Modern Optics*, 2018.
- [106] E. E. Method, "Standard Practice for Determining Electrical Conductivity Using the," *Society*, 2000.
- [107] C. B. Reid, E. Pickwell-Macpherson, J. G. Laufer, A. P. Gibson, J. C. Hebden, and V. P. Wallace, "Accuracy and resolution of THz reflection spectroscopy for medical imaging," *Phys. Med. Biol.*, vol. 55, no. 16, pp. 4825–4838, 2010, doi: 10.1088/0031-9155/55/16/013.

- [108] M. R. Leahy-Hoppa, M. J. Fitch, X. Zheng, L. M. Hayden, and R. Oslander, "Wideband terahertz spectroscopy of explosives," *Chem. Phys. Lett.*, 2007, doi: 10.1016/j.cplett.2006.12.015.
- [109] K. Kawase, Y. Ogawa, Y. Watanabe, and H. Inoue, "Non-destructive terahertz imaging of illicit drugs using spectral fingerprints," *Opt. Express*, vol. 11, no. 20, p. 2549, Oct. 2003, doi: 10.1364/oe.11.002549.
- [110] Y. L. Hoo, W. Jin, C. Shi, H. L. Ho, D. N. Wang, and S. C. Ruan, "Design and modeling of a photonic crystal fiber gas sensor," *Appl. Opt.*, 2003, doi: 10.1364/ao.42.003509.
- [111] M. Nagel, P. Haring Bolivar, M. Brucherseifer, H. Kurz, A. Bosserhoff, and R. Büttner, "Integrated THz technology for label-free genetic diagnostics," *Appl. Phys. Lett.*, vol. 80, no. 1, pp. 154–156, Jan. 2002, doi: 10.1063/1.1428619.
- [112] M. S. Islam, M. Faisal, and S. M. A. Razzak, "Dispersion flattened porous-core honeycomb lattice terahertz fiber for ultra low loss transmission," *IEEE J. Quantum Electron.*, 2017, doi: 10.1109/JQE.2017.2760361.
- [113] J. Y. Lu *et al.*, "Terahertz air-core microstructure fiber," *Appl. Phys. Lett.*, vol. 92, no. 6, 2008, doi: 10.1063/1.2839576.
- [114] G. Zhao, M. ter Mors, T. Wenckebach, and P. C. M. Planken, "Terahertz dielectric properties of polystyrene foam," *J. Opt. Soc. Am. B*, vol. 19, no. 6, p. 1476, Jun. 2002, doi: 10.1364/josab.19.001476.
- [115] S. Rana, G. K. M. Hasanuzzaman, S. Habib, S. F. Kaijage, and R. Islam, "Proposal for a low loss porous core octagonal photonic crystal fiber for T-ray wave guiding," *Opt. Eng.*, vol. 53, no. 11, p. 115107, Nov. 2014, doi: 10.1117/1.oe.53.11.115107.
- [116] M. S. Islam, S. Rana, M. R. Islam, M. Faisal, H. Rahman, and J. Sultana, "Porous core photonic crystal fibre for ultra-low material loss in THz regime," *IET Commun.*, 2016, doi: 10.1049/iet-com.2016.0227.
- [117] F. A. Mou, M. M. Rahman, M. A. Al Mahmud, M. R. Islam, and M. I. H. Bhuiyan, "Design and Characterization of a Low Loss Polarization Maintaining Photonic Crystal Fiber for THz Regime," 2019, doi: 10.1109/ICTP48844.2019.9041715.
- [118] M. S. Islam, J. Sultana, J. Atai, M. R. Islam, and D. Abbott, "Design and characterization of a low-loss, dispersion-flattened photonic crystal fiber for terahertz wave propagation," *Optik (Stuttg.)*, vol. 145, pp. 398–406, Sep. 2017, doi: 10.1016/j.ijleo.2017.07.061.
- [119] R. Islam, G. K. M. Hasanuzzaman, M. A. Sadath, S. Rana, and M. S. Habib, "Extremely low-loss single-mode photonic crystal fiber in the terahertz regime," 2016, doi: 10.1109/CEEE.2015.7428279.
- [120] M. Moshir Rahman, F. Akter Mou, M. Imamul Hassan Bhuiyan, and M. Rakibul Islam, "Design and characterization of a circular sector core cladding structured photonic crystal fiber with ultra-low EML and flattened dispersion in the THz regime," *Opt. Fiber Technol.*, 2020, doi: 10.1016/j.yofte.2020.102158.

- [121] M. Sheikholeslami, B. Rezaeianjouybari, M. Darzi, A. Shafee, Z. Li, and T. K. Nguyen, "Application of nano-refrigerant for boiling heat transfer enhancement employing an experimental study," *Int. J. Heat Mass Transf.*, 2019, doi: 10.1016/j.ijheatmasstransfer.2019.07.043.
- [122] X. Ma, M. Sheikholeslami, M. Jafaryar, A. Shafee, T. Nguyen-Thoi, and Z. Li, "Solidification inside a clean energy storage unit utilizing phase change material with copper oxide nanoparticles," *J. Clean. Prod.*, 2020, doi: 10.1016/j.jclepro.2019.118888.
- [123] H. Bao, K. Nielsen, H. K. Rasmussen, P. U. Jepsen, and O. Bang, "Fabrication and characterization of porous-core honeycomb bandgap THz fibers," *Opt. Express*, 2012, doi: 10.1364/oe.20.029507.
- [124] M. S. Islam, J. Sultana, J. Atai, D. Abbott, S. Rana, and M. R. Islam, "Ultra low-loss hybrid core porous fiber for broadband applications," *Appl. Opt.*, 2017, doi: 10.1364/ao.56.001232.
- [125] F. A. Mou, M. M. Rahman, M. R. Islam, and M. I. H. Bhuiyan, "Development of a photonic crystal fiber for THz wave guidance and environmental pollutants detection," *Sens. Bio-Sensing Res.*, 2020, doi: 10.1016/j.sbsr.2020.100346.
- [126] Z. Wu *et al.*, "Low-loss polarization-maintaining THz photonic crystal fiber with a triple-hole core," *Appl. Opt.*, 2017, doi: 10.1364/ao.56.002288.
- [127] "Max Planck Institute." <https://mpl.mpg.de/divisions/russell-division/research/>.
- [128] K. M. Kiang *et al.*, "Extruded singlemode non-silica glass holey optical fibres," *Electron. Lett.*, vol. 38, no. 12, pp. 546–547, Jun. 2002, doi: 10.1049/el:20020421.
- [129] W. Talataisong *et al.*, "Novel method for manufacturing optical fiber: extrusion and drawing of microstructured polymer optical fibers from a 3D printer," *Opt. Express*, vol. 26, no. 24, p. 32007, Nov. 2018, doi: 10.1364/oe.26.032007.
- [130] M. R. Wagner *et al.*, "Two-Dimensional Phononic Crystals: Disorder Matters," *Nano Lett.*, 2016, doi: 10.1021/acs.nanolett.6b02305.
- [131] J. M. Fini, "Microstructure fibres for optical sensing in gases and liquids," *Meas. Sci. Technol.*, 2004, doi: 10.1088/0957-0233/15/6/011.
- [132] Aihan-Yin and L. Xiong, "Highly nonlinear with low confinement losses square photonic crystal fiber based on a four-hole unit," *Infrared Phys. Technol.*, 2014, doi: 10.1016/j.infrared.2014.05.006.
- [133] H. Ademgil and S. Haxha, "Highly birefringent nonlinear PCF for optical sensing of analytes in aqueous solutions," *Optik (Stuttg.)*, 2016, doi: 10.1016/j.ijleo.2016.04.137.
- [134] M. S. Islam, J. Sultana, A. A. Rifat, A. Dinovitser, B. Wai-Him Ng, and D. Abbott, "Terahertz sensing in a hollow core photonic crystal fiber," *IEEE Sens. J.*, 2018, doi: 10.1109/JSEN.2018.2819165.

- [135] C. Jollivet, B. Samson, L. Leick, L. Shah, M. Richardson, and A. Schülzgen, "Comparative study of light propagation and single-mode operation in large-mode area fibers designed for 2- μm laser applications," *Opt. Eng.*, 2014, doi: 10.1117/1.oe.54.1.011006.
- [136] S.-P. Tai, M.-C. Chan, T.-H. Tsai, S.-H. Guo, L.-J. Chen, and C.-K. Sun, "Two-photon fluorescence microscope with a hollow-core photonic crystal fiber," *Opt. Express*, 2004, doi: 10.1364/opex.12.006122.
- [137] X. Yang, A. S. P. Chang, B. Chen, C. Gu, and T. C. Bond, "High sensitivity gas sensing by Raman spectroscopy in photonic crystal fiber," *Sensors Actuators, B Chem.*, 2013, doi: 10.1016/j.snb.2012.09.004.
- [138] D. Kacik and P. Tatar, "Photonic crystal fiber modal interferometer for refractive index sensing," *Komunikacie*, 2013, doi: 10.1364/oL37.001373.
- [139] P. Sharma and P. Sharan, "Design of photonic crystal-based biosensor for detection of glucose concentration in urine," *IEEE Sens. J.*, 2015, doi: 10.1109/JSEN.2014.2359799.
- [140] S. Roy, "Fiber optic sensor for determining adulteration of petrol and diesel by kerosene," *Sensors Actuators, B Chem.*, 1999, doi: 10.1016/S0925-4005(99)00171-9.
- [141] S. H. Kassani, R. Khazaeinezhad, Y. Jung, J. Kobelke, and K. Oh, "Suspended ring-core photonic crystal fiber gas sensor with high sensitivity and fast response," *IEEE Photonics J.*, 2015, doi: 10.1109/JPHOT.2015.2396121.
- [142] J. B. Jensen, P. E. Hoiby, G. Emiljanov, O. Bang, L. H. Pedersen, and A. Bjarklev, "Selective detection of antibodies in microstructured polymer optical fibers," *Opt. Express*, 2005, doi: 10.1364/opex.13.005883.
- [143] S. Rota-Rodrigo, A. López-Aldaba, R. A. Pérez-Herrera, M. Del Carmen López Bautista, Ó. Esteban, and M. López-Amo, "Simultaneous measurement of humidity and vibration based on a microwire sensor system using fast fourier transform technique," *J. Light. Technol.*, 2016, doi: 10.1109/JLT.2016.2580003.
- [144] H. Y. Fu *et al.*, "Pressure sensor realized with polarization-maintaining photonic crystal fiber-based Sagnac interferometer," *Appl. Opt.*, 2008, doi: 10.1364/AO.47.002835.
- [145] M. Tonouchi, "Cutting-edge terahertz technology," *Nature Photonics*. 2007, doi: 10.1038/nphoton.2007.3.
- [146] K. Lee and S. A. Asher, "Photonic crystal chemical sensors: pH and ionic strength," *J. Am. Chem. Soc.*, 2000, doi: 10.1021/ja002017n.
- [147] M. Morshed, M. Imran Hassan, T. K. Roy, M. S. Uddin, and S. M. Abdur Razzak, "Microstructure core photonic crystal fiber for gas sensing applications," *Appl. Opt.*, 2015, doi: 10.1364/ao.54.008637.
- [148] M. F. H. Arif, K. Ahmed, S. Asaduzzaman, and M. A. K. Azad, "Design and optimization of photonic crystal fiber for liquid sensing applications," *Photonic Sensors*, 2016, doi:

10.1007/s13320-016-0323-y.

- [149] S. Asaduzzaman and K. Ahmed, "Proposal of a gas sensor with high sensitivity, birefringence and nonlinearity for air pollution monitoring," *Sens. Bio-Sensing Res.*, 2016, doi: 10.1016/j.sbsr.2016.06.001.
- [150] I. Islam *et al.*, "Highly birefringent single mode spiral shape photonic crystal fiber based sensor for gas sensing applications," *Sens. Bio-Sensing Res.*, 2017, doi: 10.1016/j.sbsr.2017.04.001.
- [151] B. K. Paul, M. S. Islam, K. Ahmed, and S. Asaduzzaman, "Alcohol sensing over O+E+S+C+L+U transmission band based on porous cored octagonal photonic crystal fiber," *Photonic Sensors*, 2017, doi: 10.1007/s13320-017-0376-6.
- [152] S. Asaduzzaman, K. Ahmed, T. Bhuiyan, and T. Farah, "Hybrid photonic crystal fiber in chemical sensing," *Springerplus*, 2016, doi: 10.1186/s40064-016-2415-y.
- [153] B. K. Paul, K. Ahmed, S. Asaduzzaman, and M. S. Islam, "Folded cladding porous shaped photonic crystal fiber with high sensitivity in optical sensing applications: Design and analysis," *Sens. Bio-Sensing Res.*, 2017, doi: 10.1016/j.sbsr.2016.11.005.
- [154] S. E. Kim, B. H. Kim, C. G. Lee, S. Lee, K. Oh, and C.-S. Kee, "Elliptical defected core photonic crystal fiber with high birefringence and negative flattened dispersion," *Opt. Express*, 2012, doi: 10.1364/oe.20.001385.
- [155] T. M. Monro, W. Belardi, K. Furusawa, J. C. Baggett, N. G. R. Broderick, and D. J. Richardson, "Sensing with microstructured optical fibres," *Meas. Sci. Technol.*, 2001, doi: 10.1088/0957-0233/12/7/318.
- [156] Y. L. Hoo, W. Jin, H. L. Ho, D. N. Wang, and R. S. Windele, "Evanescent wave gas sensing using microstructure fibre," 2001, doi: 10.1117/1.1429930.
- [157] K. Saitoh, M. Koshiba, T. Hasegawa, and E. Sasaoka, "Chromatic dispersion control in photonic crystal fibers: application to ultra-flattened dispersion," *Opt. Express*, 2003, doi: 10.1364/oe.11.000843.
- [158] S. Selleri, L. Vincetti, A. Cucinotta, and M. Zoboli, "Complex FEM modal solver of optical waveguides with PML boundary conditions," *Opt. Quantum Electron.*, 2001, doi: 10.1023/A:1010886632146.
- [159] H. Ademgil and S. Haxha, "PCF based sensor with high sensitivity, high birefringence and low confinement losses for liquid analyte sensing applications," *Sensors (Switzerland)*, 2015, doi: 10.3390/s151229891.
- [160] Z. Liu *et al.*, "Reflective-distributed SPR sensor based on twin-core fiber," *Opt. Commun.*, 2016, doi: 10.1016/j.optcom.2015.12.018.
- [161] Y. Peng, J. Hou, Z. Huang, and Q. Lu, "Temperature sensor based on surface plasmon resonance within selectively coated photonic crystal fiber," *Appl. Opt.*, 2012, doi: 10.1364/AO.51.006361.

- [162] H. Yokota, H. Yashima, Y. Imai, and Y. Sasaki, "Coupling Characteristics of Fused Optical Fiber Coupler Formed with Single-Mode Fiber and Photonic Crystal Fiber Having Air Hole Collapsed Taper," *Adv. Optoelectron.*, 2016, doi: 10.1155/2016/6219895.
- [163] M. Rakibul Islam, M. M. I. Khan, F. Mehjabin, J. Alam Chowdhury, and M. Islam, "Design of a fabrication friendly & highly sensitive surface plasmon resonance-based photonic crystal fiber biosensor," *Results Phys.*, 2020, doi: 10.1016/j.rinp.2020.103501.
- [164] D. Pysz *et al.*, "Stack and draw fabrication of soft glass microstructured fiber optics," *Bull. Polish Acad. Sci. Tech. Sci.*, 2014, doi: 10.2478/bpasts-2014-0073.
- [165] V. V. R. Kumar *et al.*, "Extruded soft glass photonic crystal fiber for ultrabroad supercontinuum generation," *Opt. Express*, 2002, doi: 10.1364/oe.10.001520.
- [166] B. J. Eggleton *et al.*, "Chalcogenide photonics: fabrication, devices and applications Introduction " Photosensitive and thermal nonlinear effects in chalcogenide photonic crystal cavities," *Opt. Express Express*, 2010.
- [167] M. C. J. Large *et al.*, "Microstructured polymer optical fibres: New opportunities and challenges," 2006, doi: 10.1080/15421400500374930.
- [168] H. Ebendorff-Heidepriem, J. Schuppich, A. Dowler, L. Lima-Marques, and T. M. Monro, "3D-printed extrusion dies: a versatile approach to optical material processing," *Opt. Mater. Express*, 2014, doi: 10.1364/ome.4.001494.
- [169] Z. Liu and H.-Y. Tam, "Fabrication and Sensing Applications of Special Microstructured Optical Fibers," in *Selected Topics on Optical Fiber Technologies and Applications*, 2018.
- [170] R. Islam, M. S. Habib, G. K. M. Hasanuzzaman, R. Ahmad, S. Rana, and S. F. Kaijage, "Extremely High-Birefringent Asymmetric Slotted-Core Photonic Crystal Fiber in THz Regime," *IEEE Photonics Technol. Lett.*, 2015, doi: 10.1109/LPT.2015.2457673.
- [171] J. Sultana, M. R. Islam, M. Faisal, K. M. Abu Talha, and M. S. Islam, "Design and analysis of a Zeonex based diamond-shaped core kagome lattice photonic crystal fiber for T-ray wave transmission," *Opt. Fiber Technol.*, 2019, doi: 10.1016/j.yofte.2018.11.017.
- [172] M. S. Islam *et al.*, "A modified hexagonal photonic crystal fiber for terahertz applications," *Opt. Mater. (Amst.)*, 2018, doi: 10.1016/j.optmat.2018.03.054.
- [173] B. K. Paul, M. A. Haque, K. Ahmed, and S. Sen, "A novel hexahedron photonic crystal fiber in terahertz propagation: Design and analysis," *Photonics*, 2019, doi: 10.3390/PHOTONICS6010032.
- [174] B. K. Paul and K. Ahmed, "Analysis of terahertz waveguide properties of Q-PCF based on FEM scheme," *Opt. Mater. (Amst.)*, 2020, doi: 10.1016/j.optmat.2019.109634.
- [175] B. K. Paul *et al.*, "Extremely low loss optical waveguide for terahertz pulse guidance," *Results Phys.*, 2019, doi: 10.1016/j.rinp.2019.102666.